AARHUS UNIVERSITET
DCE - NATIONALT CENTER FOR MILJØ OG ENERGI

NIRAS

Survey of Birds for Offshore Wind Farms in Danish Waters – North Sea I

WP Birds

Energinet Eltransmission A/S

Date: 15. November 2024

Rev. no.	Date	Description	Done by	Verified by	Approved by
1.0	20.06.2024	First draft – Survey of Birds for Offshore Wind Farms in Danish Waters – North Sea I	Ib Krag Petersen (DCE) Heidi Maria Thomsen (DCE) Lindesay Scott-Hayward (CREEM) Saana Isojuuno (CREEM) Monique Mac Kenzie (CREEM) Jamie Alison (DCE) Claus Lunde Pedersen (DCE) Rune Sø Neergaard (NIRAS) Troels Eske Ortvad (DCE) Rasmus Due Nielsen (DCE) Jacob Sterup (DCE)	Ole Roland Therkildsen (DCE) Rune Sø Neergaard (NIRAS)	Søren Granskov (NIRAS)
2.0	15.09.2024	Final draft – Survey of Birds for Offshore Wind Farms in Danish Waters – North Sea I	-II-	-II-	-II-
3.0	01.11.2024	Final Version 1 - Survey of Birds for Offshore Wind Farms in Danish Waters – North Sea I	-II-	-II-	-II-
3.1	15.11.2024	Final Version 2 - Survey of Birds for Offshore Wind Farms in Danish Waters – North Sea I	-II-	-II-	-II-

Contents

Preface

This report was commissioned by Energinet. It describes results obtained from the bird survey program in connection with the planned construction of the offshore wind farms in the North Sea I area.

The report builds upon data collected under this project and analysis of those data. The report has eight main chapters. Chapter 1 is Introduction and objectives of the report. Chapter 2 provides an overview of existing data. Chapter 3 describes the data collection methods. Chapter 4 describes data analysis methods. Chapter 5 describes the results from this project. Chapter 6 provides the knowledge gaps and Chapter 7 provides discussions and conclusions from the work. Finally, Chapter 8 provides a list of references.

Front page illustration: An adult northern gannet in flight, photographed by Yann Kolbeinsson, Iceland.

Declaration

NIRAS was contracted by Energinet to undertake baseline studies of birds in relation to NSI, with Aarhus University, Danish Centre for Environment and Energy (DCE) as a subcontractor. DCE subcontracted University of St. Andrews (CREEM) to assist with parts of the data analysis.

Aarhus University (DCE) has designed and conducted the data collection for this project and analysed the data for all parts of the work. The University of St. Andrews (CREEM) conducted the distance sampling analyses and the spatial models for selected bird species in chapter 4.1.

From Aarhus University, Dept. of Ecoscience: Ib Krag Petersen (editor and responsible for field work and report writing of bird investigations), Heidi Marie Thomasen (Data analysis of ship-based data), Jamie Alison (data analysis of flight altitude information from vertical radar), Lindesay Scott-Hayward, Saana Isojuuno and Monique Mac Kenzie (Distance sampling and spatial modelling analyses of data from aerial surveys), Claus Lunde Pedersen (GIS work), Rasmus Due Nilesen, Jacob Sterup and Troels Eske Ortvad (field work aerial surveys and ship-based surveys).

From NIRAS, Rune Sø Neergaard assisted with coordination, planning and report review.

The report was peer-reviewed by Ole Roland Therkildsen, Aarhus University, and quality assured by Jesper Fredshavn at DCE, Aarhus University and Rune Sø Neergaard, NIRAS. Søren Granskov, NIRAS gave final approval for publication of the report by NIRAS.

Energinet commented on a first and second draft of the report before the final version was published, the comments and author replies can be found here:

https://dce.au.dk/udgivelser/oevrige-dce-udgivelser/eksterne-udgivelser/2024

The report is published by the Danish Energy Agency as part of the tender for offshore wind farms in North Sea I.

The report and associated investigations were financed by Energinet. Energinet wrote the initial section of the Introduction chapter.

List of key terms

A list of terms (in English and Danish) and their explanations.

Table 0.1 Terminology including Danish and English terms as well as explanations.

English (abbreviation)	Danish	Explanation
NSI		North Sea I
OWF		Offshore Wind Farm
HR3 OWF		Horns Rev 3 Offshore Wind Farm
Pre-investigation area	Forundersøgelsesområde	The area covered by the survey permit for North Sea I and the geographical scope of the technical baseline reports.
Bird survey area	Undersøgelsesområde for fugle, inkluderende en 20 km zone omkring forundersøgelsesområdet	The pre-investigation area and a 20 km buffer zone around that. This area was surveyed for birds using aerial surveys.
Distance sampling	Distance sampling	A method to record observations with distance to an observer to estimate density and total abundance for a species.
Detection function	Detektionsfunktion	Modelling the declining probability of detecting an individual or cluster of individuals with increased distance from the observer to the object.
Spatial modelling	Rumlig modellering	A method to produce distribution maps and associated uncertainty from sampled data.

Summary

In 2023 and 2024, ornithological studies were conducted to provide baseline data for EIA of future offshore wind farms in the NSI area, located in the eastern part of the Danish North Sea. These surveys aimed to gather background data for future environmental impact assessments related to upcoming offshore wind farm projects.

The ornithological studies consisted of two main components. The first component aimed to provide data on bird species abundances and distributions across the pre-investigation area and a 20 km buffer zone around it, referred to as the survey area, over the course of a year. To achieve this, eight aerial surveys were conducted between April 2023 and March 2024. During these surveys a total of 7 species groups and 28 species of birds were observed from the eight aerial surveys in the SNI area between April 2023 and March 2024. Each survey was performed using two aircraft and employed the distance sampling survey method. This approach allowed for the modelling of total abundances and distributions of selected bird species. Based on these modelled estimates, a persistency map for the survey area was created, highlighting areas of high or low importance for specific species or species groups across all surveys. Data from each of the eight surveys were used to derive information about the abundances and distributions of the following species/species groups: red-throated/black-throated diver, northern gannet, black-legged kittiwake, and razorbill/common guillemot. The maximum bird numbers per survey were 7,548 divers, 2,642 northern gannets, 3,669 black-legged kittiwakes, and 35,069 razorbills/common guillemots.

The other part aimed to describe the movements of flying birds in the pre-investigation area. Data from observations of flying birds from ship-based surveys gave information on the composition and flight altitude distribution of selected species or species groups. While almost 100% of some species flew very low over the sea surface (0-25 m), other species or species groups were recorded to fly higher. For example, common scoter and razorbill/common guillemot flew very low, whereas species of waders and gulls flew higher. Data from the ship-based surveys also gave information about the composition of species that are difficult to identify from aerial surveys, such as red-throated/black-throated divers and razorbill/common guillemots. While red-throated divers dominated the diver group, razorbills and common guillemots comprised 43% and 56% of the auk group. The species composition of the latter group varied considerably across the annual cycle.

Data from a vertical radar provided information on flight magnitude and altitude both day and night. The radar records objects that can be a single bird or a group of birds. Neither species nor group size can be inferred from data from the radar. There was both annual and diurnal variation in the bird flight activity. The movement of flying birds showed much higher flight activity in October 2023 than in any other month relating to bird autumn migration. The diurnal variation showed that the flight activity was highest at night in October 2023. Elevated activity was less pronounced during cruises in other months.

This report also presents a description of existing data. An overview of existing ornithological data from the Danish North Sea is presented. Data from an aerial survey in April/May 2019 was used to estimate abundances and distributions for selected species and species groups across the entire Danish part of the North Sea. On the basis of that dataset, total abundances and distribution of the following species could be generated: red-throated/black-throated diver, northern fulmar, northern gannet, black-legged kittiwake and razorbill/common guillemot. The total estimated abundances for these species were 22,648 divers, 46,437 northern fulmars, 31,723 northern gannets, 4,472 black-legged kittiwakes and 89,681 razorbills/common guillemots (Petersen, et al., 2024). These data can perspectivate bird abundances within the NSI area with densities and distributions in other parts of the Danish North Sea. Common scoters and red-throated divers are mainly found in the eastern parts of the bird survey area, and thus almost absent from the North Sea Energy Island study area. Bird species with a more pelagic distribution, such as northern fulmar, was found in smaller numbers in the NSI area than in the North Sea Energy Island area. Northern gannet and razorbill/common guillemot were found in comparable numbers between the two survey sites.

1. Introduction and objective

In order to accelerate the expansion of Danish offshore wind production, it was decided with the agreement on the Finance Act for 2022 to offer an additional 2 GW of offshore wind for establishment before the end of 2030. In addition, the parties behind the Climate Agreement on Green Power and Heat 2022 of 25 June 2022 (hereinafter Climate Agreement 2022) decided, that areas that can accommodate an additional 4 GW of offshore wind must be offered for establishment before the end of 2030. Most recently, a political agreement was concluded on 30 May 2023, which establishes the framework for the Climate Agreement 2022 with the development of 9 GW of offshore wind, which potentially can be increased to 14 GW or more if the concession winners – i.e. the tenderers who will set up the offshore wind turbines – use the freedom included in the agreement to establish capacity in addition to the tendered minimum capacity of 1 GW per tendered area.

The North Sea I pre-investigation area covers a total area of 2,158 km^2 which is divided into three sub-areas planned for offshore wind farms. The North Sea I area is located 20-80 km off the coast of West Jutland and from each of the three sub-areas there will be corridors for export cables connecting the offshore wind farms to the onshore grid (Figure 1.1). The overall purpose of this service is to undertake a series of surveys for birds, bats and marine mammals in a specified area of the North Sea, named North Sea I, to establish an environmental baseline for the later environmental permitting processes for the offshore wind built-out.

This report concerns baseline data and information on marine and migratory birds. Aarhus University (DCE) and the University of St. Andrews (CREEM), under a subcontract with NIRAS, carried out the study between April 2023 and March 2024 on behalf of Energinet Eltransmission A/S.

1.1 Objective

The objective of the environmental pre-investigations is to collect novel data and compile existing data and information to be handed over to future concessionaires as environmental baseline information for the environmental permitting processes. The specific objective of this technical report is to present the collected data describing the abundance and distribution of selected bird species and species groups observed by aerial surveys within the bird survey area. Furthermore, the objective is to describe the species composition and flight altitude distribution of flying birds in the area.

This technical report presents the abundance and distribution of bird species observed in the survey area through aerial surveys, comprised of the NSI pre-investigation area and a buffer of 20 km around that. It also describes bird flight volumes and altitudes based on data collected from ship-based surveys. The ship-based surveys concentrated on obtaining data on the species composition of flying birds and their flight altitudes, both diurnally by use of visual observations and nocturnally by use of vertical radar.

1.2 Survey area

The North Sea I pre-investigation area covers an area of 2,158 km^2 off the west coast of Jutland. To the south, the area extends to the north of Horns Rev. To the north, the area extends to approximately 20 km north of an east/west line from the northern end of Ringkøbing Fjord. To the west, the area reaches out to 80 to 60 km from the coast of Jutland, and to the east, the pre-investigations start from approximately 20 km from the coastline (Figure 1.1). The aerial surveys cover an area of 7,640 km^2 and constitute the pre-investigation area plus a 20 km buffer zone.

The pre-investigation area has water depths from ca. 15-35 m, while the survey area covers water depths from the coastline (0 m) to approximately 45 m. The pre-investigation area has a minimum distance to the HR3 OWF of 7.5 km and a minimum distance to the Vesterhav Syd OWF site of 10 km. The Thor OWF site is approximately 5 km north of the pre-investigation area and is largely within the survey area of this project (Figure 1.1).

The pre-investigation area is adjacent to the EU Special Protection Area number 113 in the southeastern part of the pre-investigation area, with no overlap between the two.

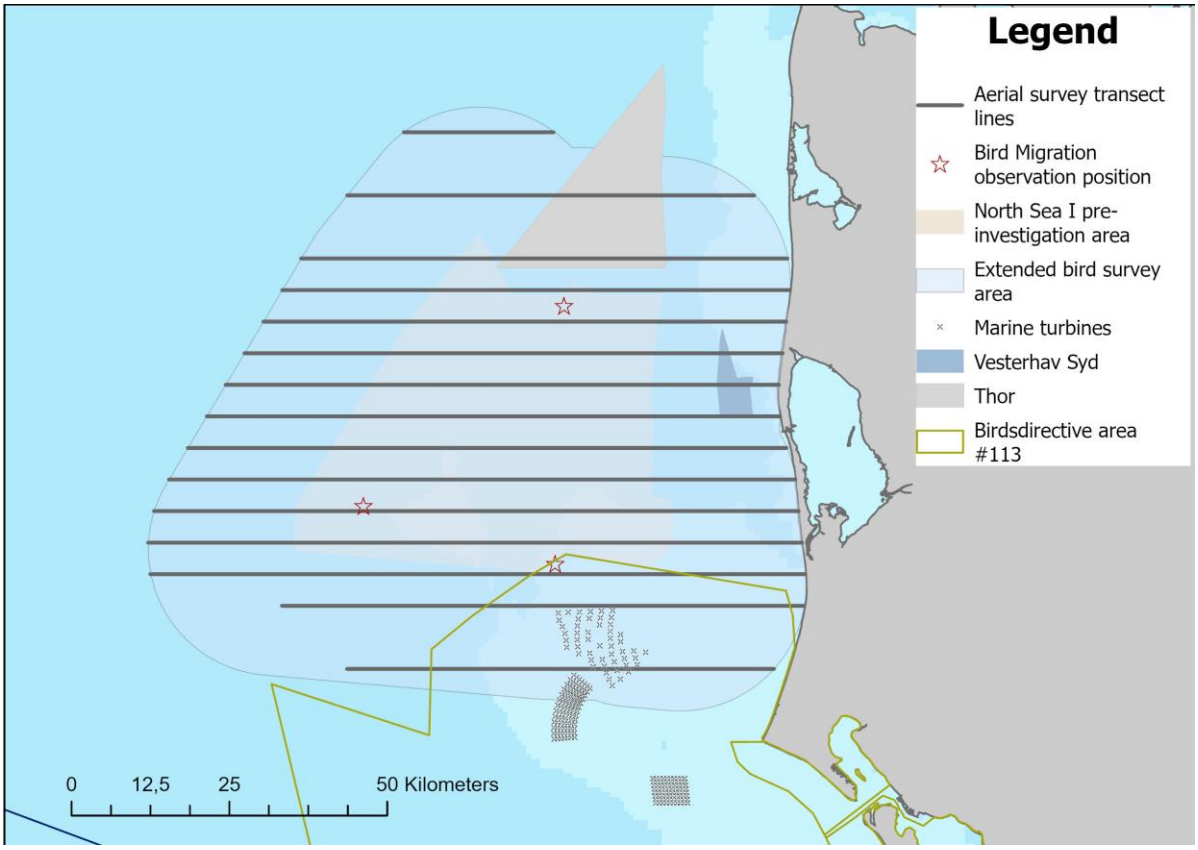

Figure 1.1 The North Sea I pre-investigation area and the survey area for the description of bird abundances and distributions. The aerial survey transect lines and bird migration observation positions are indicated. Moreover, the Horns Rev wind turbines, the Vesterhav Syd OWF site and the Thor OWF site are also shown. Finally, the extension of the EU Special Protection Area number 113 is shown.

2. Existing data

While the inner Danish waters have been surveyed for birds for many years, data on bird distributions further out in the North Sea are relatively scarce. The Danish part of the North Sea was surveyed for birds through ship-based surveys in the 1970s and 1980s (Tasker, Webb, Hall, Pienkowski, & Langslow, 1987; Stone, et al., 1995; Skov, Durinck, Leopold, & Tasker, 1995) and aerial surveys in the 1980s (Laursen, et al., 1997).

Since then, relatively few bird surveys have been conducted in the North Sea. The most notable activity has been a long series of aerial line transect surveys related to wind energy development in the Horns Rev area, starting in 1999 and continuing until 2012. These surveys, totalling around 50, were spread across the annual cycle but covered a relatively small geographical area.

The southern part of the Danish North Sea has been surveyed irregularly since 2002, mainly focusing on the presence of red-throated divers and black-throated divers concerning the designation of a Birds Directive area for these two species (Petersen, Nielsen, & Clausen, 2016; Petersen, Nielsen, & Clausen, 2019).

Since 2015, the central-eastern parts of the Danish North Sea, from Blåvand in the south to Thyborøn in the north, and extending approximately 70 km out to sea, have been surveyed irregularly by aerial surveys. Most surveys were conducted in late spring, focusing on red-throated divers in relation to the Marine Strategic Framework Directive. In 2019, five surveys were conducted in this area in relation to a strategic environmental assessment of wind farm plans (Petersen & Sterup, 2019).

In the northern parts of the North Sea, a series of aerial surveys focused on marine birds along the southern flank of the Norwegian Trench. The Environmental Agency requested these surveys in relation to plans for designating a Birds Directive Special Protection Area for seabirds such as the northern fulmar (Petersen, Nielsen, & Clausen, 2016).

In 2012 and 2013, five aerial surveys were conducted in a geographically restricted area in Jammerbugten, commissioned by Vattenfall in relation to OWF plans (Nielsen & Petersen, 2014).

Between March 2022 and November 2023 12 aerial surveys were conducted in the North Sea Energy Island area, situated to the northwest of the North Sea I bird survey area, covering an area of more than 4,800 km^2 (Petersen, et al., 2024).

The only recent survey with comprehensive, large scale bird coverage in the Danish North Sea was conducted over three days in April/May 2019 (Petersen, Nielsen, & Clausen, 2019; Petersen, et al., 2024).

To supplement the data presented in the rest of this report, data from the 2019 aerial surveys were used to model total abundances and spatial distributions of four bird species or species groups: northern fulmar, red-throated/black-throated diver, northern gannet, black-legged kittiwake, and razorbill/common guillemot. These data were gathered and analysed in the same way as the data presented earlier in the report, apart from the fact that for these data, there was access to more environmental covariates, such as sea surface temperature and salinity.

3. Survey methods

The ornithological surveys in the bird survey area were designed to provide baseline data to support the process of developing environmental impact assessments for OWFs in the area.

The bird data consists of two main parts: one that describes the abundance and distribution of bird species in the area throughout the annual cycle and another that describes bird migration and flight activity in the area.

Eight aerial surveys, conducted between April 2023 and March 2024, collected data on bird abundance and distribution. These surveys used the distance sampling method, which enables the modelling of density and fine-scale distribution of selected bird species.

Data on bird flight in the area was collected using ship-based surveys, during which ornithological observers recorded bird densities and flight altitude from three pre-defined positions within the pre-investigation area. During the day, visual observations enabled species identification of the passing birds, while at night, a vertical radar recorded general bird movements and flight altitudes without the option of getting species-specific data.

The two general survey methods are described below.

3.1 Aerial surveys

Data on bird abundance and distribution were collected using standard methods. Human observers visually gathered data during aerial surveys by flying transects between designated GPS waypoints at regular speeds and altitudes

(Figure 1.1). Twin-engine, high-wing aircraft, specifically the Cessna 337 and the Partenavia P-68, were used for the surveys. Observations were recorded within distance bands (NOVANA Technical Specification TA A188) parallel to the aircraft to allow for the modelling of differential detectability at increasing distances from the observers (Petersen & Sterup, 2019), following standard distance sampling line transect survey methods (Buckland, et al., 2001; Buckland, Rexstad, Marques, & Oedekoven, 2015).

The data collection was performed from a flight altitude of 76 m. Two trained observers recorded birds from either side of the aircraft. The bird species or species group was noted for each record, along with information on flock size, behaviour, perpendicular distance from the survey track and time. In addition, the environmental conditions at the time (e.g. sea state and sun glare) were registered. The perpendicular distance was classified in predefined distance bands with increasing distance from the survey track line to 1.5 km on either side of the aircraft (Figure 3.1).

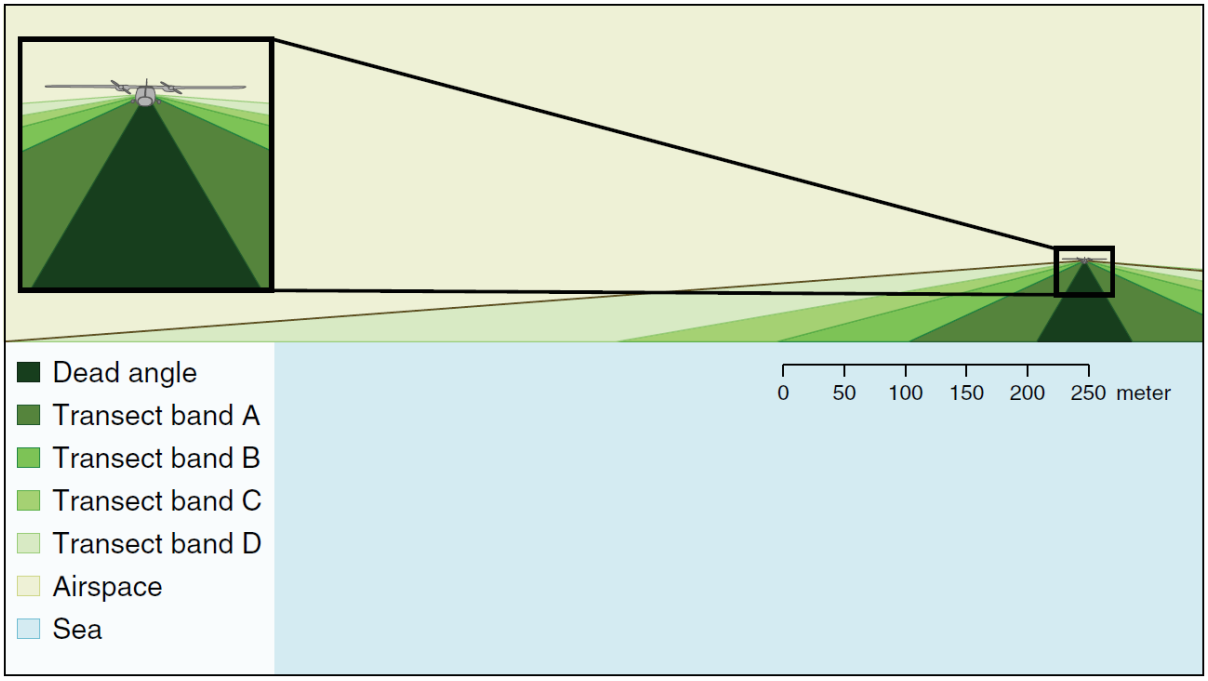

Figure 3.1 The transect band definitions for aerial line transect surveys. From the survey altitude of 76 m, there is a dead angle of 44 m on each side of the survey track that the observers could not cover.

The survey transect lines were designed as parallel east-west oriented lines, covering the survey area. The 15 transect lines were separated by 5 km for most transects, although in parts of the area outside of the pre-investigation area, the distance between transects was 10 km (Figure 1.1). The species distribution maps in Chapter 5.1 present the precise survey track lines covered during each survey.

The data used for this assessment derives from eight surveys undertaken between April 2023 and March 2024, all of which were completed over a single day (Table 3.1).

Table 3.1 Overview of the eight aerial surveys conducted in the study. The total transect length covered in the southern (South) and northern (North) parts of the survey area is given for each survey.

Date	Transect length (km)			Aircraft type
	South	North	Total	
2023-04-30	592.9	658.0	1,250.8	Partenavia P-68 and Cessna 337
2023-07-07	592.0	657.1	1,249.1	Partenavia P-68 and Cessna 337
2023-09-05	595.5	637.3	1,232.7	Partenavia P-68
2023-11-26	593.0	658.0	1,251.0	Partenavia P-68 and Cessna 337
2023-12-14	611.8	640.2	1,252.0	Partenavia P-68
2024-02-08	593.1	643.3	1,236.4	Partenavia P-68
2024-02-25	594.5	657.4	1,252.0	Partenavia P-68 and Cessna 337
2024-03-21	599.9	622.9	1,222.8	Partenavia P-68 and Cessna 337

3.2 Ship-based surveys

Between April 2023 and March 2024, eight ship-based surveys were conducted in the North Sea I pre-investigation area (Figure 1.1). Each survey included an average of 5 (± 0.5) days and 59.7 (± 9.9) hours of bird observation. Combined, the eight surveys comprised 40 observation days and 477.4 bird observation hours.

Table 3.2 Overview of the eight ship-based surveys conducted in the North Sea I pre-investigation area. The table shows each survey's start and end dates and the number of observation days (N = 40) and hours (N = 477.4).

Survey ID	Start date	End date	Observation days	Observation hours
S1	2023-04-27	2023-04-30	4	59.5
S2	2023-05-18	2023-05-22	5	80.8
S3	2023-06-13	2023-06-18	6	102.5
S4	2023-08-11	2023-08-16	6	81.1
S5	2023-09-15	2023-09-22	7	61.7
S6	2023-10-08	2023-10-10	3	32.2
S7	2023-12-03	2023-12-08	6	41.2
S8	2024-02-08	2024-02-10	3	18.4

Observers spent approximately equal observation days (Appendix 1 Table 8.1) and hours (Appendix 1 Table 8.2) at each of the three pre-defined observation positions within the pre-investigation area (Figure 1.1) during the ship-based surveys. On average, each survey included 1.9 (± 0.3), 1.5 (± 0.3) and 1.6 (± 0.3) observation days, and 20.5 (± 4.2), 18.6 (± 4.1), 20.6 (± 4.3) observation hours at the North, Southeast, and Southwest observation positions, respectively. However, three surveys (S1, S6, and S8) only included observations from two positions. Overall, 37.5%, 30% and 32.5% of the observation days, and 34.3%, 31.2% and 34.5% of the observation hours were spent at the North, Southeast and Southwest observation positions, respectively.

3.2.1 Species observations

The ship-based bird observations were made at the three pre-defined observation positions within the pre-investigation area (Figure 1.1) using two ship-based survey methods: transect surveys and stationary surveys. During transect surveys, observers recorded birds while the ship sailed along a straight line, covering an area of 300 m perpendicular to the ship's course on one or both sides, depending on observer conditions. Furthermore, some observers continued counting when the ship was stationary to assess species composition. Observers measured the

perpendicular distance to birds using a laser rangefinder, and estimating the distance by eye when using the rangefinder was not feasible. During snapshot observations, observers recorded all birds within a 300 x 1000 m area in front of the vessel at 15-minute intervals. Data collected using both methods were used to analyse flight altitude (Chapter 4.2.1) and species composition (Chapter 4.2.2).

3.2.2 Flight altitude recording

Flight altitude recordings were made in all directions around the ship mainly from a stationary position, and only occasionally during active sailing between stations or to and from the survey area. Flight altitude was recorded for birds flying alone and in flocks, and flock size was recorded. Observers aimed to limit the recordings to birds that appeared to be little or unaffected by the ship's presence. Consequently, flight altitude recordings were obtained as far away from the ship as possible to eliminate data from individuals potentially attracted to the vessel.

In general, flight altitude recordings were made using a laser rangefinder. Whenever possible, especially during undulating flight, observers measured the altitude multiple times for each individual or flock to capture the range and variation in flight altitude. Repeated measures of the same individual or flock were recorded with the same observation ID. However, it was not possible to use the laser rangefinder on some occasions due to high waves. In these cases, the observer would estimate the flight altitude. Observers continuously estimated the flight altitudes and verified them using a laser rangefinder to refine and improve their estimation accuracy.

3.2.3 Vertical radar counts

Observers recorded 28,813 images from the ship-borne radar system between April 2023 and March 2024. The images were recorded during, immediately before, or after the eight ship-based surveys in eight sessions (Table 3.3). The September 2023 session had a relatively low number of images due to a gap in recording from the morning of 19 September to the morning of 21 September due to technical problems. None of the images from September 2023 were manually annotated. This is because a large portion of images from other surveys made a sufficient background for incorporation of annotation data.

Table 3.3 Details of the eight radar recording sessions. Pulse length is a setting on the radar system, while resolution is a setting in the screen-grab software. The annotator highlights which observers, if any, were responsible for labelling birds in images.

Start date	End date	Pulse length	Resolution	Images	Annotator
2023-04-26	2023-05-01	Medium	1920×1080	2,811	TEO
2023-05-17	2023-05-22	Medium	1800×1800	3,883	TEO
2023-06-13	2023-06-18	Medium	2400×1900	4,378	TEO
2023-08-10	2023-08-16	Short	2400×1900	4,211	RDN
2023-09-15	2023-09-23	Short	2400×1900	4,114	None
2023-10-07	2023-10-11	Short	2400×1900	2,658	TEO + RDN
2023-12-02	2023-12-08	Medium	2400×1900	4,641	RDN
2024-02-05	2024-02-11	Medium	2400×1900	2,117	TEO

The eight radar recording sessions were annotated using the VGG image annotator software. The radar annotations represent the presence of birds in the image as objects. The objects can represent a single bird or a group of birds. However, the images cannot infer bird species or flock size data. Therefore, with the radar data, "bird number" or "putative bird number" more precisely refers to object number.

The annotators were two experienced ornithologists familiar with the vessel-borne radar systems and the survey environments. Only one annotator would generally make annotations for each radar recording session. However, both

annotators generated labels for October 2023 (the session containing the highest number of birds), while no annotator generated labels for September 2023. Annotators were instructed to annotate objects they believed to be birds and to overlook images with clear signs of interference or bad weather, e.g., precipitation or heavy fog (Figure 3.2). They were also shown examples of circular (Figure 3.3) and radial artefacts (Figure 3.4), which they should not annotate. The annotators were informed 1) that annotation of birds is a subjective process, 2) that they should make their best judgement, and 3) to dismiss any weak or highly persistent signals.

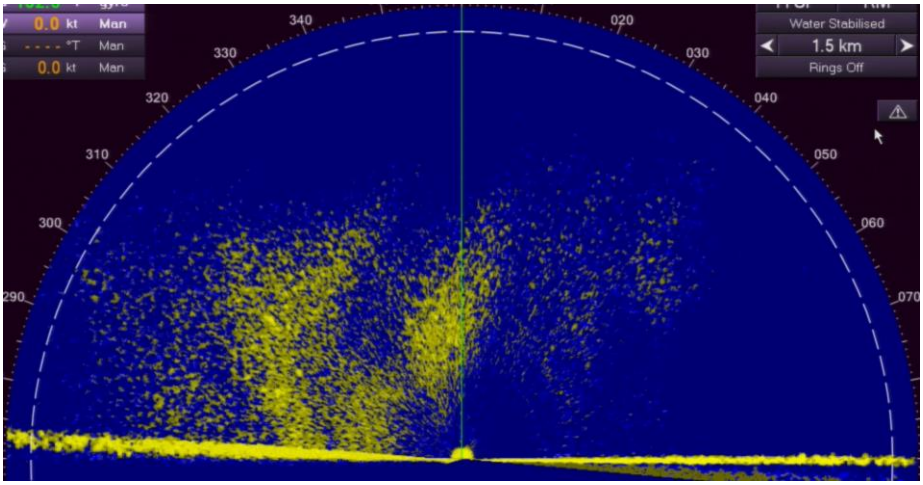

Figure 3.2 Example of a screen grab with clear evidence of bad weather.

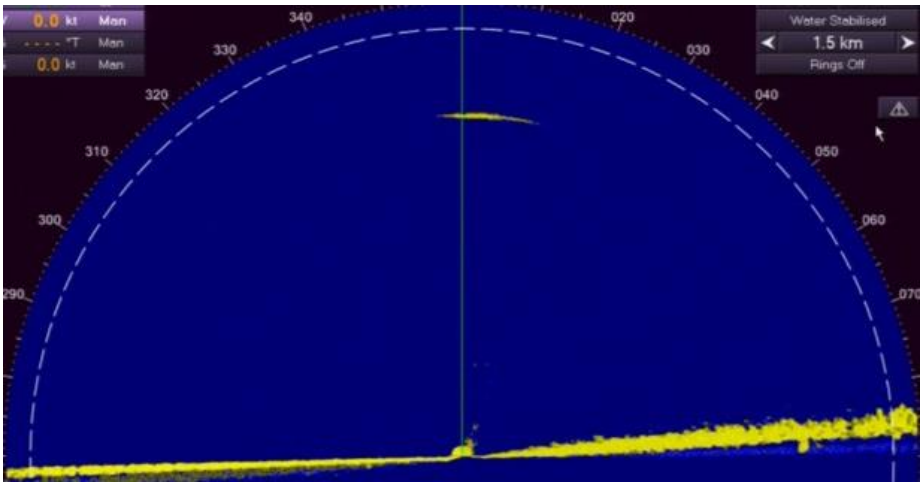

Figure 3.3 Example of a screen grab with a circular artefact.

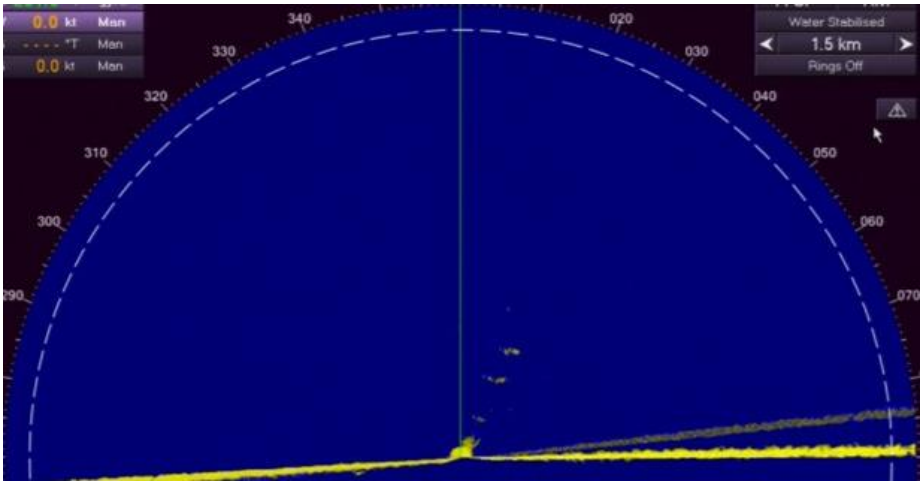

Figure 3.4 Example of a screen grab with a radial artefact.

4. Data analysis

4.1 Aerial surveys

4.1.1 Data for abundance estimation

Data was collected so that the declining probability of detecting a bird or a group of birds with increased distance from the survey track line could be modelled (Chapter 3.1). The detections were recorded in four bins or distance bands (A-D) with categories of 0-119 m (A), 119-388 m (B), 388-956 m (C) and 956-1,456 m (D). The detections were predominantly observed from both sides of the aircraft. No band under the aircraft was recorded, and the bins were adjusted to reflect this. Band D was subsequently removed from analysis for all species except the northern gannet, owing to little or no observations, with no adverse effects on the results.

Each transect was divided into approximately 500 m long and up to 1000 m wide segments and detections associated with the nearest segment. The transects for the surveys are shown in Table 4.1.

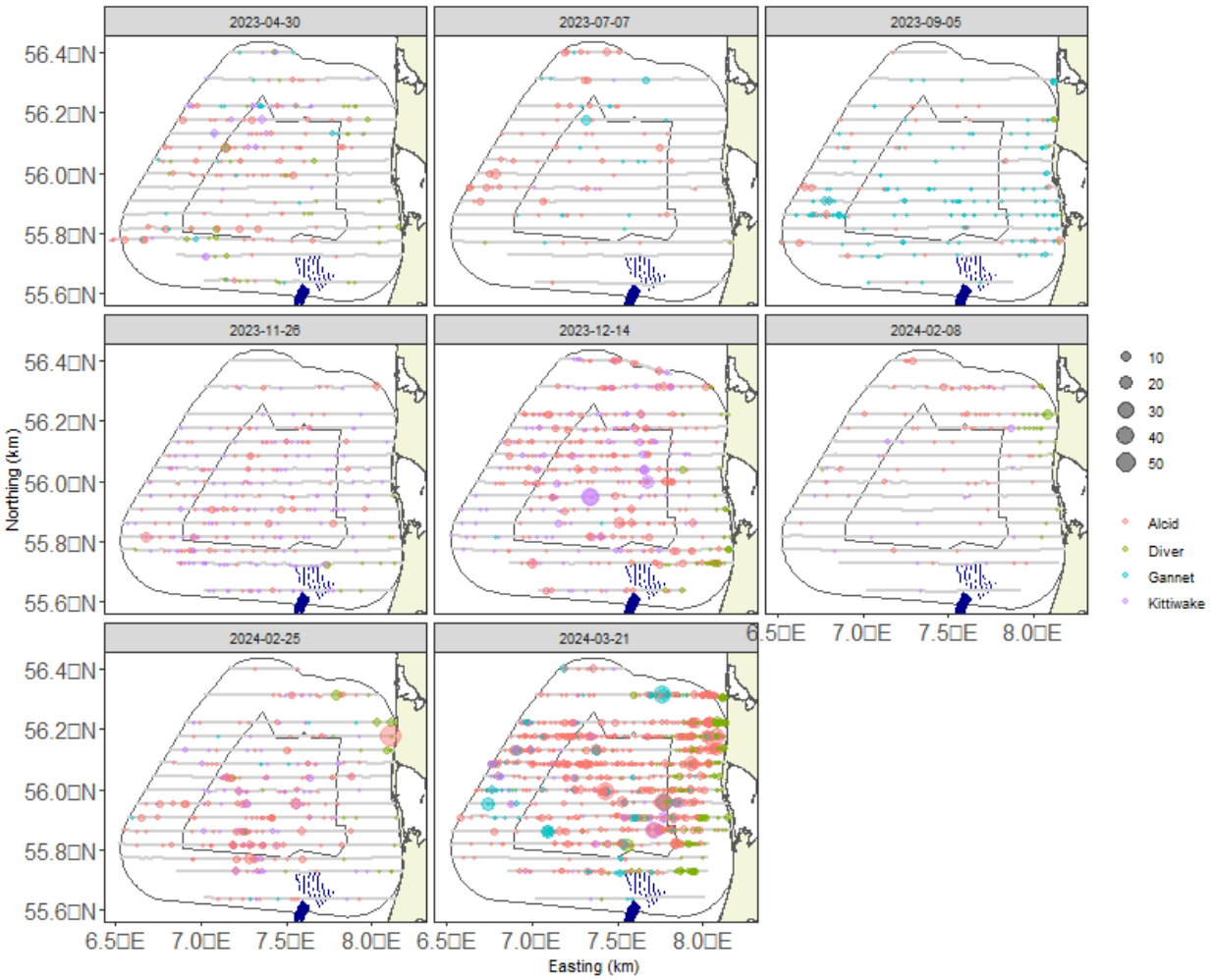

Table 4.1 Table detailing the survey effort (number of segments) for each of the eight surveys.

Survey date	Number of segments
2023-04-30	2,514
2023-07-07	2,513
2023-09-05	2,479
2023-11-26	2,514
2023-12-14	2,517
2024-02-08	2,486
2024-02-25	2,518
2024-03-21	2,460

For the spatial modelling, the latitude and longitude of the locations of the segment centroids were converted to UTM using UTM Zone 32N.

4.1.2 Distance sampling analysis

All survey data were collected using visual aerial methods and so correction for declining detectability with increasing distance from the plane was accounted for using Distance sampling methodology (Multiple Covariate Distance Sampling, MCDS) (F. F. C. Marques and Buckland 2004; T. A. Marques et al. 2007; Buckland et al. 2001). Analyses were conducted for each of the modelled species or species group datasets by pooling the information across all surveys. The distance analysis models the decreased probability of detecting a bird or group of birds with increased distance away from the track line of the survey aircraft.

To allow for the detectability of birds varying due to external factors (not just distance from observer) other covariates were included in the distance model. The candidate variables trialled were bird group size, behaviour, observer, glare and sea state (see Table 4.2). For some observers there were too few observations so in those cases, the observers' observations were combined with the next smallest. Observations with a sea state greater than four were removed from the analysis. Sea state is a measure of wave activity, and the more wave activity the more difficult it becomes to detect birds with increased distance away from the survey track line. Both half-normal and hazard rate detection functions were trialled (allowing different steepness/shape of the decline in detectability with distance) and the best of all competing models chosen using BIC. Further details on the distance analysis can be found in Appendix 2. The effects of glare, and any mitigations as a result, was approached using a dedicated analysis.

Table 4.2 Table detailing the covariates used in the detection function fitting.

Covariates	Values
Behaviour	S (sitting or diving) and F (flying or flushing)
Observer	7 Observers
Glare	1 (full sun), 2, 3 (cloudy), 9 (changeable)
Sea state	0, 0.5, 1, 1.5, 2, 2.5, 3, 3.5 (calm to rough)

4.1.2.1 Mitigating the effects of glare

Sighting conditions, such as sun glare and sea state, can influence the detection of sea birds from aerial surveys. Data to describe sighting conditions is usually collected in situ. However, when this is absent, alternative methods are required to identify (and adjust for) heterogeneity in the detection probability. Accounting for such heterogeneity is particularly important for distance sampling, where near-perfect detection at the track line is often a required assumption.

Detection information from band A was used for the left-hand and right-hand sides of the aircraft to identify transect lines with likely poor sighting conditions. For all species except flying northern gannets and black-legged kittiwakes, which are much easier to see even when glare is present, the identified transects removed observations from the affected side and reduced the coverage to one side (i.e., returning a one-sided transect).

The effects of glare and any mitigations, as a result, were approached using a dedicated analysis. The analysis was designed to quantify the extent to which directional sun glare can lead to left-hand or right-hand side bias in counts within a single transect line with the same direction of travel. Specifically, it was assumed that the proportion of left or right sightings in band A should be 0.5 and follow a binomial distribution. The proportions for each transect were then compared to a critical value calculated as the quantile of the binomial $(n, p = 0.5)$ distribution at three standard errors greater than the mean and where n equals the number of observations on the transect. This is a common measure in extreme value theory (Leys, Ley, Klein, Bernard, & Licata, 2013). Any transects with values greater than the critical value had the observations from the smaller side removed and the coverage reduced to a single side.

4.1.3 Spatial analysis framework

The following sections describe the spatial modelling methods employed and a description of the outputs which follow. The spatial analysis takes the distance corrected outputs and provides a density surface and associated

uncertainty at a fine geographical scale (grid squares of 1x1 km). For a more detailed description of the methods, see Appendix 2.

4.1.3.1 Modelling summary

The outputs from the detection function analysis give a detectability corrected count (abundances) in a small area (segment of approximately 500 m). Spatial models are used to turn these distances corrected counts along transect lines into spatial distribution maps, whilst accounting for data characteristics and modelling assumptions. The spatial modelling process was undertaken using a Generalised Additive Model framework (GAM) with an error family suitable for count per unit area response data, the Tweedie distribution. The effort associated with each observation varied depending on the associated segment length and width. Segment area was therefore included as a log-scale offset term in the model.

As each of the 8 surveys were analysed separately, only spatial explanatory variables were considered. The candidate variables for inclusion in the spatial model were a set of one-dimensional terms, water depth (Figure 4.1) and distance to coast (Figure 4.2), that were permitted to change linearly or non-linearly with the response and a two-dimensional term using geographic coordinates to account for surface patterns, which could be a result of unmodelled environmental variability. The flexibility of any smooth functions (1D or 2D) and the choice between competing models (inclusion or exclusion of variables) was determined using a five-fold cross-validation procedure.

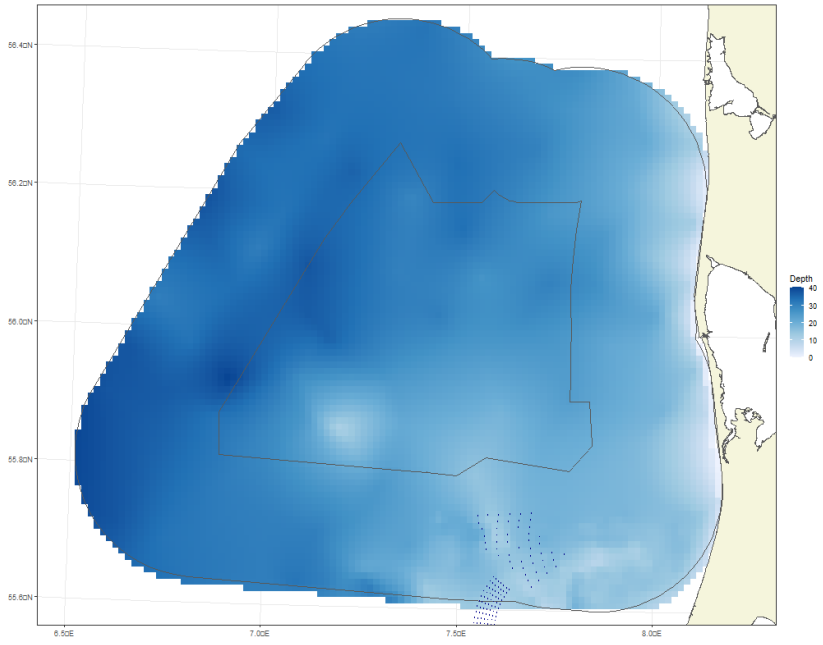

Figure 4.1 Visual representation of bathymetry (water depth).

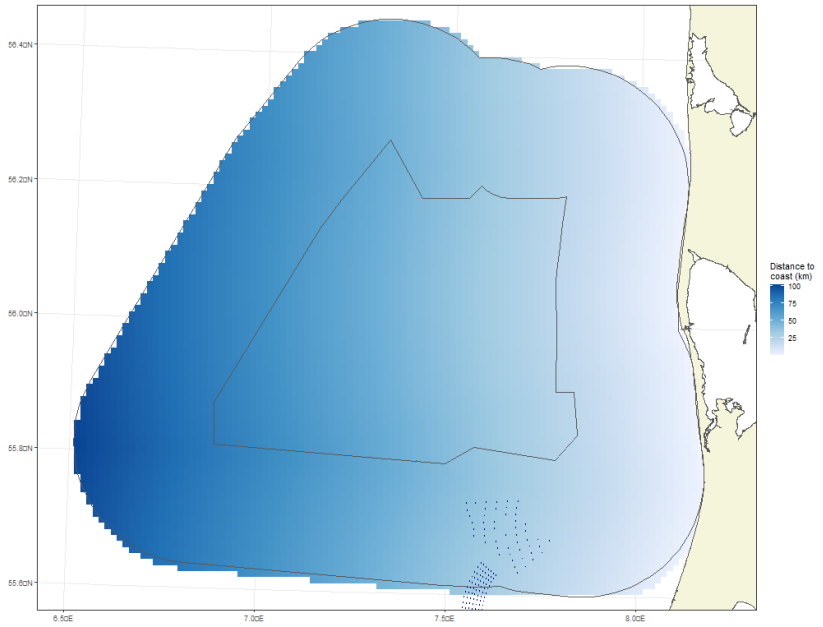

Figure 4.2 Visual representation of distance to the coast (DC).

The response data were collected along survey lines in sequence, and so consecutive observations were likely to be correlated in space and time. With a spatial term included, any resulting temporal auto-correlation in model residuals was accounted for by using robust standard errors as part of the modelling framework. These essentially inflate the standard errors in relation to the positive correlation observed within pre-specified blocks (here, transects) of residuals.

Uncertainty in the outputs was estimated using both the detection model and spatial model in a process called bootstrapping. This involves repeatedly sampling from the parameter distributions of each model and obtaining a new set of predicted abundances across the spatial grid. From this process, we have 500 sets of plausible predictions for every grid cell. These may be used in a variety of ways to estimate uncertainty and answer questions such as "does the spatial distribution vary between two surveys or phases".

All models were fitted using the ***MRSea R*** package (Scott-Hayward, Mackenzie, & Walker, 2023; R Core Team, 2024) and subjected to various diagnostic checks (e.g. assessment of the assumed mean-variance relationship, a key assumption check).

Further methodological details on model specification, fitting, and diagnostics are available in Appendix 2

4.1.3.2 Model specifics

More specifically, the MRSea package uses CReSS-SALSA based spatially adaptive generalized additive models, with targeted flexibility, to allow for non-linear relationships between the one-dimensional and two-dimensional covariates and the response (Scott-Hayward, Mackenzie, Donovan, Walker, & Ashe, 2014; Scott-Hayward, Mackenzie, & Walker, 2023; Walker, Mackenzie, Donovan, & O'Sullivan, 2010). CReSS is a complex-region spatial smoother, whilst SALSA is a Spatially Adaptive Local Smoothing Algorithm both developed to examine animal survey data for signs of changes in animal abundance and distribution following marine renewables development. However the methods are suitable for a wide range of applications.

The 1D smooth terms (for depth or distance to coast) were specified to be either a quadratic (degree 2) *B*-spline (*df* = 3,4,5) or a natural cubic spline (*df* = 2,3,4). In cases where these degrees of freedom boundaries were reached, however, a broader range of parameters were trialled instead. The degrees of freedom for these terms determine the flexibility of these smooth (and nonlinear) relationships - the more degrees of freedom, the more flexible the relationship can be.

The spatial patterns in each analysis were based on a two-dimensional CReSS-based (Complex Region Spatial Smoother) surface using a Gaussian radial basis function (*df* = [2,100]) (Scott-Hayward, Mackenzie, Donovan, Walker, & Ashe, 2014). The flexibility of both the spatial and 1D elements constituted part of the model selection procedure and, for each survey, was determined using SALSA and the BIC measure of fit.

Uncertainty about model parameter estimates proceeded via robust standard errors due to the nature of the survey procedure (consecutive observations are likely to be correlated in space and time). These essentially work by inflating the standard errors (normally obtained under traditional approaches) in relation to the positive correlation observed within pre-specified blocks of residuals. In cases where this residual correlation is minimal, the adjustments are small, and when the correlation is more extreme, the inflation is larger.

A transect-based blocking structure was used to reflect potential correlation within blocks while independence (i.e., no correlation) between blocks was assumed. To ensure this assumption was realistic, the decay of any residual correlation to zero (i.e., independence) with the distance between points (within blocks along transects) was assessed visually. Specifically, transects in each survey were used as the blocking structure.

4.1.3.3 Modelling diagnostics

For all modelling there are assumptions made and the violation of these can lead to spurious results. To assess the adequacy of model fit and assumptions a range of diagnostic measures were used.

1) ACF plot: A blocking structure was used to account for potential residual non-independence for each model and a robust standard error approach was based on unique transects. Figure 4.3 shows an example ACF plot with the temporal correlation within each transect shown in grey and the average in red. The plot shows a mean lag one correlation of approximately 0.25 followed by a reassuring decay to zero. This indicates that the robust standard errors were necessary for this model (no residual correlation is indicated by a lag 1 correlation of near zero) and that the blocking structure is appropriate.

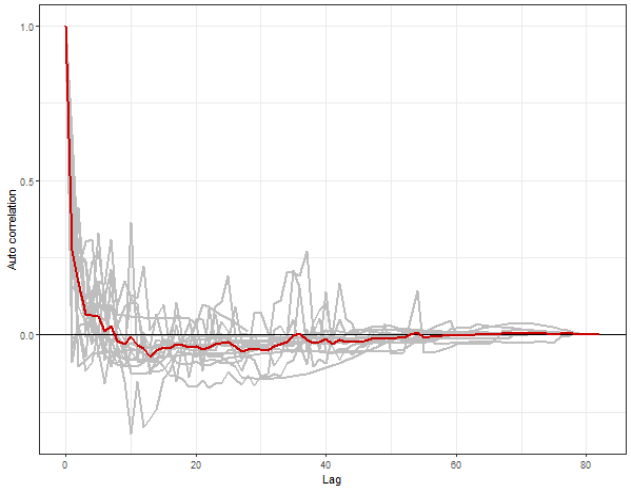

Figure 4.3 Example ACF plot: the grey lines represent the residual correlation observed in each transect and the red line the average of these values across transects.

2) Mean-Variance plot: The assumed mean-variance relationship under the model was assessed visually using plots of the model's fitted values against the residuals' variance. In this analysis, Tweedie models were employed, which assume a nonlinear mean-variance relationship. Figure 4.4 shows an example plot. The observed residual variance is calculated in bins relating to quantiles of the fitted values (hence the irregular spacing). These are plotted as the black dots and agreement between these and the assumed relationship (Tweedie, dotted blue line) indicates the mean-variance assumption is appropriate. As the Quasi-Poisson and Poisson families are special cases of the Tweedie, these are included on the plot for comparison.

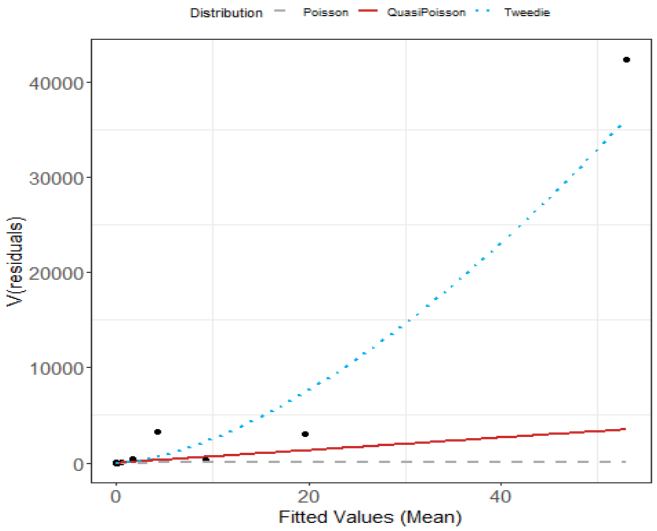

Figure 4.4 Plot showing the estimated Tweedie mean-variance relationship (blue dashed line). The red line shows the $V(\mu)=\phi\mu$ relationship and the grey line the 1:1 relationship. The black dots are the observed residual variances.

3) DHARMa diagnostic plots: QQ plots and residuals against predicted values plots were assessed to ascertain the level of agreement between the data and the model. These plots were created using the DHARMa R package and using simulated residuals. Given these outputs, we would expect that a correctly specified model shows:
    a. a straight 1-1 line, and no compelling evidence against the null hypothesis of a correct overall residual distribution, as indicated by the p-values for the associated tests in the QQ-plot.
    b. visual homogeneity of residuals in both the vertical and horizontal directions, in the residuals against predictor plot.

Figure 4.5 shows examples of these plots

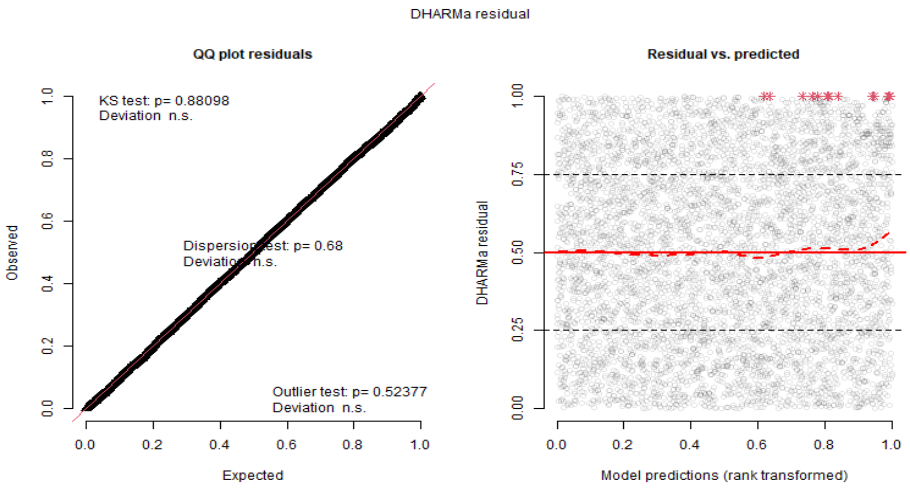

Figure 4.5 Example DHARMa plots: QQplot (left) and residuals against predicted values (right). The red stars are outliers and the red line is a smooth spline around the mean of the residuals

Figure 2 8.

4) Pearson residuals for each model were also spatially visualised to ensure no areas of consistent bias across the survey area. This would be indicated by clusters of negative or positive residuals in spatially similar locations.

4.1.3.4 Model predictions and estimates of uncertainty

Based on each selected model, predictions of counts were made to a grid of points (each point representing a 1 km^2 grid cell) across the survey area. Additionally, abundances within the survey-based prediction region were obtained by summing the grid cell counts across the relevant areas.

The uncertainty in the detection function was reflected using a parametric bootstrap ($\boldsymbol{n = 500}$) of the fitted distance sampling model. This generated new estimated counts for each segment. The selected spatial model was then re-fitted to each of the new datasets to obtain a new set of parameter estimates for the model. The final output of this process was a parametric bootstrap procedure using the robust variance-covariance matrix from each parametric bootstrap model. These were used to calculate 500 sets of model predictions, which generated 95% percentile-based intervals and allowed for calculating a coefficient of variation for each grid cell. If it was impossible to fit a spatial model to the data, the abundance estimates for the survey were calculated from the distance analysis parametric bootstraps.

4.1.3.5 Additional Outputs

A calculation of 'persistence' was also undertaken across surveys using the geo-referenced estimates of density (abundance/associated area) across the survey area. Distributional persistence allows the reader to get a measure of intra/inter-annual variability across multiple surveys. For example, there may be areas of consistent usage, despite survey-to-survey variability, which can provide context to the ability to detect post-construction changes. Persistence scores were calculated for every grid cell in the following way. Each bootstrap replicate was allocated a binary value based on whether or not the estimate in each location was above the mean estimated density (1) throughout the survey area or below this mean estimated density (0). This was performed for all 500 sets of plausible predictions in each grid cell (based on the bootstrap replicates), and the proportion of these bootstrap predictions above the mean (indicated by the value of 1) was calculated for each grid cell to give a persistence score for that location. The scores range

between 0 and 1, where 1 indicates that the density in that grid cell was estimated to be above average in every bootstrap replicate in every survey (so uniformly above the mean; high persistence/consistent usage), while a value of 0.1 indicates that just 10% of the estimates were above the estimated mean, and thus indicates low persistence in that location. A zero would result from the density in every survey and every bootstrap being below average.

4.2 Ship-based surveys

4.2.1 Flight altitude

For flight altitude analyses, rangefinder measurements were preferred over observer estimates. However, flight altitude estimates were used when rangefinder data was unavailable or produced negative values (e.g. if birds flew between waves).

Flight altitudes were divided into 25 m interval bands from 0 to 250 m, and the number of altitude recordings and individuals occurring in each interval was analysed. These analyses were done for each species individually. However, related species, such as passerines, were sometimes grouped to improve sample size or when they were difficult to distinguish in the field. Furthermore, the analyses were limited to species or species groups with ten or more flight altitude recordings.

Since some individuals and flocks had multiple flight altitude measurements, these repeated measures were not considered independent. Instead, the mean flight altitude for each observation ID with multiple measurements was used.

4.2.2 Species composition

The species ratios were calculated for those species groups that were difficult to identify during aerial surveys. These groups included divers, gulls (excluding black-headed gulls and black-legged kittiwakes), terns, and auks (common guillemots, black guillemots and razorbills). The ratios were based on the number of individuals observed and were calculated for each of the eight surveys. They included all types of observations at all observation positions.

4.2.3 Vertical radar analysis

4.2.3.1 Annotation

Labels from both annotators for the October 2023 session were compared to quantify the subjectivity of the annotation process. The average level of agreement between annotators on the presence of a given bird was 89.7%. Therefore, a computer vision model is not expected to achieve higher than 90% accuracy.

4.2.3.2 Computer vision pipeline

A computer vision (CV) algorithm was designed to work towards a more efficient method to generate labels of putative (i.e. supposed, assumed) birds while accounting for the shifting horizon of ship-borne radar systems. While computer vision encompasses some machine learning tools, it was chosen not to use machine learning at this stage for two reasons. Firstly, there is insufficient training data to highlight the exact angle of the horizon when an image is recorded, and there were very few bird labels available in the early stages of the project. Secondly, training machine learning models requires not only large amounts of data but also time and computational resources, which were not available given the time pressure of the project.

The CV algorithm primarily uses the 'opencv2' Python package and comprises four stages: 1) scan area detection, 2) foreground segmentation, 3) horizon detection, 4) bad weather and noise detection and 5) bird filtering. These are described in detail in Appendix 3.

4.2.3.3 Training

The CV algorithm was trained using a training subset of 5,617 birds annotated by one observer (RDN) in all images from 8 October 2023, which was the busiest day of the survey in terms of bird traffic. These birds represented 42.8% of the total number of birds annotated across all other survey days and 23.4% of the total number of birds annotated by both observers combined.

The CV algorithm had ten trainable parameters, further explained in Appendix 3. Sensible initial values were selected for each parameter (Table 4.3), which were then optimised using a simple hill-climbing algorithm. This was essentially an iterative univariate search, whereby parameters were varied in turn across a specified range of between five and twenty values until a local optimum was found.

Table 4.3 Trainable parameters in the computer vision algorithm, including initial and end values (i.e. values post-training).

Parameter	Initial value	End value
Foreground hue	30	42
Foreground hue range	5	20
Minimum saturation	60	0
Minimum horizon strength	20	28
Minimum radial artefact strength	20	18
Horizon buffer angle	4	0
Min area	5	0
Max area	600	740
Min distance	50	100
Min l/w ratio	5	8

4.2.3.4 Evaluation

The optimum CV algorithm was determined based on a balance between precision, i.e. the proportion of correct predictions, and recall, i.e. the proportion of annotated birds correctly predicted. The metric used to optimise the algorithm is F1 accuracy, which was already 79.1% with the initial parameter values. The algorithm was trained across four sessions, each taking over 12 hours, shifting the specified ranges of parameters when they were limiting the search space. The result was an algorithm with 88% F1 accuracy within the training subset, with a lower accuracy expected outside the training subset.

4.2.3.5 Prediction

The CV algorithm was used to make predictions across June, August, September, October and December 2023, which were the months where images had the appropriate resolution (2400×1900). While February 2024 had the appropriate resolution (Table 3.3), technical issues led to background colour changes, which made running the model inappropriate. Therefore, data from the manual annotation was used.

Predictions were post-processed to correct bird positions considering the shifting horizon, remove areas of the radar sweep which frequently presented artefacts, and exclude periods of bad weather. First, the distances and angles of birds relative to the radar sensor were determined based on the pixel locations of birds and the parameters of the scan area ellipse. Angles were corrected, assuming the shifted horizon angles represent a flat horizon in real space. Real positions and distances of birds in meters were then calculated based on the parameters of the scan area ellipse. Subsequently, predictions within 5° of the horizons were excluded because the rolling of the boat often presented artefacts in this range. Furthermore, following quality checks from annotators, we excluded the 15-45° range for August and October 2023 and the range 0-90° for December due to the high prevalence of radial artefacts. Finally,

predictions during "noisy" hours were excluded, where the mean noise and weather indicator was above one and one hour on either side.

The number of birds per hour (= 30 radar sweeps) is presented for temporal analyses. However, to analyse bird numbers in space, the depth of the scan at different distances from the sensor is accounted for to produce comparable measurements of bird density at 50×50 m resolution. When analysing the effect of altitude on bird density, a generalised additive model was used to account for the effects of distance from the radar sensor on the detectability of birds (accounting for the fact that birds very close to or very far from the sensor cannot be detected properly). The algorithm was fitted with the 'gam' function in the 'mgcv' package in R using a Tweedie error distribution.

5. Survey results

5.1 Aerial surveys

A total of 7 species groups and 28 species of birds were observed from the eight aerial surveys in the North Sea I area between April 2023 and March 2024 (Table 5.1).

Table 5.1 The bird species or species groups observed from aerial surveys in the study area during eight surveys between April 2023 and March 2024. The number of observed individuals per species or species group is indicated. The numbers thus is not an estimation of total abundances of birds. The total number of each species or group observed is shown.

Species	Total	2023-04-30	2023-07-07	2023-09-09	2023-11-11	2023-12-14	2024-02-08	2024-02-25	2024-03-21
Diver sp.	163	14			3	2	9		135
Red-throated diver	423	39	2	7	8	56	48	40	223
Black-throated diver	1						1		
White-billed diver	1	1							
Red-necked grebe	1					1			
Northern fulmar	205	3	167	10	7	1	4	3	10
Manx shearwater	1		1						
Northern gannet	623	36	29	173		2		11	372
Great cormorant	47		40	1		1	2	1	2
Eurasian teal	12	5							7
Common goldeneye	12								12
Common eider	28			1	10		1	14	2
Common scoter	17,245	2,509	1,115	1,857	4,066	882	1,126	5,410	280
Velvet scooter	13	1			11			1	
Red-breasted merganser	8								8
Sanderling	17			17					
Wader sp.	3			3					
Great skua	1			1					

Species	Total	2023-04-30	2023-07-07	2023-09-09	2023-11-11	2023-12-14	2024-02-08	2024-02-25	2024-03-21
Arctic skua	2			2					
Skua sp.	1							1	
Common gull	478	3	6	13	9	275	7	28	137
European herring gull	2,136	14	1'381	136	84	235	29	108	149
Lesser black-backed gull	323	2	263	38	1				19
Great black-backed gull	95	12	28	16	1	9	5	12	12
Black-headed gull	30	1	3	2				21	3
Little gull	56	10		1	3	2	3	21	16
Black-legged kit-tiwake	887	54	4	2	157	276	54	124	216
Gull sp.	617	6	51	11	14	477	53	4	1
Arctic tern	5			5					
Arctic/common tern	590	580	10						
Sandwich tern	17	9	6	1					1
Tern sp.	153	150		3					
Razorbill	148				14	76	4	8	46
Raorbill/common guillemot	2,290	100	55	29	112	320	148	240	1,286
Common guil-lemot	682	46	56	38	27	41	21	95	358

It was possible to model detection functions and spatial distribution for red-throated/black-throated divers, northern gannet, black-legged kittiwake, and razorbill/common guillemot. To model a detection function there needs to be a minimum number of observations, which was the case for these species and species groups. The following chapters present the results of the data collected on bird abundances and distributions for selected species or species groups.

5.1.1 Divers (Gaviidae)

Three species of divers were observed during the eight surveys: red-throated, black-throated, and white-billed diver. The most frequently observed diver was the red-throated diver, with 423 birds recorded. The two other species were only recorded on a single occasion. Divers are difficult to identify during aerial surveys, and 163 birds could not be identified as species (Table 5.1). Divers were recorded during all aerial surveys. Most birds were recorded in March and April. In July and September, only a few divers were recorded (Figure 5.1). There were 389 records of divers across the eight surveys. The average flock size was 1.5, and the maximum flock size was 18 birds.

Divers were primarily recorded in the eastern parts of the study area and were recorded less frequently in the central and western parts of the area (Figure 5.2). In April 2023, divers were observed more widespread in the study area. This is a time close to migration towards the breeding grounds, which might explain the difference in distribution.

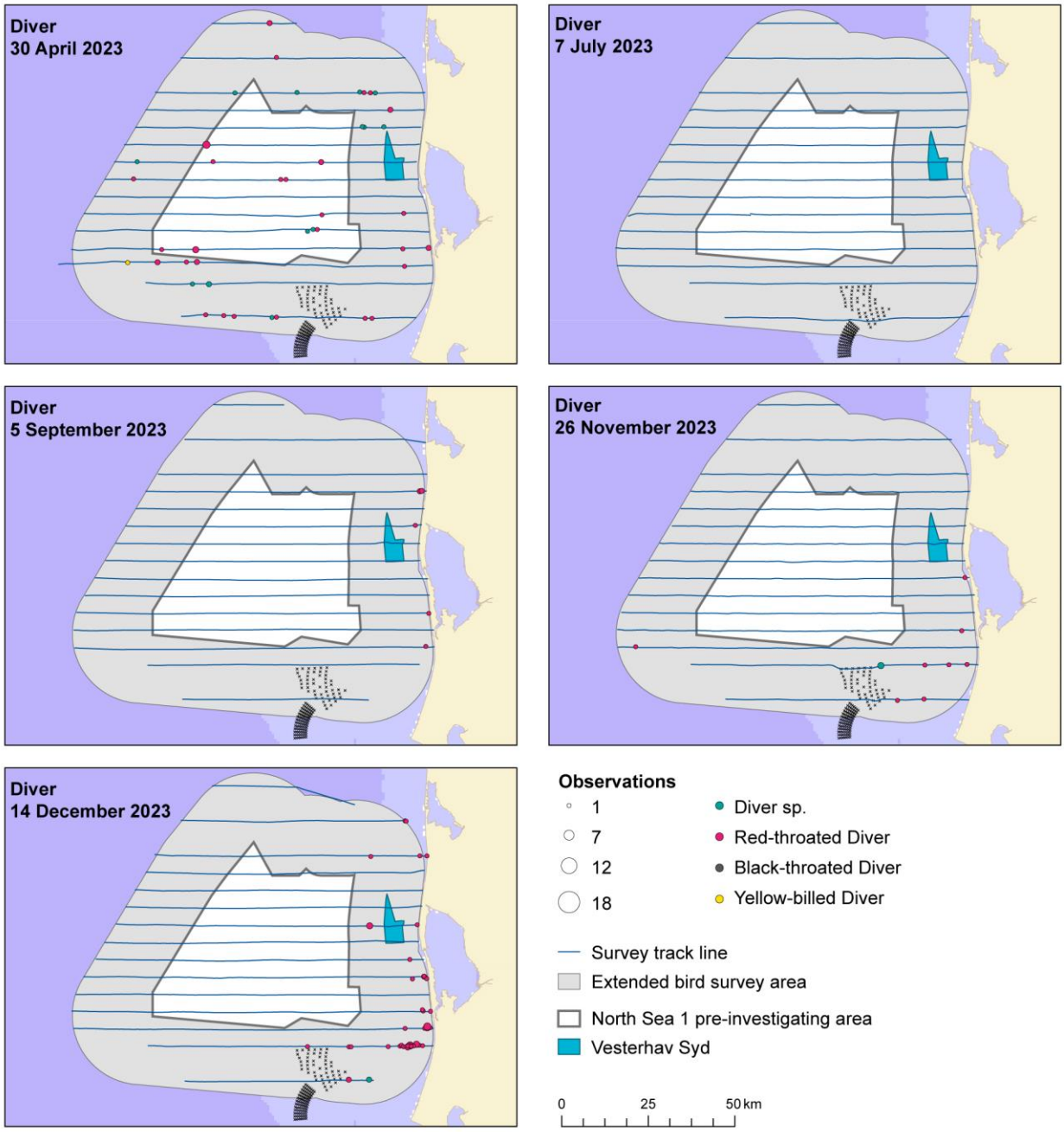

Figure 5.1 The numbers and distribution of divers observed during five surveys in 2023 in the North Sea I survey area.

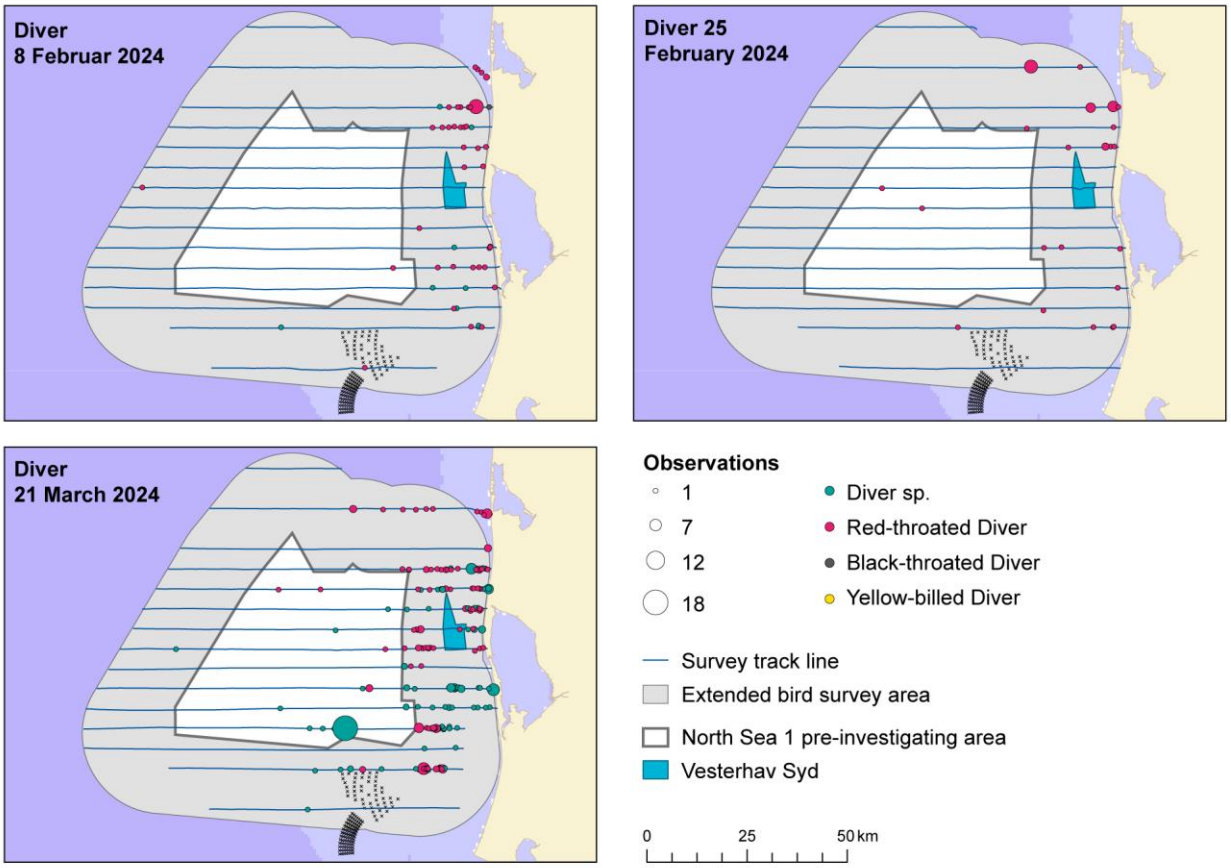

Figure 5.2. The numbers and distribution of divers observed during three surveys in 2024 in the North Sea I survey area.

5.1.1.1 Distance analysis

The average probability of sighting divers was estimated to be 0.23 (CoV = 0.04). This probability was estimated using a half-normal detection function, and no covariates were selected (Figure 5.3).

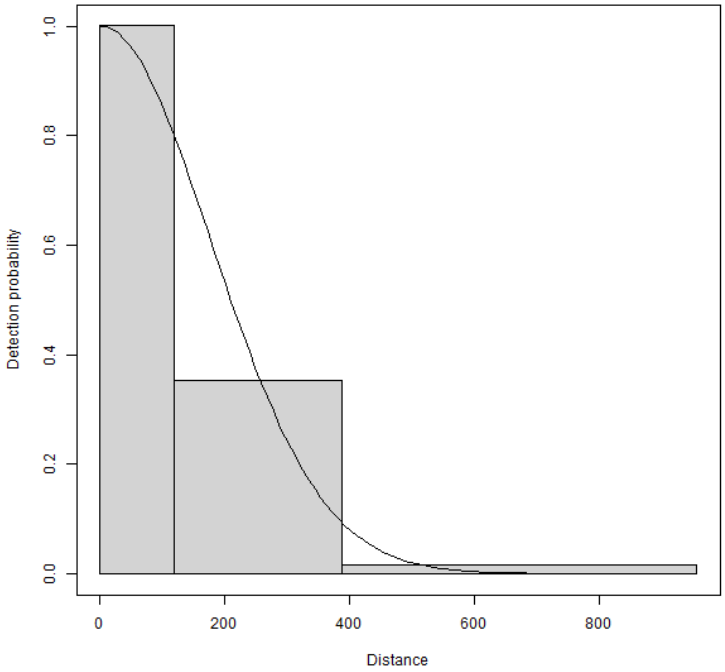

Figure 5.3 Figure showing the estimated detection function. The histogram represents the distances of the observed sightings.

5.1.1.2 Spatial analysis

Figure 5.4 shows the distribution of the distance corrected counts for each of the eight surveys.

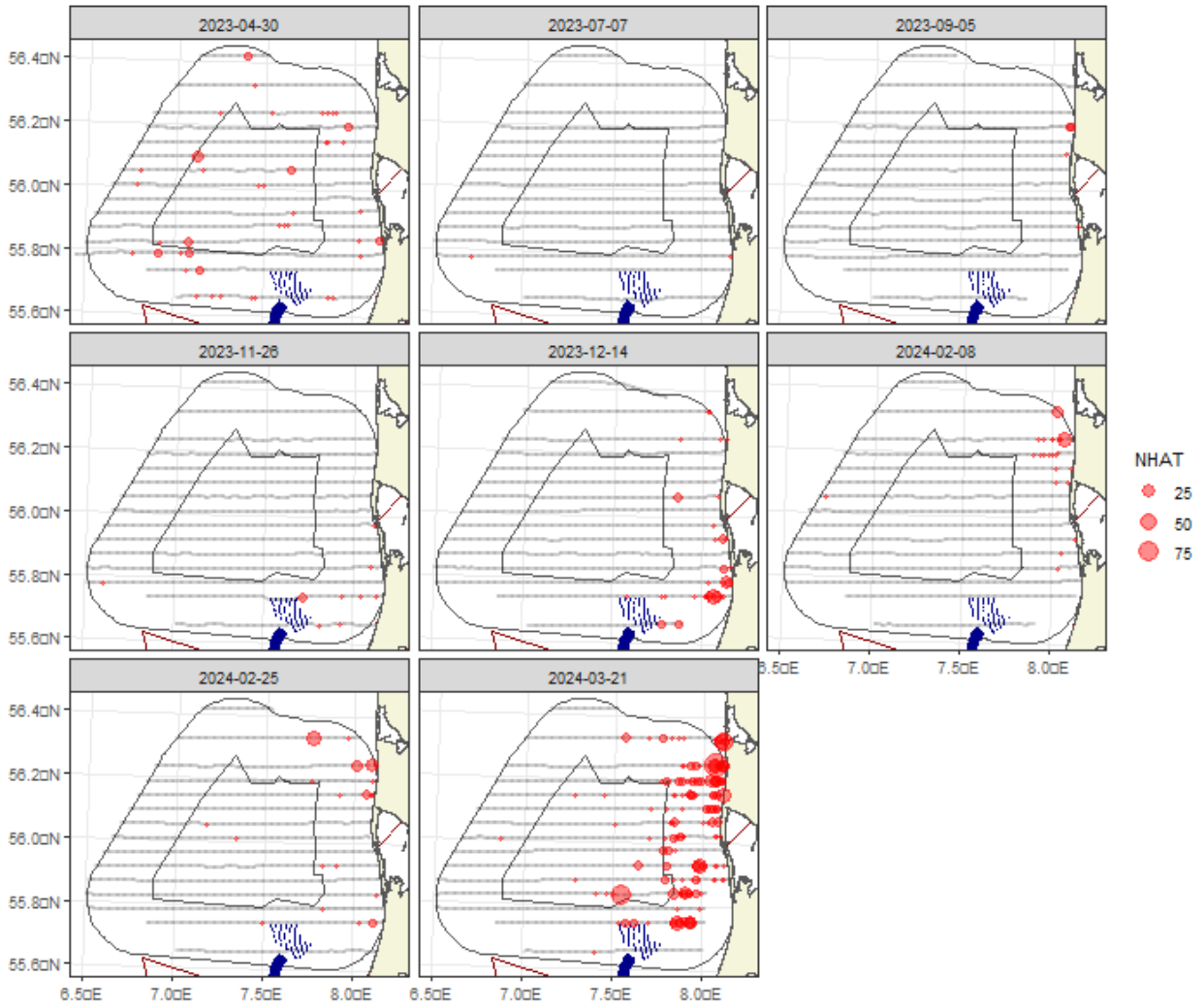

Figure 5.4 Distance-corrected counts for divers across the eight surveys. The red circles indicate the distance-corrected counts along the transect lines. The grey dots are segments with a count of zero.

5.1.1.3 Model selection

There was not enough data for two of the eight surveys to fit a spatial model, namely the July and September surveys in 2023 (Table 5.2). The models selected in the remaining six surveys included a spatial term (of varying complexity). The depth covariate was not selected for any models, while the distance to coast covariate was selected as a linear term for one. This shows there was compelling evidence for non-uniform spatial patterns in most surveys, but given these spatial patterns, there was little to no evidence of depth or distance to the coast relationships. The spatial surfaces selected ranged from four to 11 parameters for the spatial term (Table 5.2).

Table 5.2 Model selection results for divers for each survey. The model column represents the terms in the model.

Name	Model	Distribution	Variable 1D	Variable 2D	Number of parameters	Dispersion parameter	Tweedie parameter
2023-04-30	2D Only	quasipoisson	NA	s(x,y, df=7)	8	7.2	NA
2023-07-07	No Model	NA	NA	NA	NA	NA	NA
2023-09-05	No Model	NA	NA	NA	NA	NA	NA

Name	Model	Distribution	Variable 1D	Variable 2D	Number of parameters	Dispersion parameter	Tweedie parameter
2023-11-26	2D Only	quasipoisson	NA	s(x,y, df=3)	4	0.9	NA
2023-12-14	2D Only	quasipoisson	NA	s(x,y, df=10)	11	5.0	NA
2024-02-08	2D Only	quasipoisson	NA	s(x,y, df=10)	11	0.6	NA
2024-02-25	2D Only	Tweedie	NA	s(x,y, df=7)	8	13.3	1.26
2024-03-21	Best 1D2D	Tweedie	distcoast, df=1	s(x,y, df=2)	4	42.2	1.22

The estimated abundances, densities and associated 95% confidence intervals for each month are given in Table 5.3 and Figure 5.5. There was not enough data to fit a spatial model for the July and September surveys in 2023, so the abundance estimates were calculated using the Horvitz-Thompson method (H-T). The estimated total abundance in the survey area reached 31 to 7,548 individuals, which equals a density of 0.0 to 1.0 birds/km^2. The highest abundances were observed in winter and early spring (Table 5.3 and Figure 5.5).

Table 5.3 Estimated abundance and density of divers for each survey. The 95% CI is a percentile-based confidence interval.

Month	Area (km^2)	Estimator type	Estimated count	95% CI count	Estimated density	95% CI density
2023-04-30	7833	Spatial	1289	(653, 2722)	0.2	(0.1, 0.3)
2023-07-07	7833	H-T	31	(29, 34)	0.0	(0, 0)
2023-09-05	7833	H-T	89	(83, 97)	0.0	(0, 0)
2023-11-26	7833	Spatial	209	(90, 543)	0.0	(0, 0.1)
2023-12-14	7833	Spatial	936	(431, 3526)	0.1	(0.1, 0.5)
2024-02-08	7833	Spatial	1921	(798, 5407)	0.2	(0.1, 0.7)
2024-02-25	7833	Spatial	776	(367, 1895)	0.1	(0, 0.2)
2024-03-21	7833	Spatial	7548	(4797, 12752)	1.0	(0.6, 1.6)

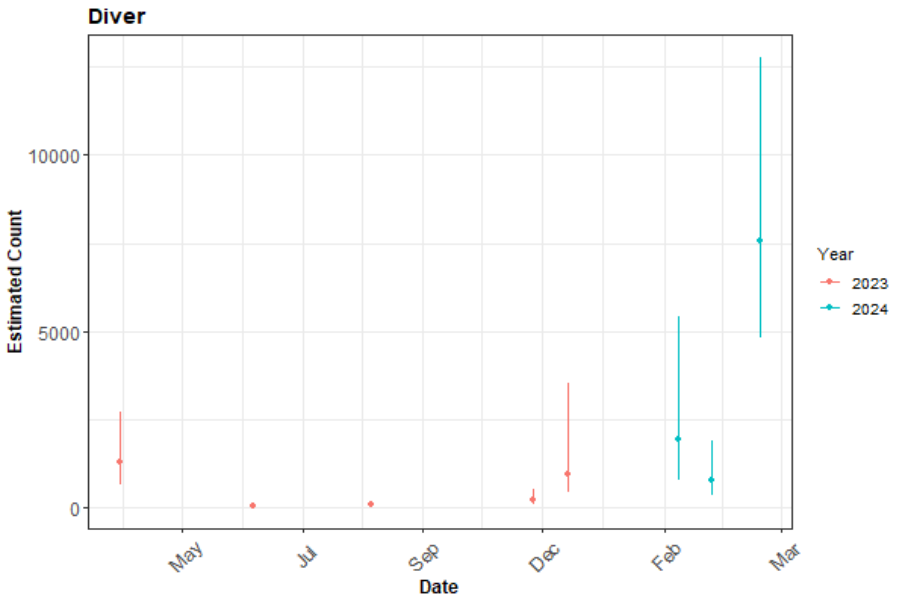

Figure 5.5 The estimated count of divers for each survey. The 95% CI is a percentile-based confidence interval and is from a parametric bootstrap with 500 replicates.

5.1.1.4 *Spatial results*

Figure 5.6 shows the estimated counts of divers in each 1 km^2 grid cell for each month. Generally, the estimated abundances fitted well with the raw data, and there were no notable misalignments. In areas where the estimated counts were systematically higher, the abundances were also relatively high, and there were no areas with large estimated abundances unsupported by the data.

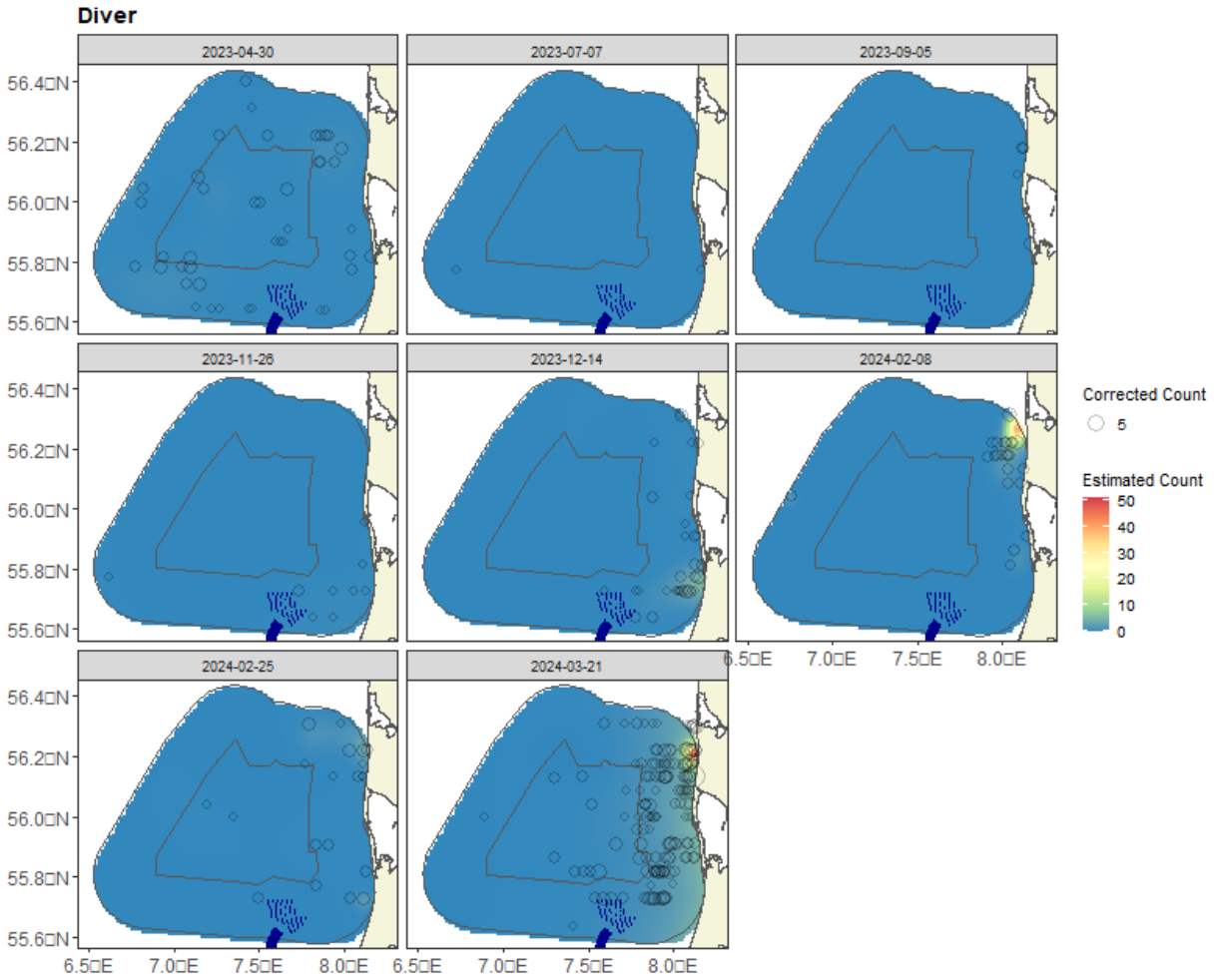

Figure 5.6 Figure showing the estimated diver abundance across the study site for each of the surveys. The estimated counts are per 1 km x 1 km grid cell. The open circles show the corrected counts.

5.1.1.5 *Uncertainty in spatial predictions*

Broadly, the highest coefficient of variation (CoV) scores were associated with the `almost zero' predictions, and it is known that the CoV metric is highly sensitive to any uncertainty for very small predictions. There was one larger value for the eastern side of the survey area for one of the surveys that was otherwise absent of data. There was no material overlap between high values of the CoV metric and the transect lines/locations with non-zero counts, resulting in no concerns in this case (Figure 5.7).

For cases when the very small predicted values were excluded (Figure 5.8), the CoV for all surveys was almost <1.5 and so there was no material concern. Those areas that remain with high CoVs were also areas with very low abundance, so again, of little concern.

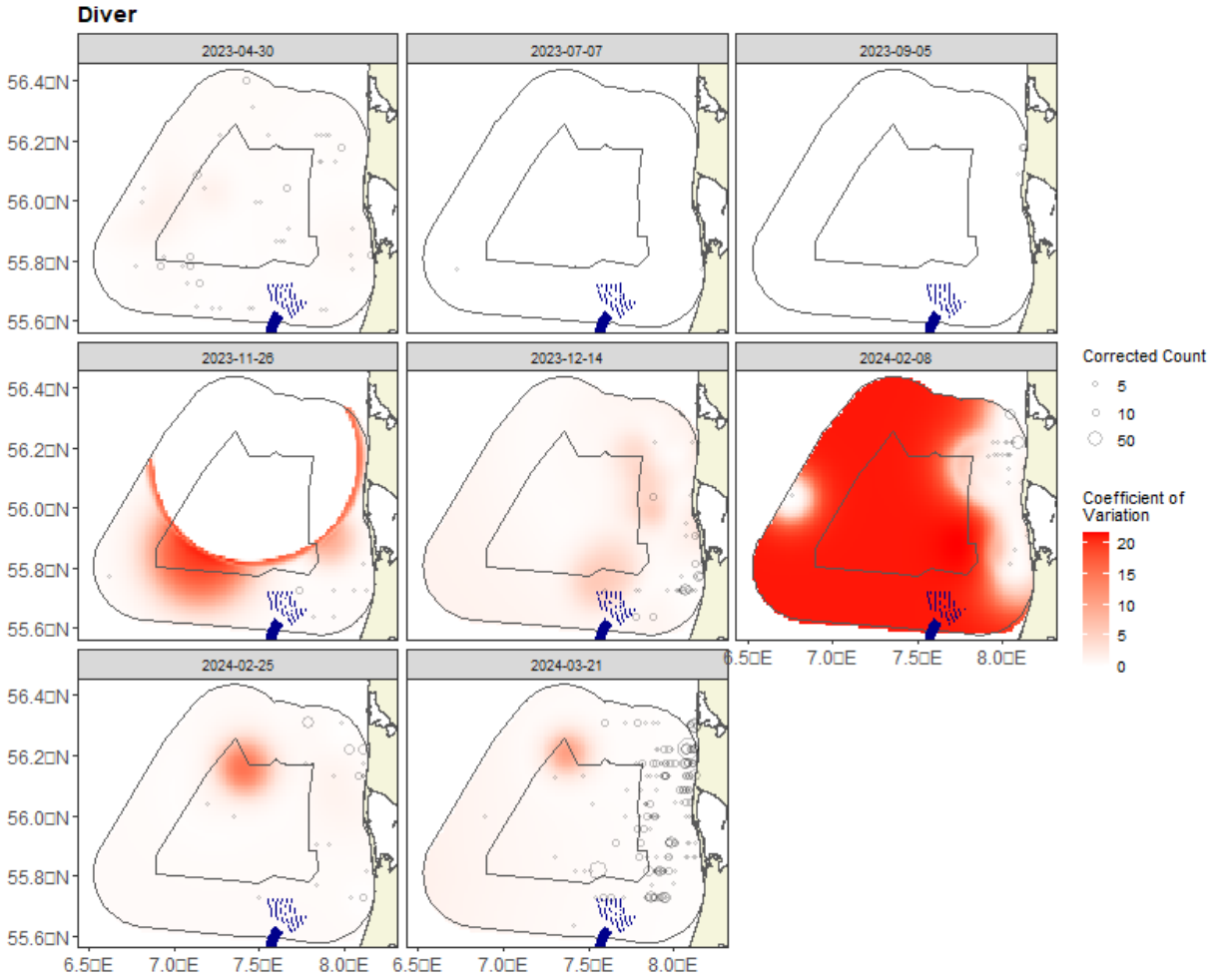

Figure 5.7 Figure showing the coefficient of variation (CoV) across the study region for each survey. The open circles show the distance corrected counts. The presence of dark red CoV scores in areas with virtually zero predictions is an artefact of the very small prediction rather than any notable concern.

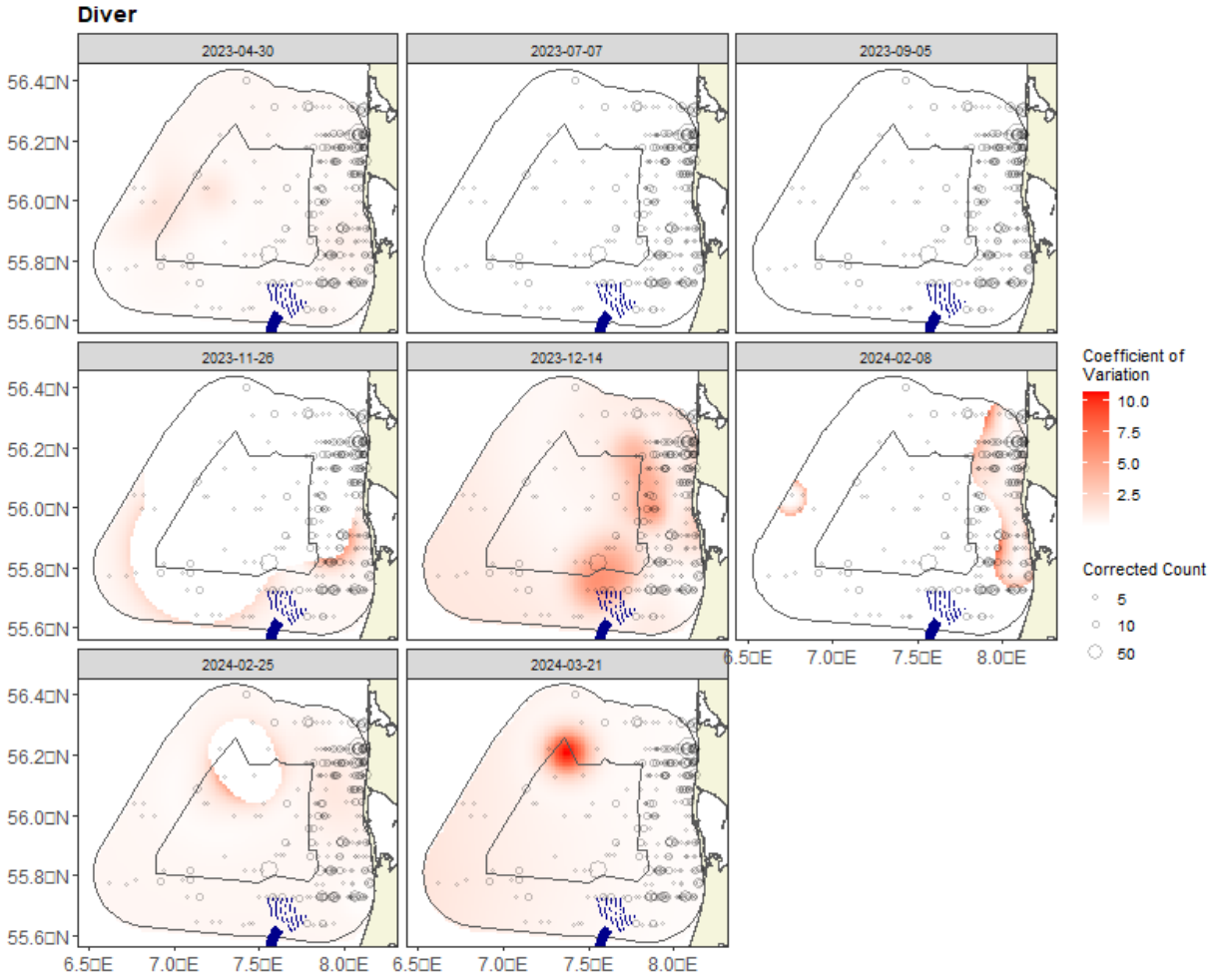

Figure 5.8 Figure showing the coefficient of variation (CoV) for all cells above a density of 0.001. The open circles show the distance corrected counts. The presence of dark red CoV scores in areas with virtually zero predictions is an artefact of the very small prediction rather than any notable concern.

5.1.1.6 Model diagnostics

A blocking structure was used to account for potential residual non-independence for each model, and a robust standard error approach was based on unique transects. In each case, a reassuring decay to zero was seen (indicated by the red and grey lines in Figure 5.9), implying that an appropriate blocking structure was used.

The assumed mean-variance relationship was examined, and agreement was generally shown between the assumed (red) lines and the observed values. Figure 5.10 and Figure 5.11 show example relationships for a quasi-Poisson and Tweedie model. Figure 5.12 shows an example of a diagnostics QQ plot.

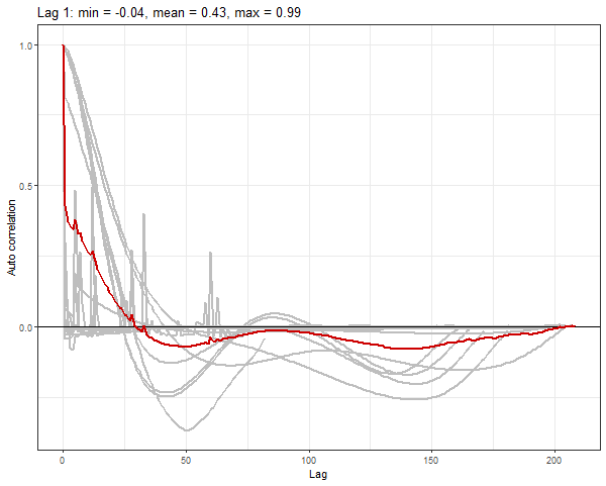

Figure 5.9 Example diagnostics. The grey lines represent the residual correlation observed in each transect, and the red line is the average of these values across transects.

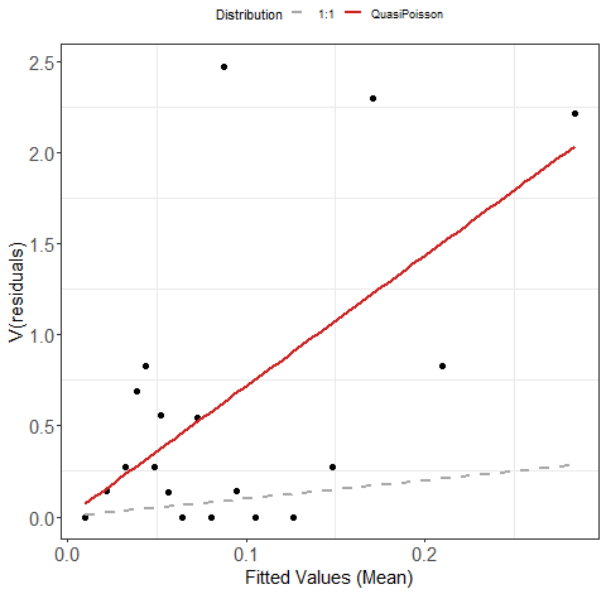

Figure 5.10 Example diagnostics. The plot shows the estimated quasi-Poisson mean-variance relationship (red line) and actual (black dots). The black dots are based on 20 quantiles of the model residuals, and for reference, the grey dashed line shows the 1:1 relationship.

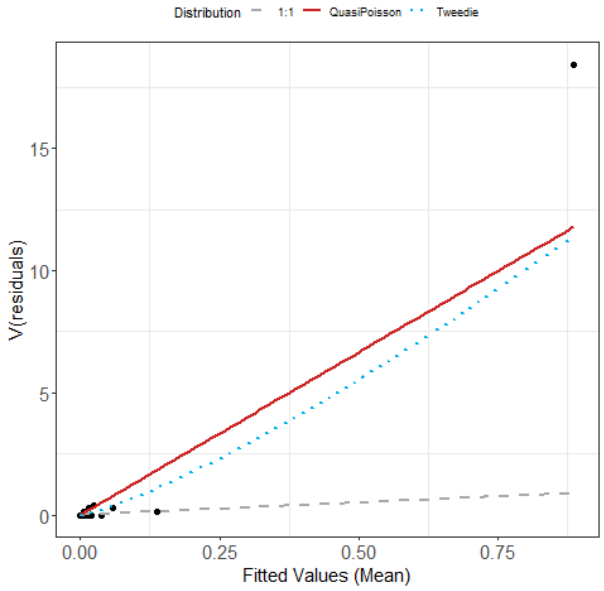

Figure 5.11 Example plot showing the estimated Tweedie mean-variance relationship (blue dashed line). The red line shows the $V(\mu)=\phi\mu$ relationship, and the grey line shows the 1:1 relationship.

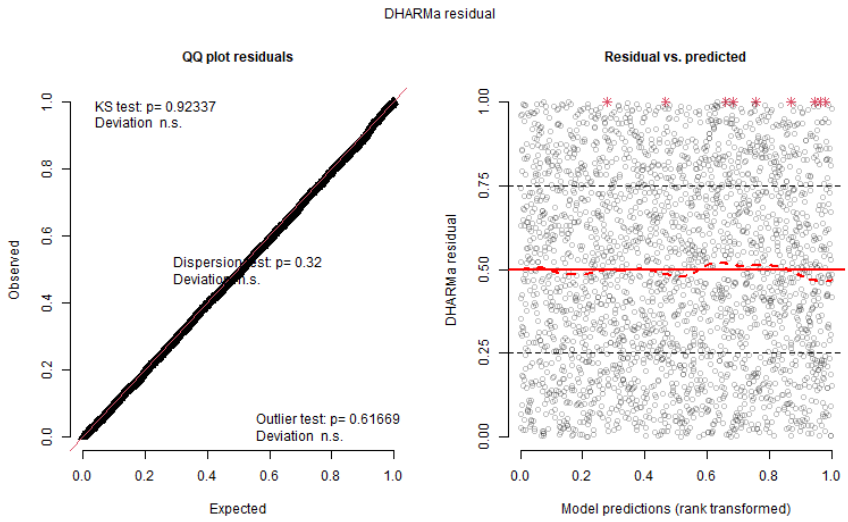

Figure 5.12 Example diagnostics. QQplot (left) and residuals against predicted values (right). The red stars are outliers, and the red line is a smooth spline around the mean of the residuals.

5.1.1.7 Areas of persistence

Across the eight surveys, there is generally moderate persistence across the survey area (Figure 5.13). The highest persistence (~ 60%) occurs in the northeastern part of the survey area along the coastline. The plot shows that when divers are present during these surveys, they are mainly in the eastern parts of the survey area.

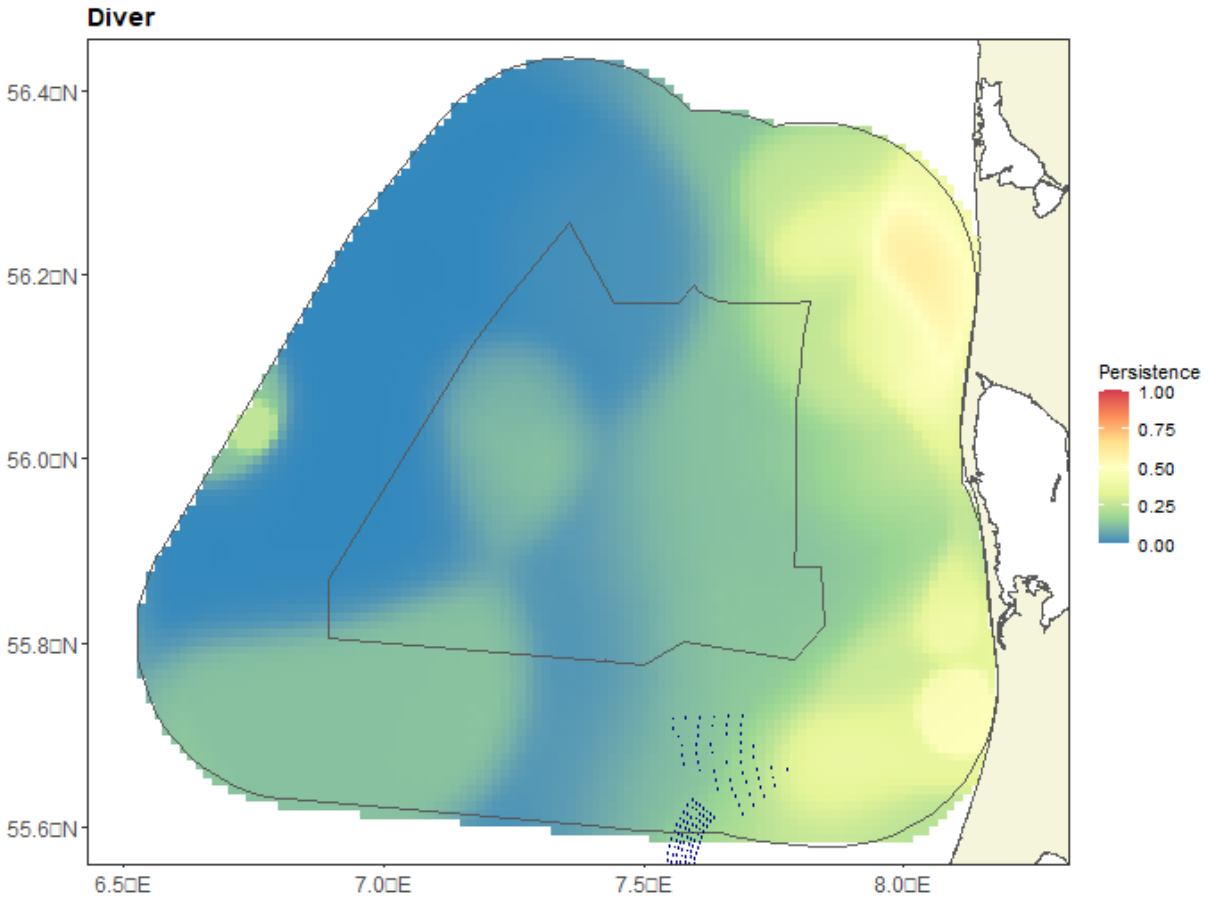

Figure 5.13 Persistence scores for divers across the eight surveys. The polygon represents the pre-investigation area (black line).

5.1.2 Northern fulmar (*Fulmarus glacialis*)

Northern fulmars were recorded in relatively low numbers in the survey area. In total, 205 individuals were recorded. The majority of these were recorded in July 2023 (167 birds). Across the remaining surveys, a maximum of 10 birds were observed per survey (Table 5.1). There were 98 records of northern fulmars across the eight surveys. The average flock size was 2.1, and the maximum flock size was 100 birds.

The northern fulmars were mainly recorded in the western parts of the survey area, although in July 2023 and February 2024, few birds were recorded in the central parts of the survey area (Figure 5.14 and Figure 5.15). The northern fulmar data did not allow for the estimation of total abundances and distribution due to the low number of observations.

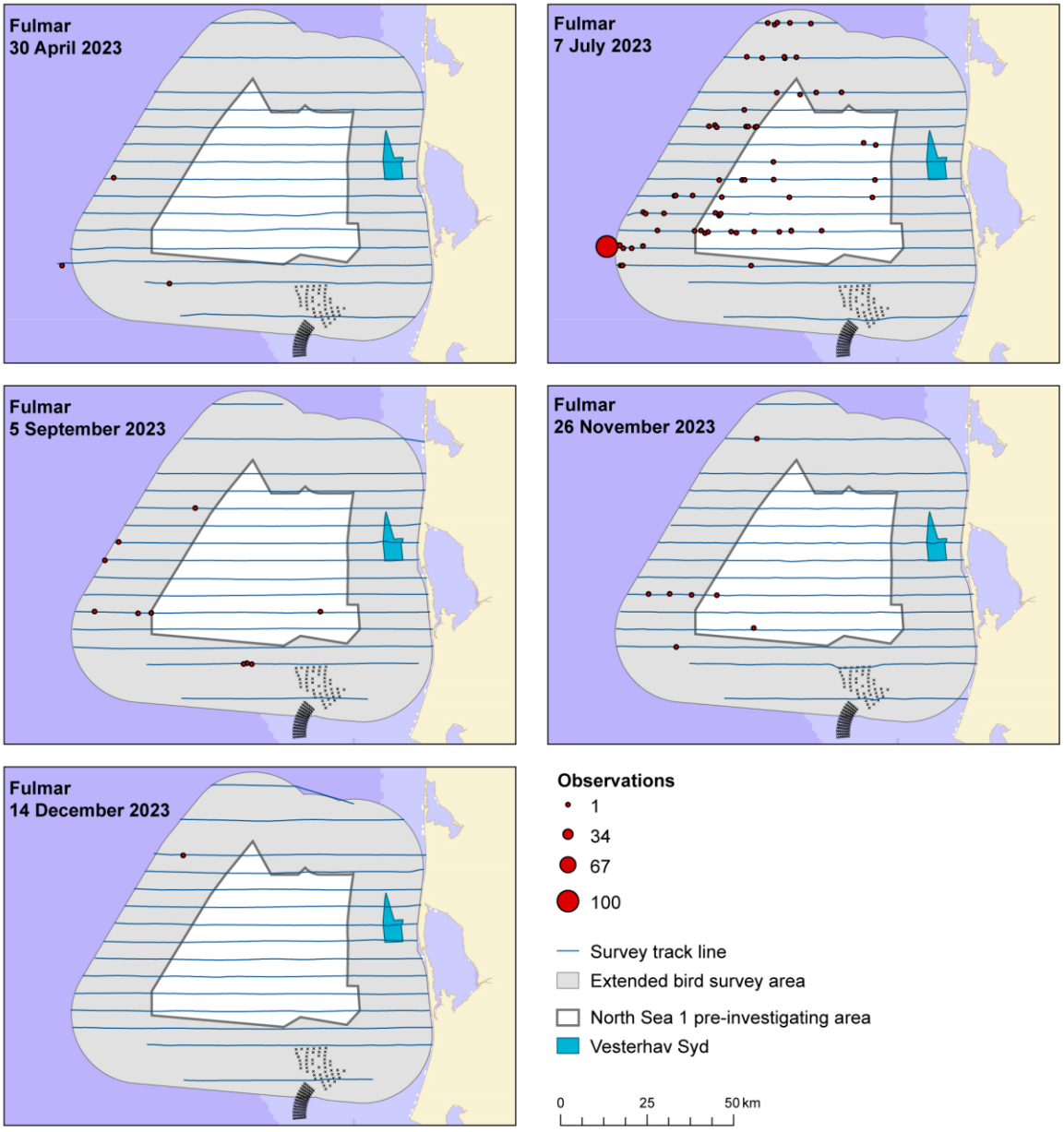

Figure 5.14 The numbers and distribution of northern fulmars observed during five surveys in 2023 in the North Sea I survey area.

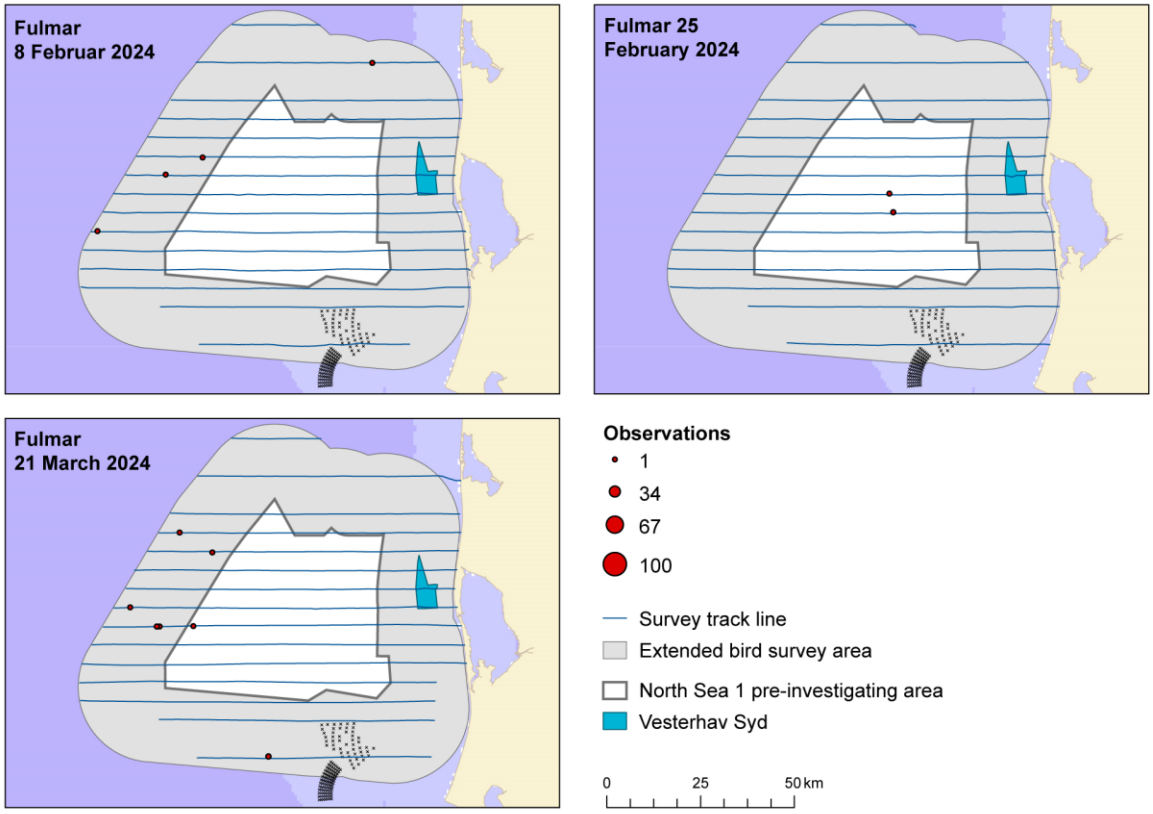

Figure 5.15. The numbers and distribution of northern fulmars observed during three surveys in 2024 in the North Sea I survey area.

5.1.3 Northern gannet (*Morus bassanus*)

Northern gannets were recorded during most surveys in the area. A total of 623 birds were encountered, most of which were seen in March 2024 (372 birds) and September 2023 (173 birds). During the November 2023 and the early February 2024 surveys, no northern gannets were recorded (Table 5.1).

Northern gannets were seen throughout the survey area (Figure 5.16 and Figure 5.17). There were 369 records of northern gannets across the eight surveys. The average flock size was 1.7, and the maximum flock size was 40 birds.

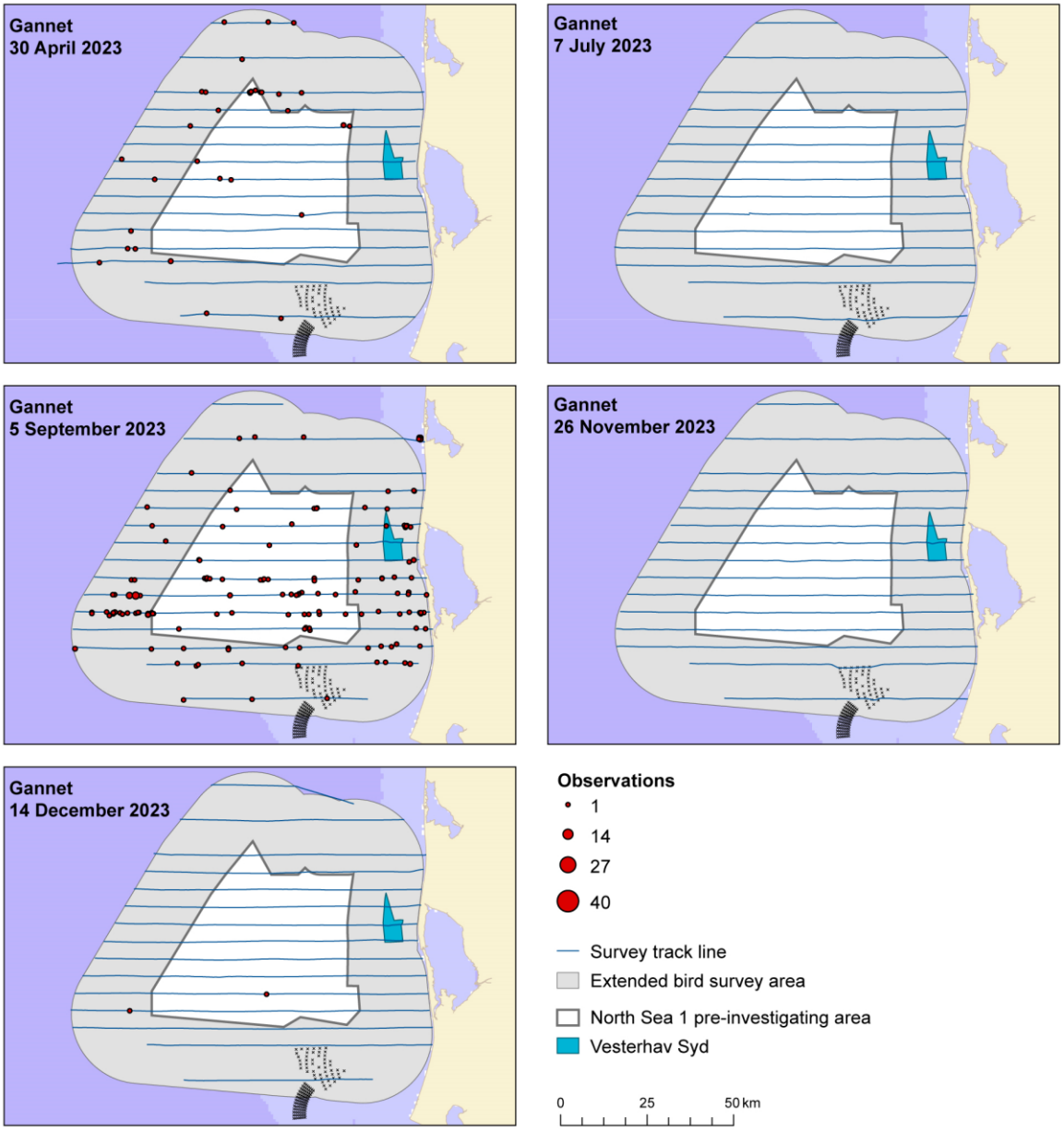

Figure 5.16 The numbers and distribution of northern gannets observed during five surveys in 2023 in the North Sea I survey area.

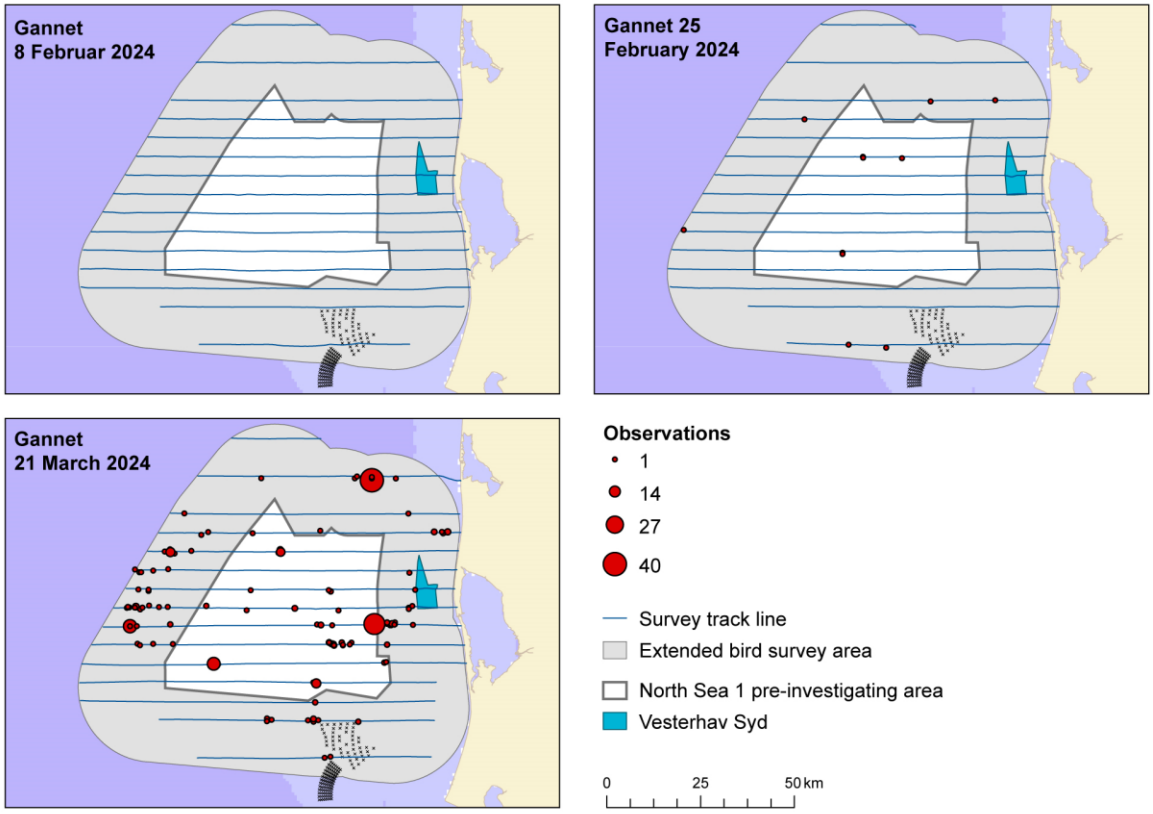

Figure 5.17 The numbers and distribution of northern gannets observed during five surveys in 2024 in the North Sea I survey area.

5.1.3.1 Distance analysis

The average probability of sighting a northern gannet was estimated to be 0.31 (CoV = 0.04). This probability was estimated using a half-normal detection function with group size as a covariate (Figure 5.18). The probability of detection of larger groups is slightly higher for all distance bands.

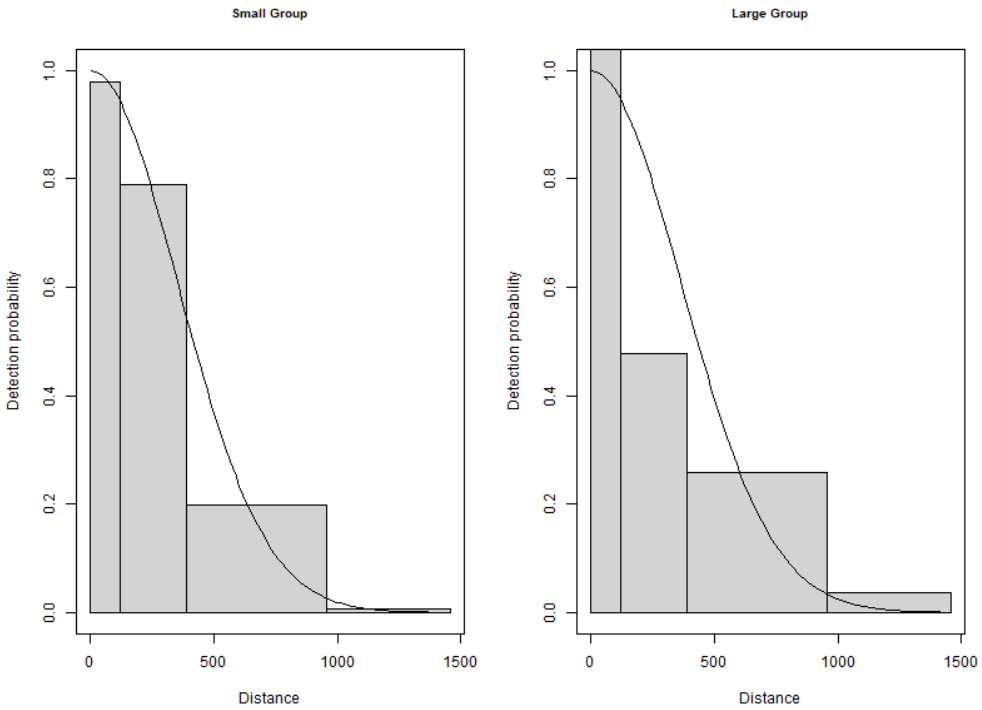

Figure 5.18 Figure showing the estimated detection function for a small and large group. The histogram represents the distances of the observed sightings.

5.1.3.2 Spatial analysis

Figure 5.19 shows the distribution of the distance corrected counts for each of the two months of surveys.

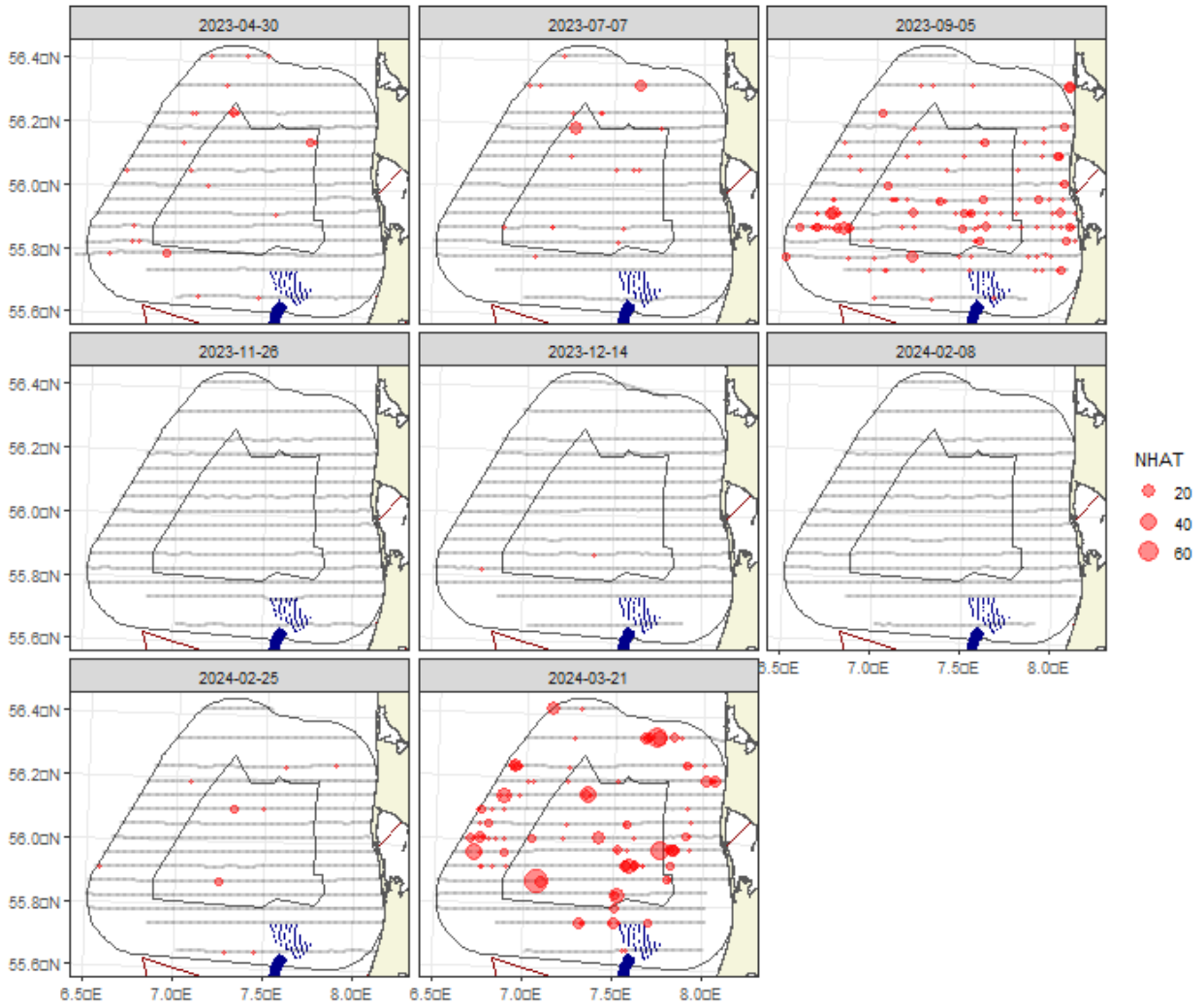

Figure 5.19 Distance-corrected counts for the northern gannet across the eight surveys. The red circles indicate the distance-corrected counts along the transect lines. The grey dots are segments with a count of zero.

5.1.3.3 Model selection

There was insufficient data for three of the eight surveys to fit spatial models, namely the November and December 2023 and the February 2024 surveys (Table 5.4). For the other five surveys, the models included a spatial term (of varying complexity). Neither the depth nor distance to the coast covariates (either as a linear or smooth term) were selected for any surveys. This shows compelling evidence for non-uniform spatial patterns in each survey, but given these spatial patterns, there was no evidence of depth or distance to the coast relationships. The spatial surfaces selected ranged from two to eight parameters for the spatial term (Table 5.4).

Table 5.4 Model selection results for northern gannet for each survey. The model column represents the terms in the model.

Name	Model	Distribution	Variable 1D	Variable 2D	Number of parameters	Dispersion parameter	Tweedie parameter
2023-04-30	2D only	quasipoisson	NA	s(x,y, df=4)	5	5.0	NA
2023-07-07	2D only	quasipoisson	NA	s(x,y, df=2)	3	5.2	NA
2023-09-05	2D only	quasipoisson	NA	s(x,y, df=8)	9	6.3	NA

Name	Model	Distribution	Variable 1D	Variable 2D	Number of parameters	Dispersion parameter	Tweedie parameter
2023-11-26	No model	NA	NA	NA	NA	NA	NA
2023-12-14	No model	NA	NA	NA	NA	NA	NA
2024-02-08	No model	NA	NA	NA	NA	NA	NA
2024-02-25	2D only	quasipoisson	NA	s(x,y, df=2)	3	2.9	NA
2024-03-21	2D only	quasipoisson	NA	s(x,y, df=2)	3	24.8	1.42

The estimated abundances, densities and associated 95% confidence intervals for each survey are given in Table 5.5 and Figure 5.20There was not enough data to fit a spatial model for the November and December 2023 and the first February 2024 surveys, so the abundance estimates were calculated using the Horvitz-Thompson method (H-T).

During the eight surveys, total numbers were estimated to be between 0 and 2,642 individuals. Highest numbers were estimated for March 2024 and September 2023, respectively. This corresponds to densities between 0 and 0.3 birds/km^2 (Table 5.5).

Table 5.5 Estimated abundance and density of northern gannet for each survey. The 95% CI is a percentile-based confidence interval.

Month	Area (km^2)	Estimator type	Estimated count	95% CI count	Estimated density	95 % CI density
2023-04-30	7,833	Spatial	332	(147, 890)	0.0	(0, 0.1)
2023-07-07	7,833	Spatial	221	(97, 556)	0.0	(0, 0.1)
2023-09-05	7,833	Spatial	1,137	(601, 2,271)	0.1	(0.1, 0.3)
2023-11-26	7,833	H-T	0	(0, 0)	0.0	(0, 0)
2023-12-14	7,833	H-T	15	(14, 16)	0.0	(0, 0)
2024-02-08	7,833	H-T	0	(0, 0)	0.0	(0, 0)
2024-02-25	7,833	Spatial	124	(47, 329)	0.0	(0, 0)
2024-03-21	7,833	Spatial	2,642	(1,713, 4,439)	0.3	(0.2, 0.6)

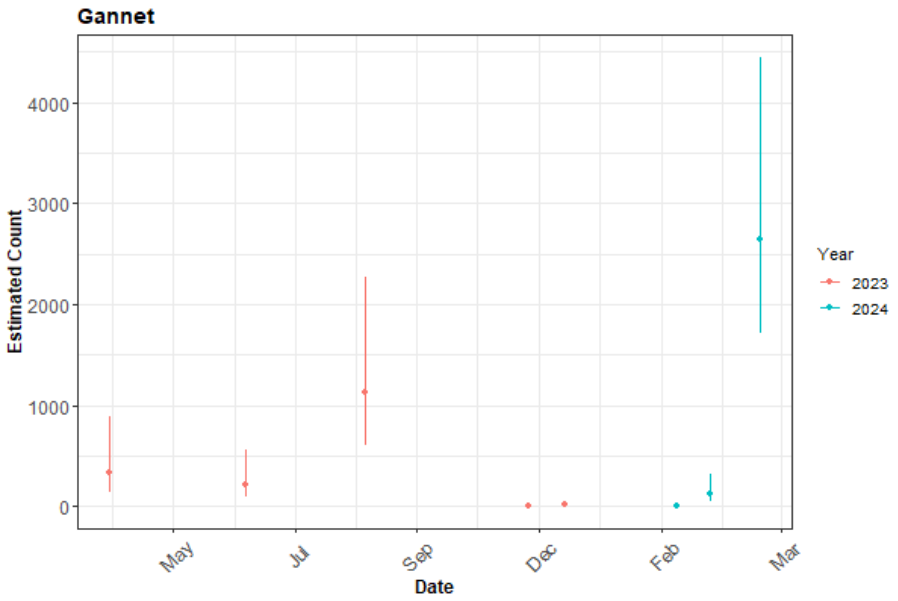

Figure 5.20 The estimated count of northern gannet for each survey. The 95% CI are percentile-based confidence intervals are from a parametric bootstrap with 500 replicates.

5.1.3.4 Spatial results

Figure 5.21 shows the estimated counts of northern gannets in each 1 km^2 grid cell for each of the eight surveys. Generally, the estimated abundances fit well with the raw data, and there were no notable misalignments. In areas where the estimated counts were systematically higher, the abundances were also relatively high, and there were no areas with large estimated abundances unsupported by the data.

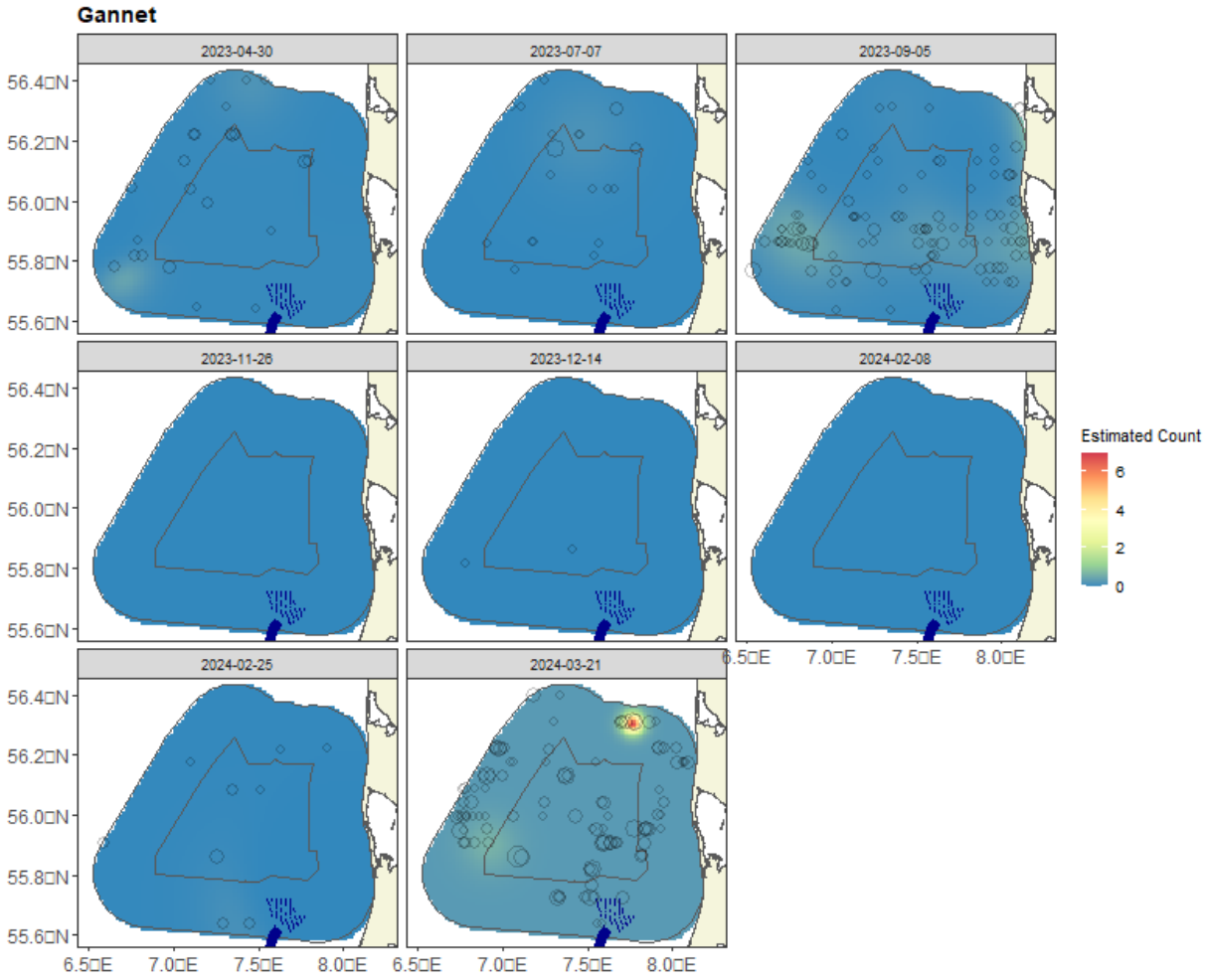

Figure 5.21 Figure showing the estimated northern gannet abundance across the study site for each survey. The estimated counts are per 1 km x 1 km grid cell. The open circles show the observed corrected count. The coloured graphics represent the predicted counts in each location.

5.1.3.5 Uncertainty in spatial predictions

Broadly, the highest coefficient of variation (CoV) scores were associated with the `almost zero' predictions, and it is known that the CoV metric is highly sensitive to any uncertainty for very small predictions. There was one larger value in the centre of the survey area on 30-07-2022, but that was otherwise absent from the data. There was no material overlap between high values of the CoV metric and the transect lines/locations with non-zero counts, resulting in no concerns in this case (Figure 5.22).

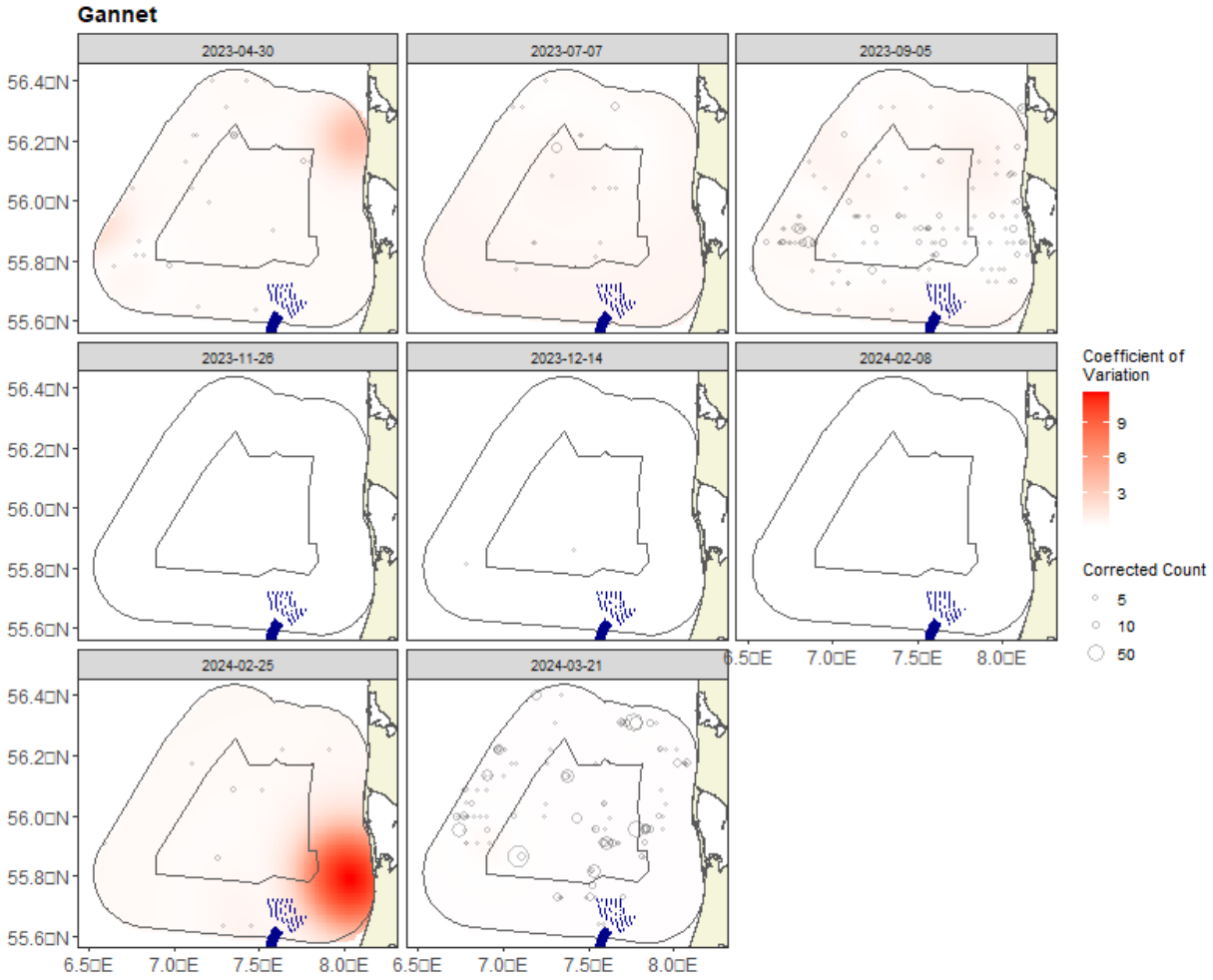

Figure 5.22 Figure showing the coefficient of variation across the study region for each survey. The open circles show the distance corrected counts, where applicable, and the polygons represent the pre-investigation area (black line). The presence of dark red CoV scores in areas with virtually zero predictions is an artefact of the very small prediction rather than of any notable concern.

For the case when the very small predicted values were excluded (Figure 5.23), the CoV for most surveys was <1, and so was of no material concern. For one survey, there remained some high uncertainty around very small values, which play a role in the related confidence intervals for the abundances (Table 5.5 and Figure 5.20).

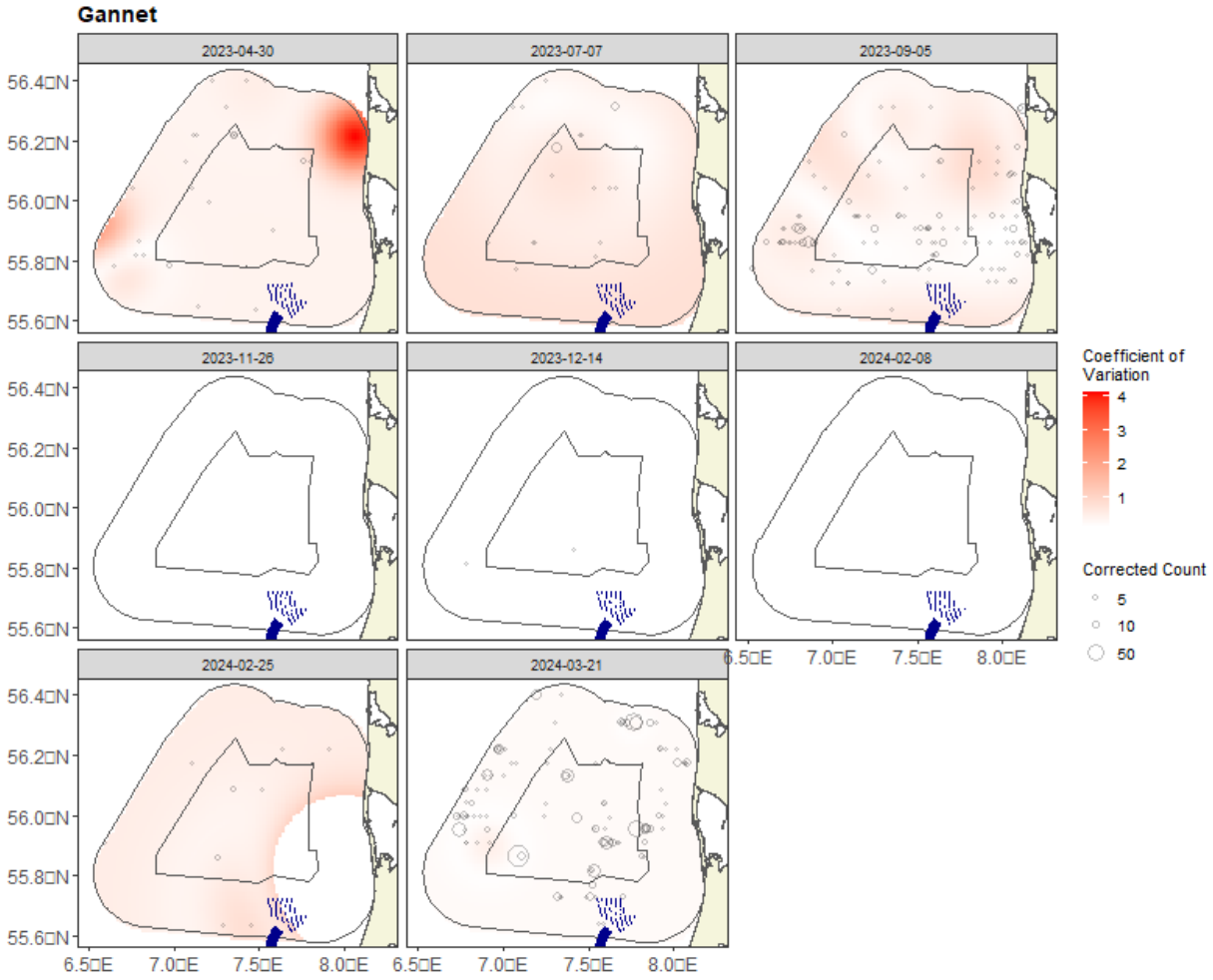

Figure 5.23 Figure showing the coefficient of variation for all cells above the 25% quantile of predicted values. The open circles show the distance corrected counts, where applicable, and the polygons represent the pre-investigation area (black line). The presence of dark red CoV scores in areas with virtually zero predictions is an artefact of the very small prediction rather than any notable concern.

5.1.3.6 Model diagnostics

A blocking structure was used to account for potential residual non-independence for each model, and a robust standard error approach was based on unique transects. In each case, a reassuring decay to zero was seen (indicated by the red and grey lines in Figure 5.24), implying that an appropriate blocking structure was used.

The assumed mean-variance relationship was examined, and agreement was generally shown between the assumed (red) lines and the observed values. Figure 5.25 shows example relationships for a quasi-Poisson model. No models used a Tweedie mixing parameter greater than 1.

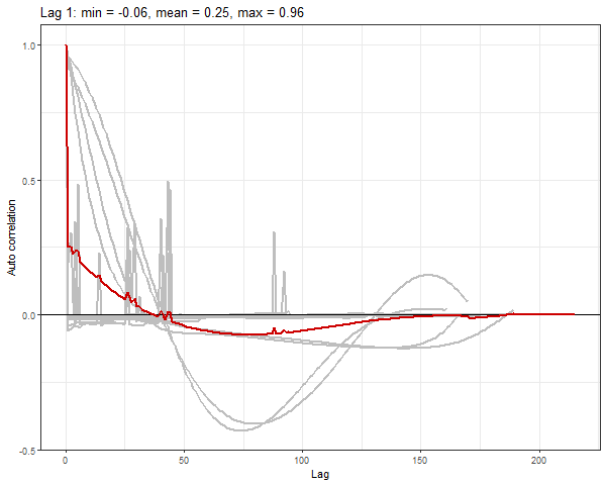

Figure 5.24 Example ACF plot. The grey lines represent the residual correlation observed in each transect, and the red line is the average of these values across transects.

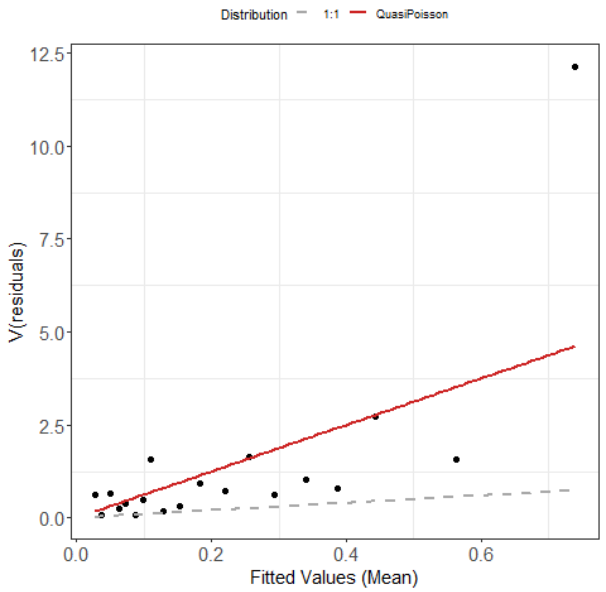

Figure 5.25 Example plot showing the estimated quasi-Poisson mean-variance relationship (red line) and actual (black dots). The black dots are based on 20 quantiles of the model residuals, and for reference, the grey dashed line shows the 1:1 relationship.

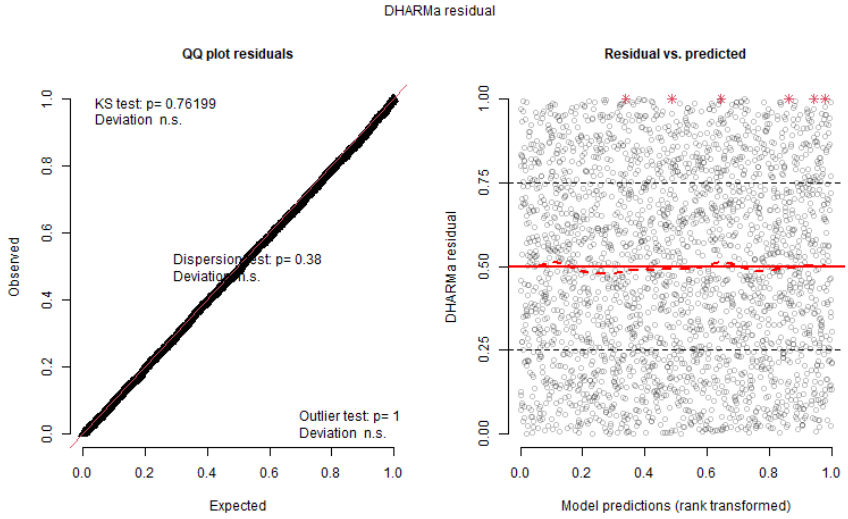

Figure 5.26 Example diagnostics. QQplot (left) and residuals against predicted values (right). The red stars are outliers and the red line is a smooth spline around the mean of the residuals.

5.1.3.7 Areas of persistance

Across the eight surveys, there is moderate to low persistence (Figure 5.27). This shows that northern gannets do not consistently use specific regions of the survey area but use the whole area more generally.

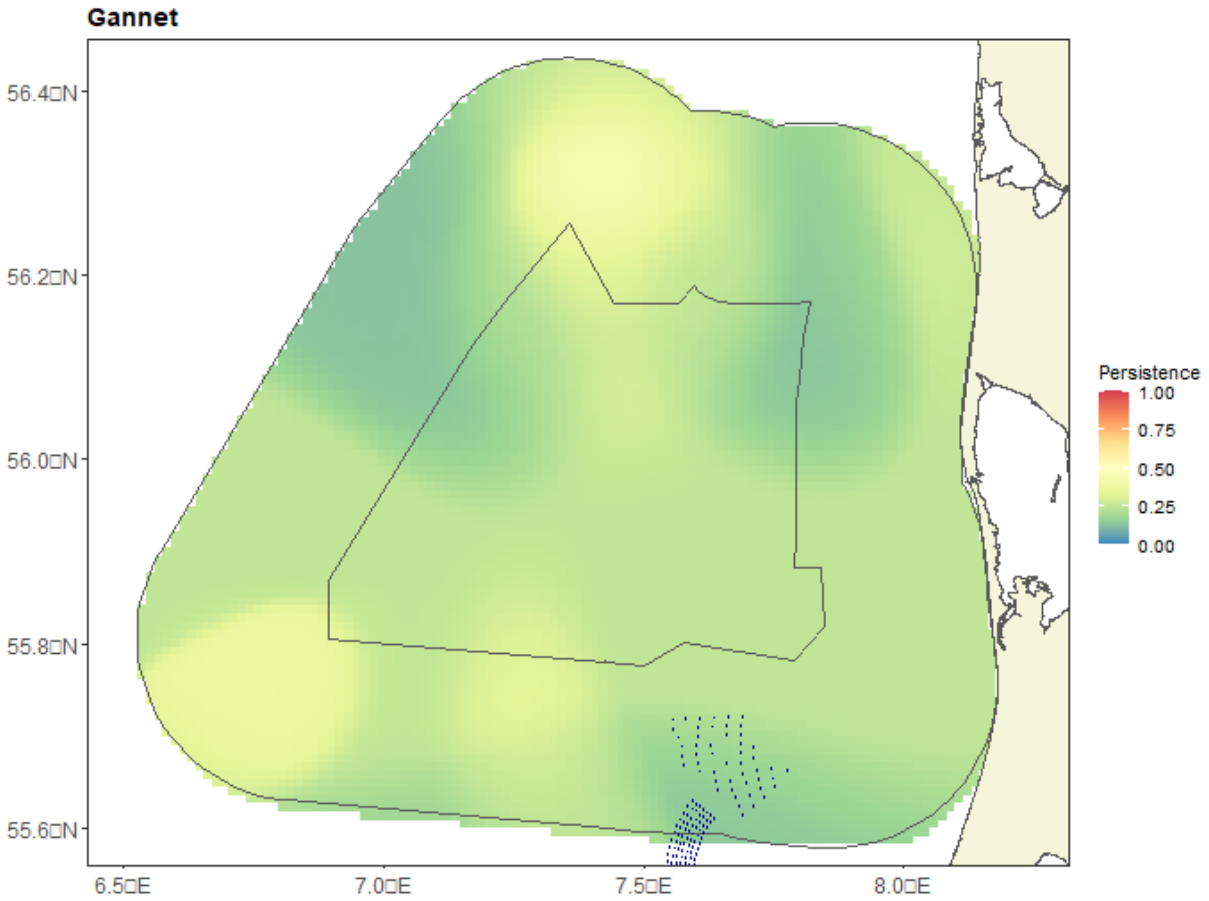

Figure 5.27 Persistence scores across the eight surveys. The polygon represents the pre-investigation area (black line).

5.1.4 Common scoter (*Melanitta nigra*)

Common scoters were recorded in the survey area during all eight surveys. A total of 17,245 birds were counted. The highest numbers during a single survey were 5,410 birds on 25 February 2024. The lowest number was 280 birds, recorded in March 2024. The surveys in April and November 2023 both recorded numbers of common scoters above 2,000 individuals (Table 5.1).

The common soters were almost entirely recorded in the eastern and coastal parts of the survey area and at Horns Rev, with a water depth of less than 25 m. Few observations were recorded of offshore birds. These represent flying individuals (Figure 5.28 and Figure 5.29).

No attempt has been made to estimate the total abundances and spatial distribution of common scoters from this data. The species was recorded in a very clumped distribution and with few observations per survey, which challenges the analysis. Across the 407 records of common scoters, the mean flock size was 42.4 birds, and the maximum flock size was 1,100 individuals.

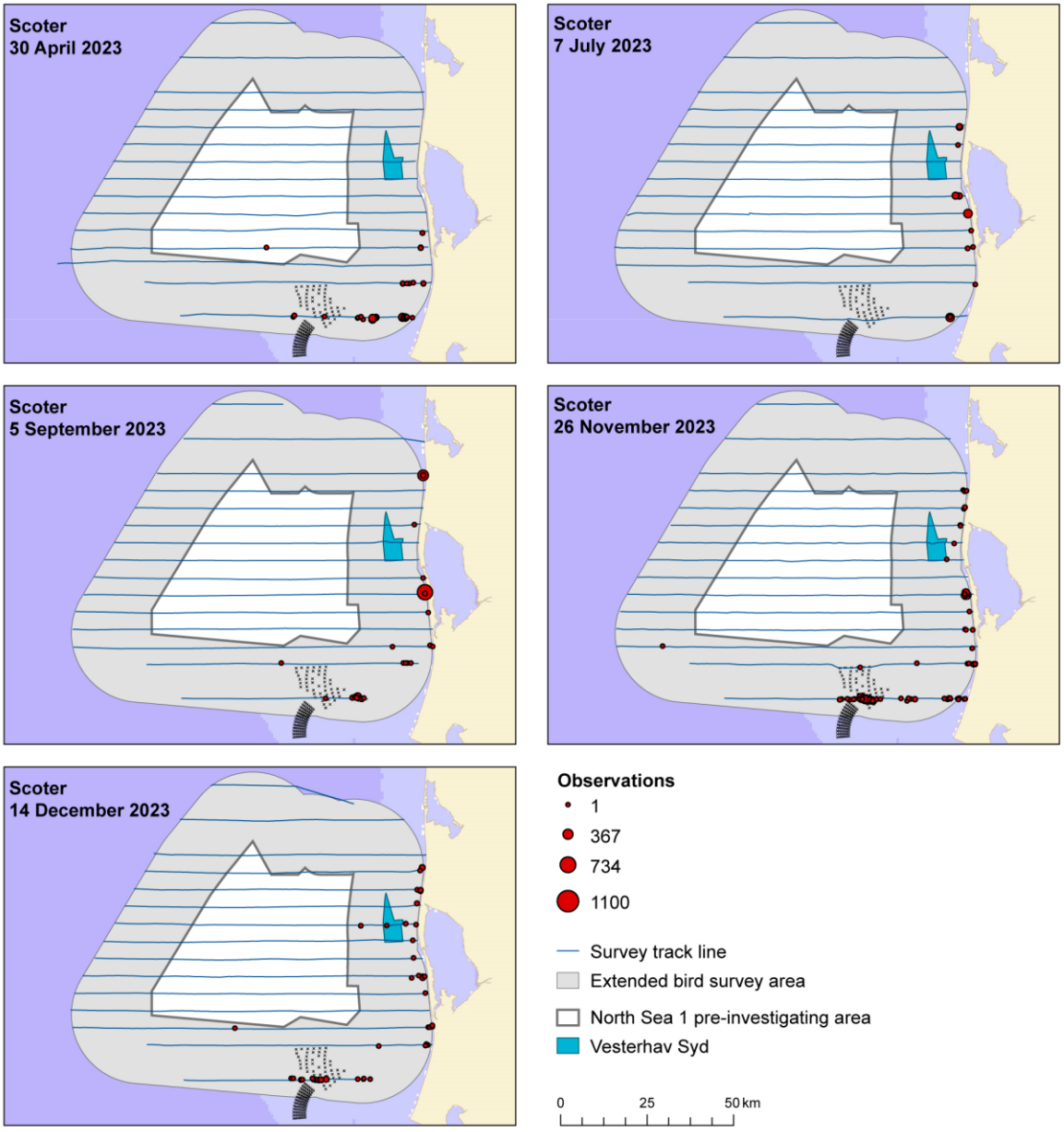

Figure 5.28 The numbers and distribution of common scoters observed during five surveys in 2023 in the North Sea I survey area.

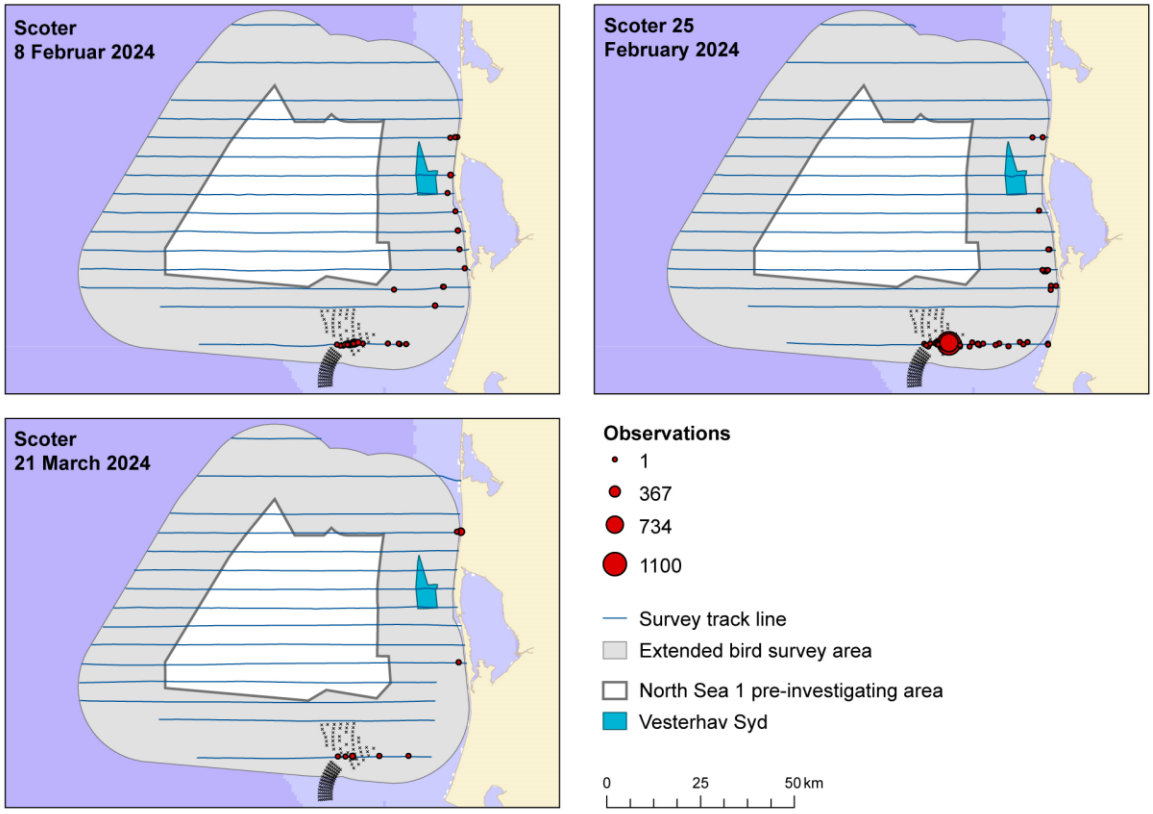

Figure 5.29 The numbers and distribution of common scoters observed during three surveys in 2024 in the North Sea I survey area.

5.1.5 Black-legged kittiwake (*Rissa tridactyla*)

Black-legged kittiwake was observed during all eight surveys. 887 individuals were recorded across all surveys, and the maximum number of observed birds for a single survey was 276 individuals in December 2023. Most black-legged kittiwakes were recorded over the winter and spring period, while few birds were recorded in July and September (Table 5.1).

Black-legged Kittiwake was recorded across the entire survey area, although less frequently in the very eastern coastal parts (Figure 5.30 and Figure 5.31). There were 554 records of black-legged kittiwakes, with a mean flock size of 1.6 birds. The recorded number per flock ranged from 1 to 40 individuals.

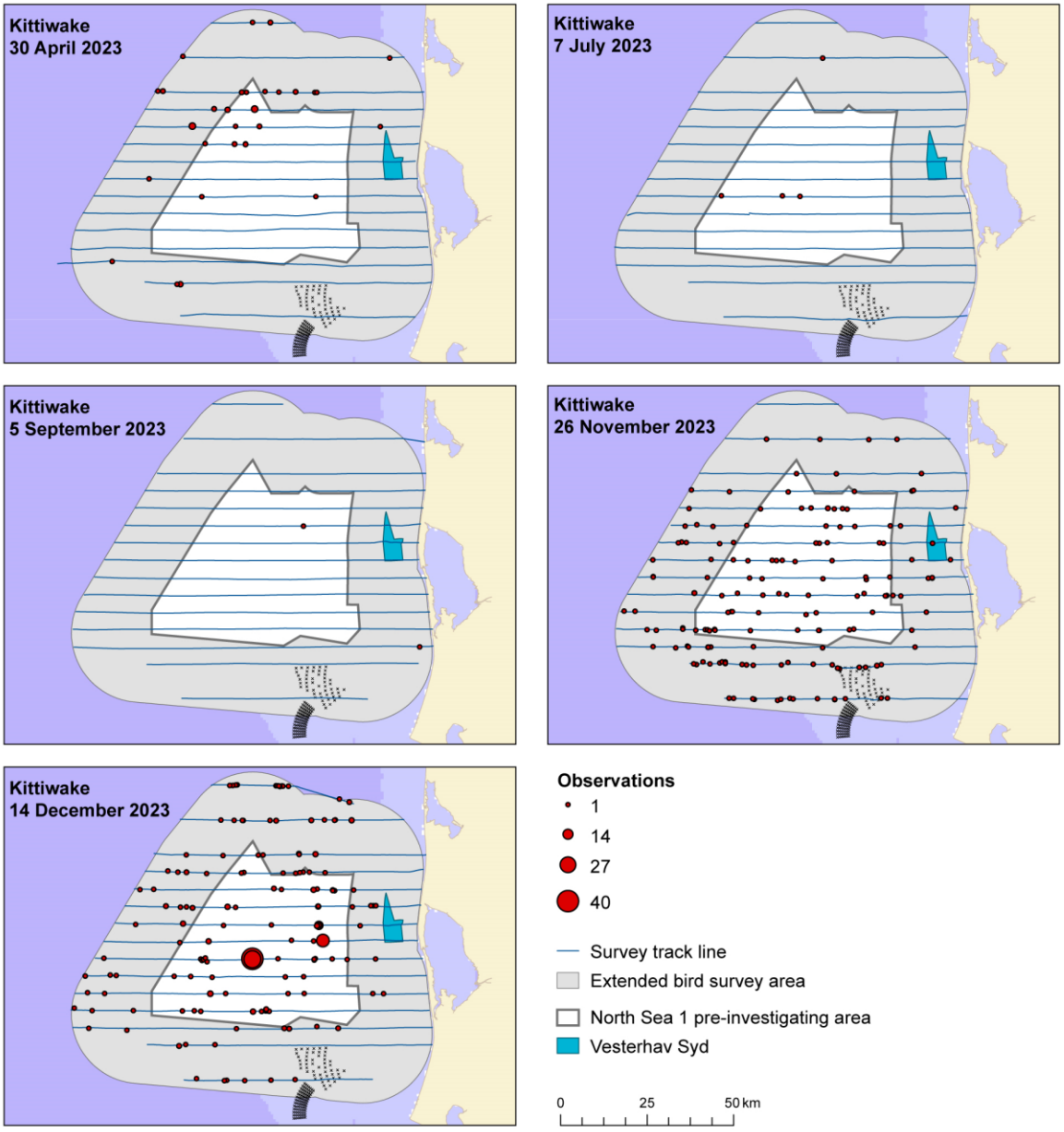

Figure 5.30 The numbers and distribution of black-legged kittiwakes observed during five surveys in 2023 in the North Sea I survey area.

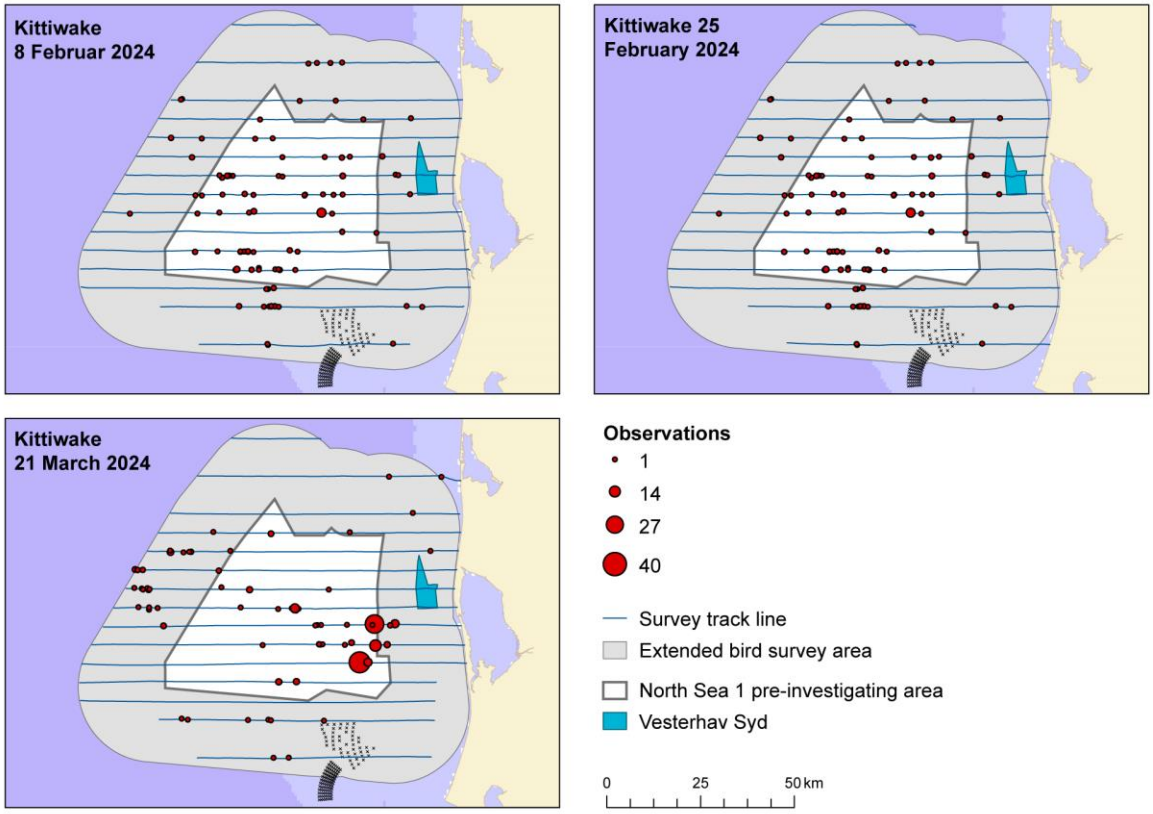

Figure 5.31 The numbers and distribution of black-legged kittiwakes observed during three surveys in 2024 in the North Sea I survey area.

5.1.5.1 Distance analysis

The average probability of sighting a black-legged kittiwake was estimated to be 0.22 (CoV = 0.04). This probability was estimated using a hazard rate detection function, and no covariates were selected (Figure 5.32).

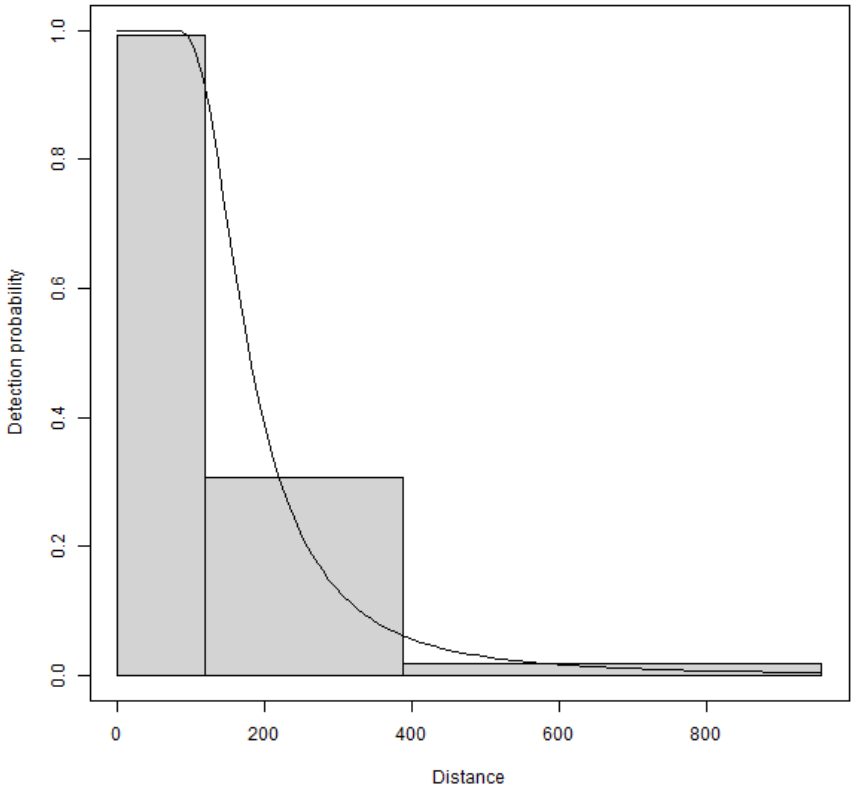

Figure 5.32 Figure showing the estimated detection function. The histogram represents the distances of the observed sightings.

5.1.5.2 Spatial analysis

Figure 5.33 shows the distribution of the distance corrected counts for each of the eight surveys.

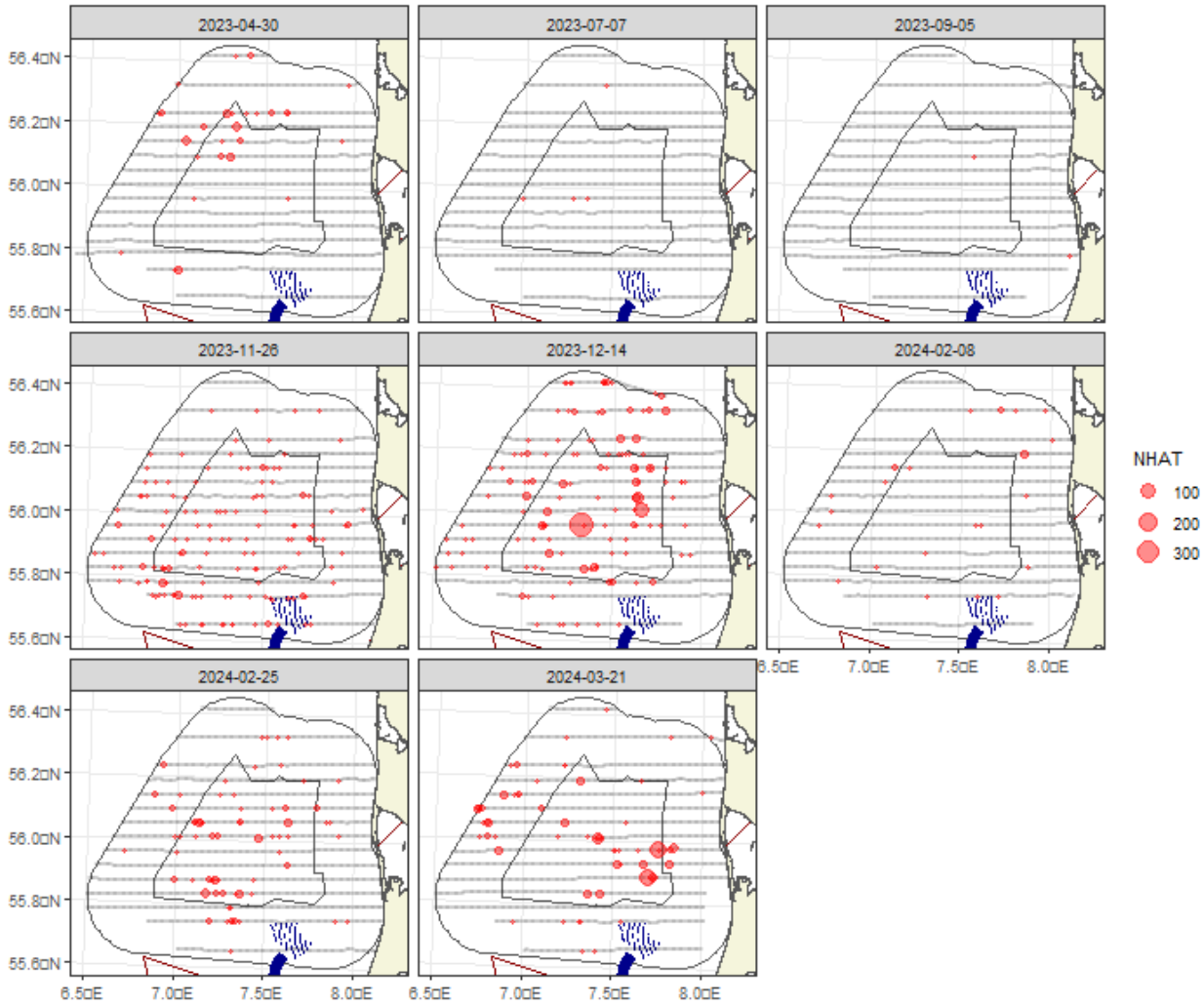

Figure 5.33 Distance-corrected counts for the black-legged kittiwake across the 8 surveys. The red circles indicate the distance-corrected counts along the transect lines. The grey dots are segments with a count of zero.

5.1.5.3 Model selection

There was insufficient data for two of the eight surveys to fit a spatial model, namely the July and September 2023 surveys (Table 5.6). The models selected for the remaining six surveys included a spatial term (of varying complexity), while the depth covariate (either linear or smooth term) was not selected for any surveys. The distance from the coast covariate was selected as a smooth term for one survey. This shows there was compelling evidence for non-uniform spatial patterns in each survey. However, given these spatial patterns, there was little evidence for depth or distance to the coast relationships. Thus, other important factors are driving the distribution of the birds, factors that we do not have access to, such as for instance food availability. The spatial surfaces selected ranged from 4 to 12 parameters for the spatial term (Table 5.6).

Table 5.6 Model selection results for black-legged kittiwake for each survey. The model column represents the terms in the model.

Name	Model	Distribution	Variable 1D	Variable 2D	Number of parameters	Dispersion parameter	Tweedie parameter
2023-04-30	2D only	Tweedie	NA	s(x,y, df=7)	8	11.1	1.22
2023-07-07	No model	NA	NA	NA	NA	NA	NA

Name	Model	Distribution	Variable 1D	Variable 2D	Number of parameters	Dispersion parameter	Tweedie parameter
2023-09-05	No model	NA	NA	NA	NA	NA	NA
2023-11-26	Best 1D2D	quasipoisson	s(distcoast, df=2)	s(x,y, df=9)	12	5.0	NA
2023-12-14	2D only	Tweedie	NA	s(x,y, df=5)	6	47.0	1.44
2024-02-08	2D only	quasipoisson	NA	s(x,y, df=3)	4	5.5	NA
2024-02-25	2D only	quasipoisson	NA	s(x,y, df=9)	10	6.0	NA
2024-03-21	2D only	Tweedie	NA	s(x,y, df=10)	11	33.5	1.49

Table 5.7 and Figure 5.34 give each survey's estimated abundances, densities, and associated 95% confidence intervals. In 2023, there was not enough data for the July and September surveys to fit a spatial model, so the abundance estimates were calculated using the Horvitz-Thompson method (H-T).

While the summer surveys from July and September 2023 had estimations of less than 100 individuals, all other surveys had estimated total abundances of between 785 and 3,669 birds. This corresponds to densities of 0.1 to 0.3 birds/km^2 (Table 5.7 and Figure 5.34).

Table 5.7 Estimated abundance and density of black-legged kittiwake for each survey. The 95% CI is a percentile-based confidence interval.

Month	Area (km^2)	Estimator type	Estimated count	95% CI count	Estimated density	95% CI density
2023-04-30	7,833	Spatial	1,382	(620, 3,582)	0.2	(0.1, 0.5)
2023-07-07	7,833	H-T	66	(61, 71)	0.0	(0, 0)
2023-09-05	7,833	H-T	32	(29, 34)	0.0	(0, 0)
2023-11-26	7,833	Spatial	2,339	(1,475, 3,977)	0.3	(0.2, 0.5)
2023-12-14	7,833	Spatial	3,669	(1,917, 7,664)	0.5	(0.2, 1)
2024-02-08	7,833	Spatial	785	(367, 1,879)	0.1	(0, 0.2)
2024-02-25	7,833	Spatial	1,929	(1,091, 3,549)	0.2	(0.1, 0.5)
2024-03-21	7,833	Spatial	3,349	(1,480, 8,419)	0.4	(0.2, 1.1)

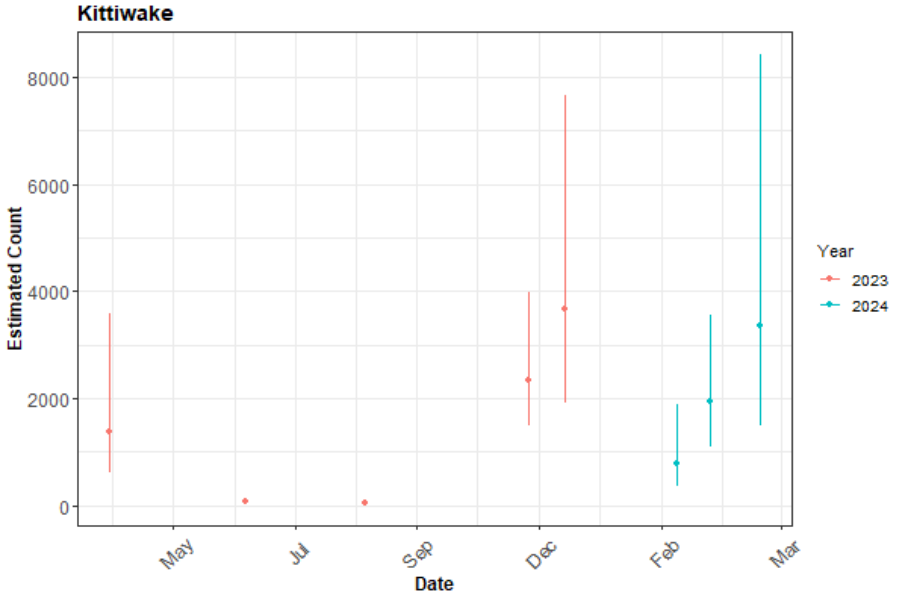

Figure 5.34 The estimated count of black-legged kittiwakes for each survey. The 95% CI are percentile-based confidence intervals are from a parametric bootstrap with 500 replicates.

5.1.5.4 Spatial results

Figure 5.35 shows the estimated counts of black-legged kittiwakes in each 1 km^2 grid cell for each month. Generally, the estimated abundances fitted well with the raw data, and there were no notable misalignments. In areas where the estimated counts were systematically higher, the abundances were also relatively high, and there were no areas with large, estimated abundances unsupported by the data.

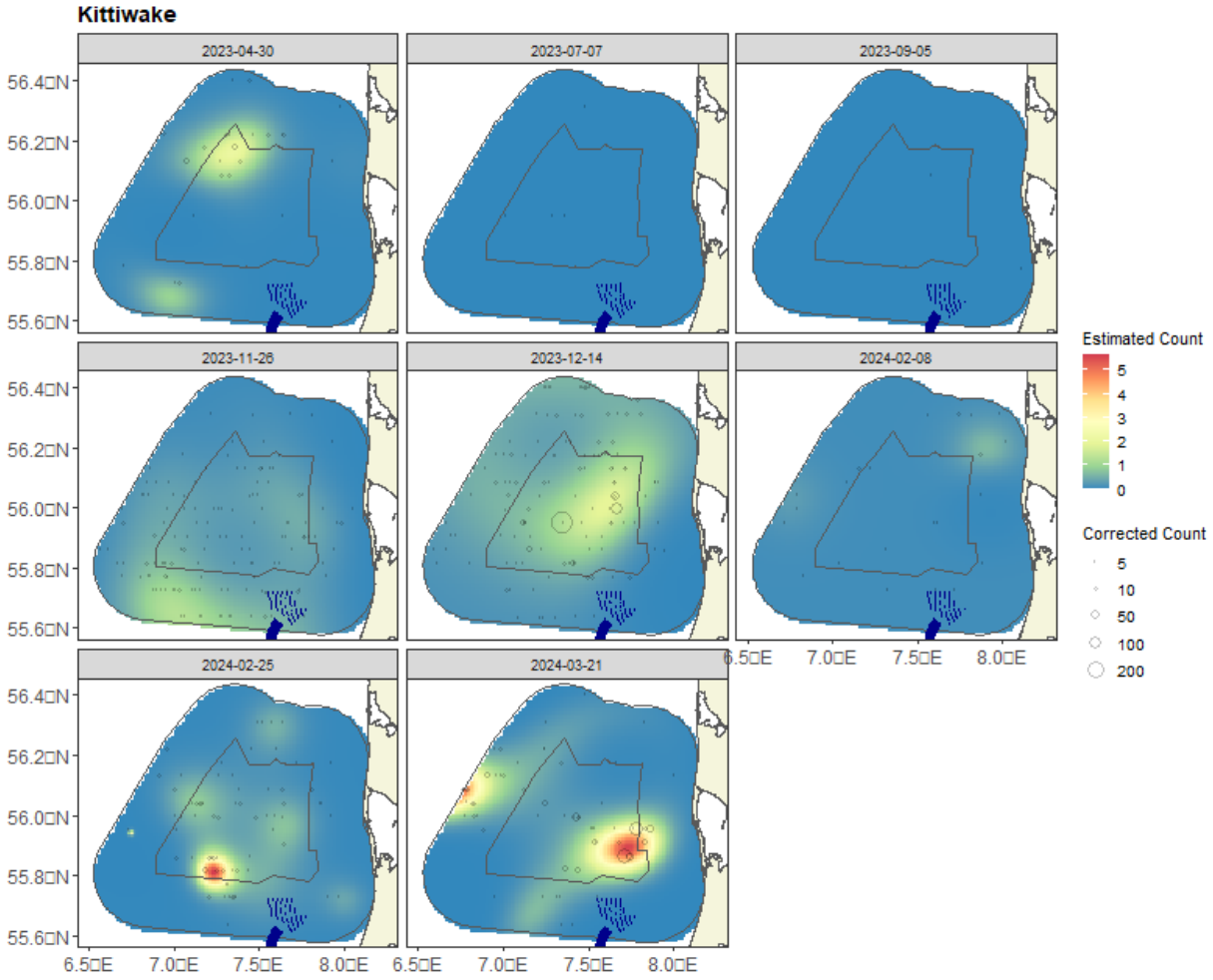

Figure 5.35 Figure showing the estimated black-legged kittiwake abundance across the study site for each survey. The estimated counts are per 1 km x 1 km grid cell. The open circles show the observed corrected counts.

5.1.5.5 Uncertainty in spatial predictions

Broadly, the highest coefficient of variation (CoV) scores were associated with the `almost zero' predictions, and it is known that the CoV metric is highly sensitive to any uncertainty for very small predictions. There was one larger value in the western edge of the survey area but that was otherwise absent of data. There was no material overlap between the high values of the CoV metric and the transect lines/locations with non-zero counts. Therefore, there were no concerns in this case (Figure 5.36).

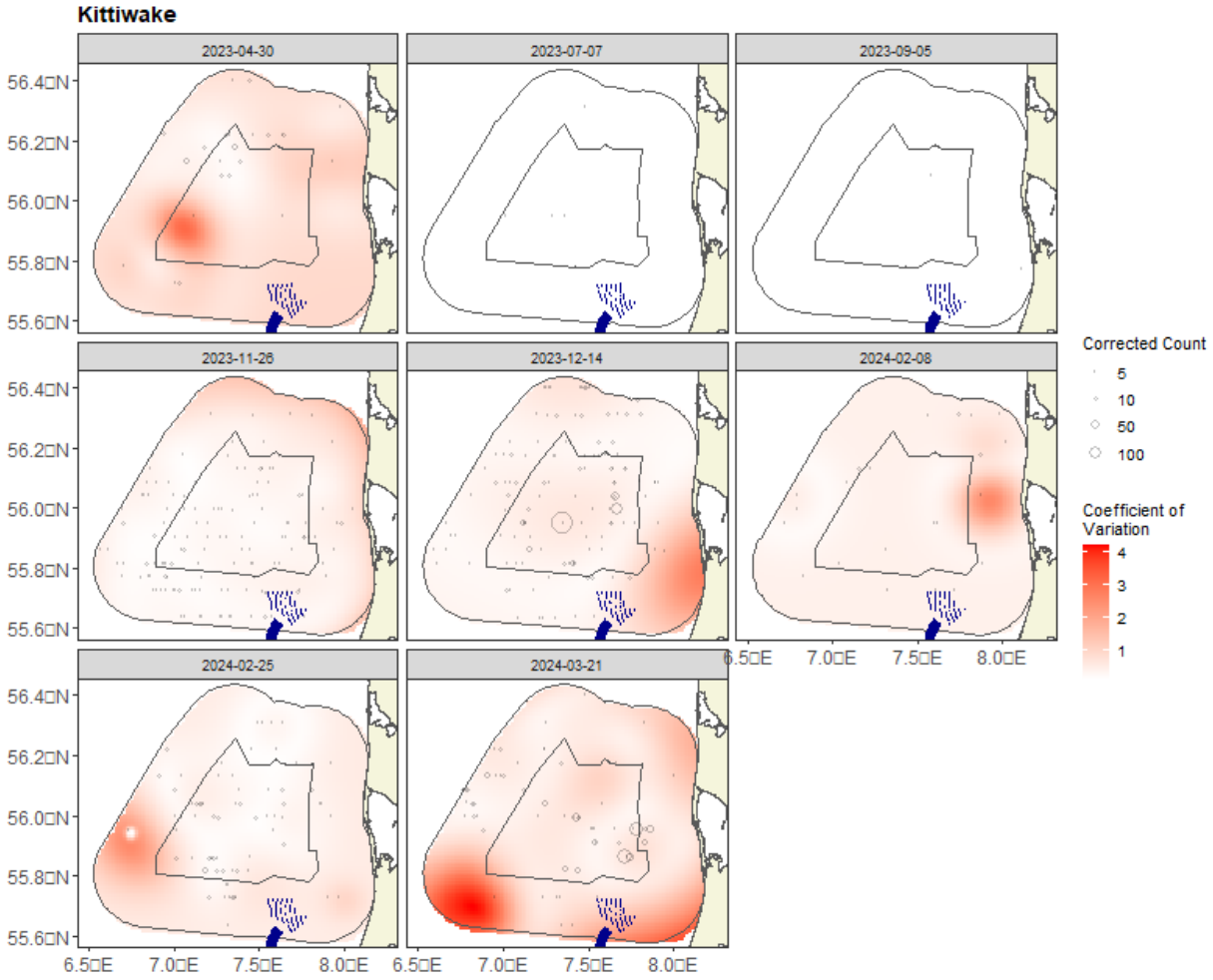

Figure 5.36 Figure showing the coefficient of variation (CoV) across the study region for each survey. The open circles show the distance corrected counts. The presence of dark red CoV scores in areas with virtually zero predictions is an artefact of the very small prediction rather than of any notable concern.

For the case when the very small predicted values were excluded (Figure 5.37), the CoV for all surveys was <1 for most surveys and so of no material concern. There remains some high uncertainty for some surveys, reflected in the large confidence interval for the abundance (Table 5.7 and Figure 5.34).

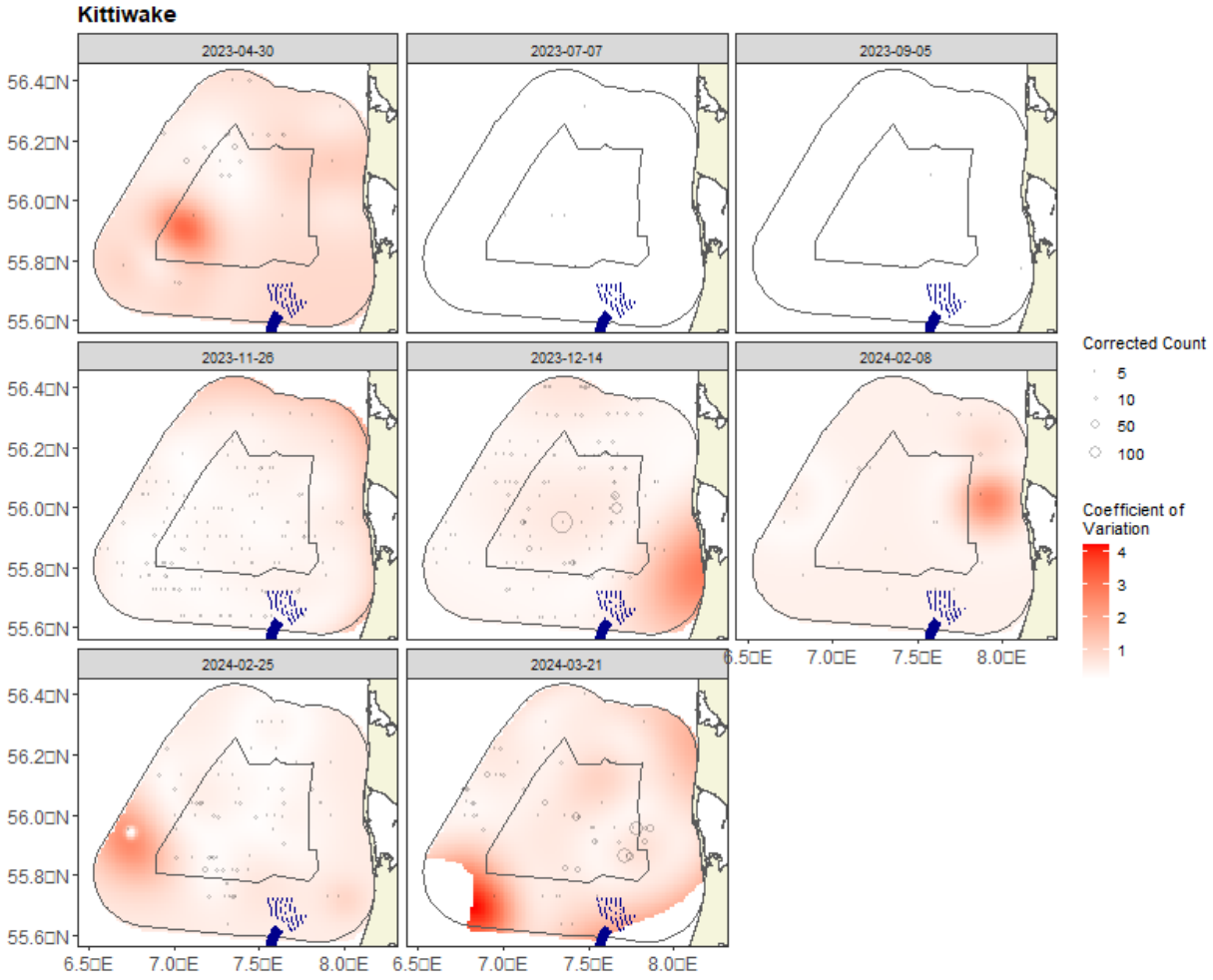

Figure 5.37 Figure showing the coefficient of variation for all cells with density > 0.001. The open circles show the distance corrected counts. The presence of dark red CoV scores in areas with virtually zero predictions is an artefact of the very small prediction rather than of any notable concern.

5.1.5.6 Model diagnostics

A blocking structure accounted for potential residual non-independence for each model, and a robust standard error approach was based on unique transects. In each case, a reassuring decay to zero was seen (indicated by the red and grey lines in Figure 5.38), implying that an appropriate blocking structure was used.

The assumed mean-variance relationship was examined, and generally showed agreement between the assumed (red) lines and the observed values. Figure 5.39 and Figure 5.40 show example relationships for a quasi-Poisson and Tweedie model.

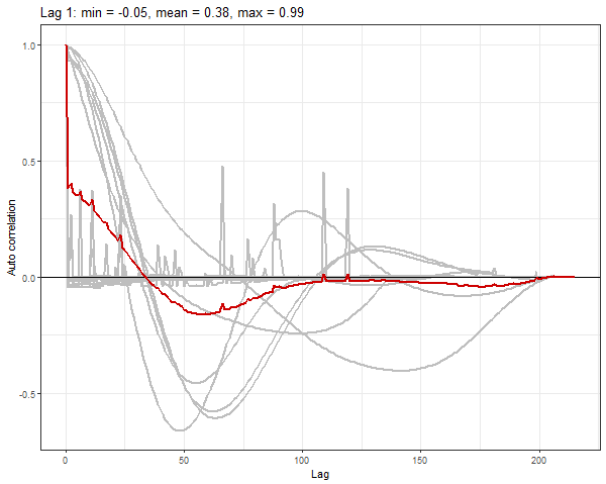

Figure 5.38 Example ACF plot. The grey lines represent the residual correlation observed in each transect, and the red line is the average of these values across transects.

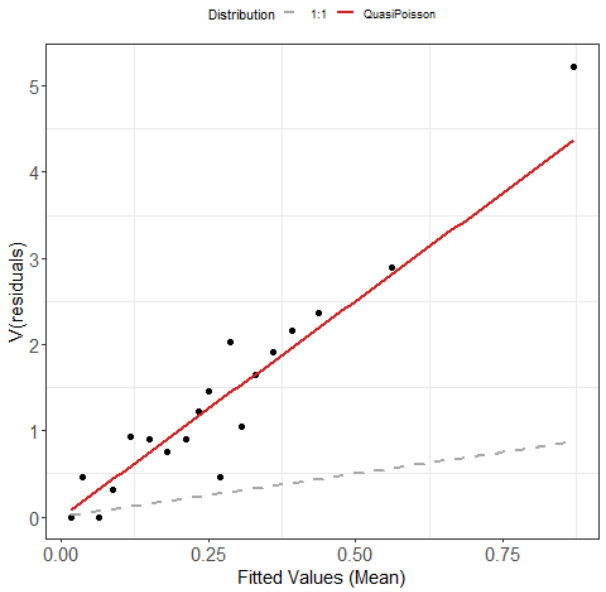

Figure 5.39 Example plot showing the estimated quasi-Poisson mean-variance relationship (red line) and actual (black dots). The black dots are based on 20 quantiles of the model residuals, and for reference, the grey dashed line shows the 1:1 relationship.

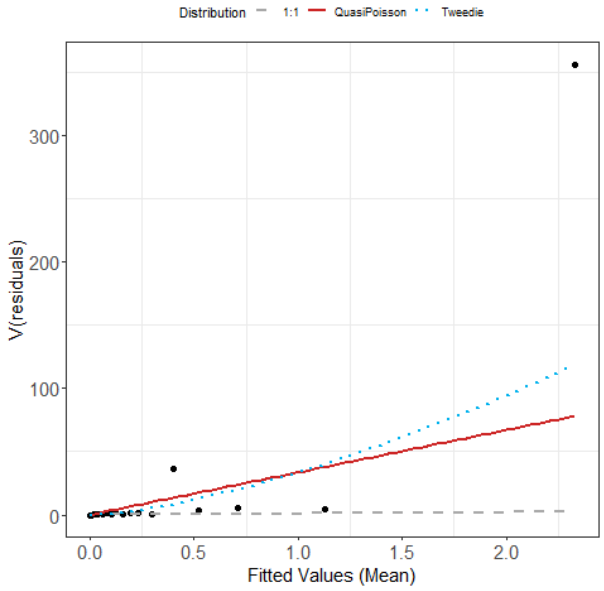

Figure 5.40 Example plot showing the estimated Tweedie mean-variance relationship (blue dashed line). The red line shows the V(μ)=ϕμ relationship, and the grey line shows the 1:1 relationship.

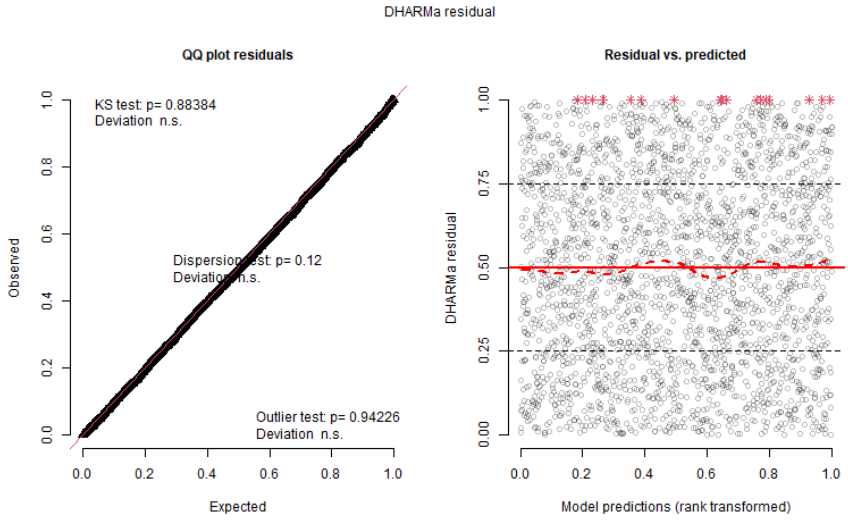

Figure 5.41 Example diagnostics. QQplot and residuals against predicted values. The red stars are outliers and the red line is a smooth spline around the mean of the residuals.

5.1.5.7 Areas of persistence

Across the eight surveys, black-legged kittiwake has moderate persistence (~ 60%), focused on the centre west of the study area (Figure 5.42). There was low persistence towards the coast, particularly in the southeast of the survey area, indicating that black-legged kittiwake utilize that area less..

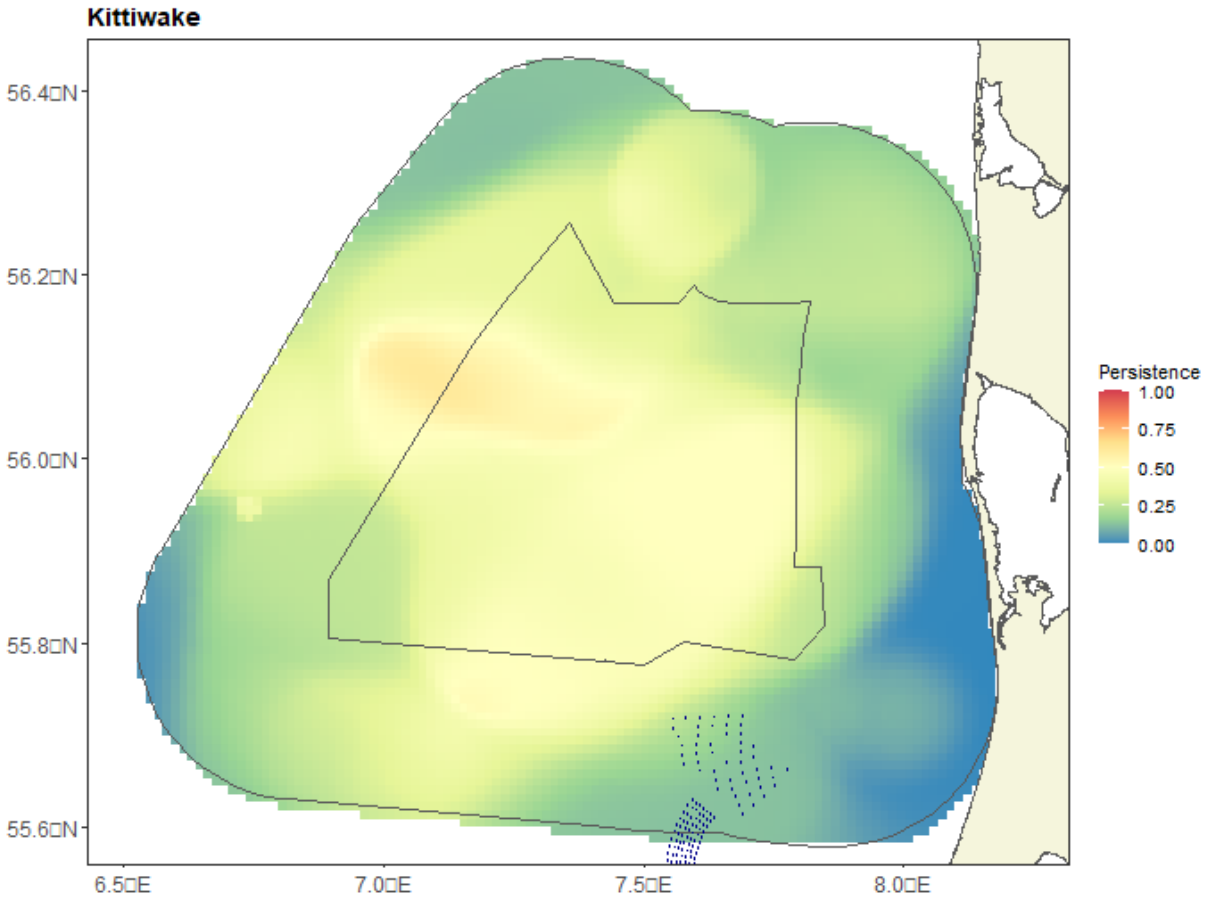

Figure 5.42 Persistence scores for black-legged kittiwake across the eight surveys. The polygon represents the pre-investigation area (black line).

5.1.6 Little gull (*Hydrocoloeus minutus*)

Little gulls were recorded in low numbers in the survey area. 56 individuals were recorded, with the highest numbers recorded in late February 2024 (21 birds). No little gulls were recorded in July 2023, and only one bird was seen during the September 2023 survey. The species is most abundant in the area in winter and early spring.

Most of the recorded little gulls were seen in the southern and eastern parts of the survey area (Figure 5.43 and Figure 5.44). The observations of little gulls contain 37 records, with a mean flock size of 1.5 birds and a maximum flock size of 6 birds.

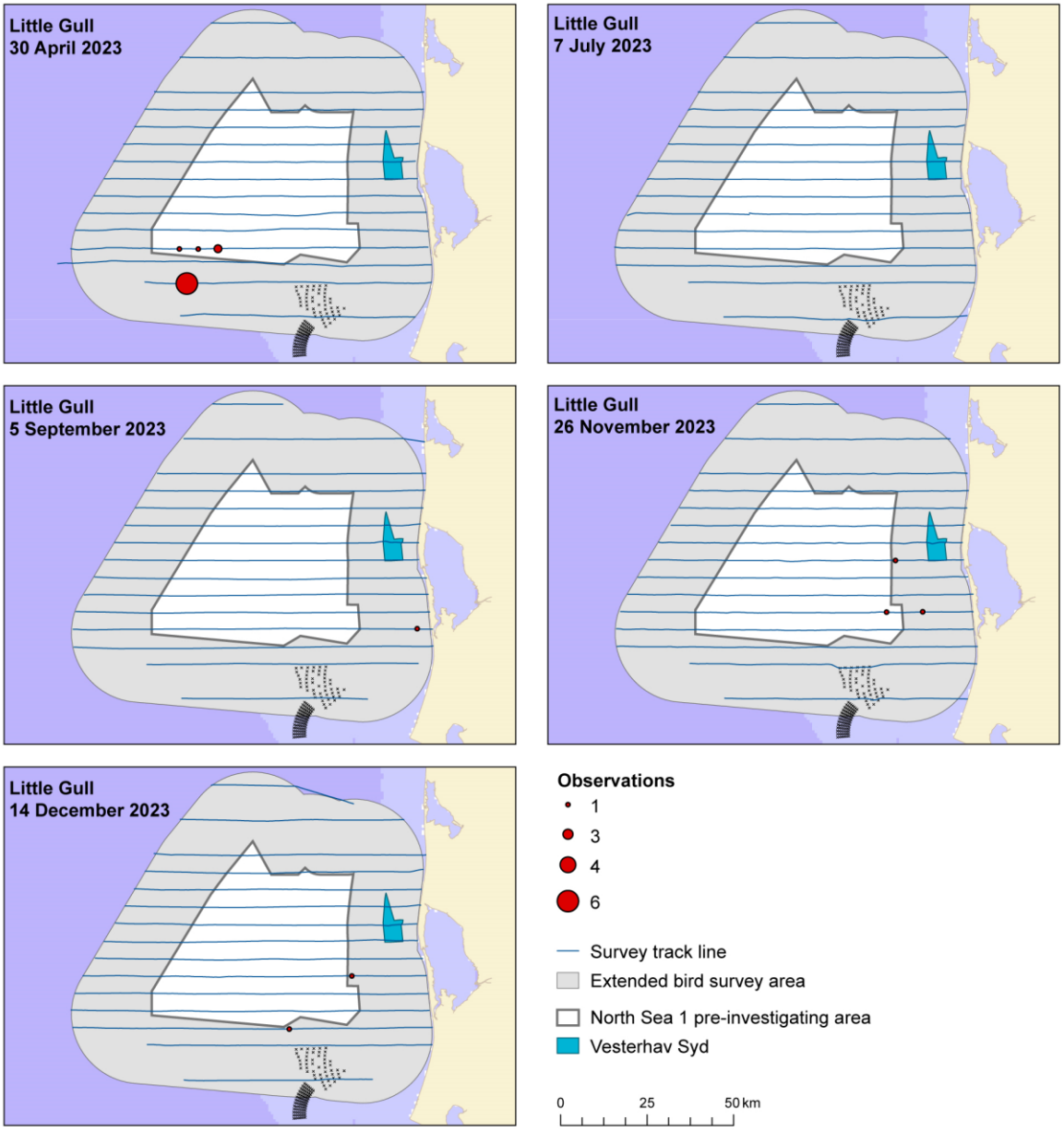

Figure 5.43 The numbers and distribution of little gulls observed during five surveys in 2023 in the North Sea I survey area.

The little gull data did not allow for estimating the total abundances and distribution due to a low number of observations.

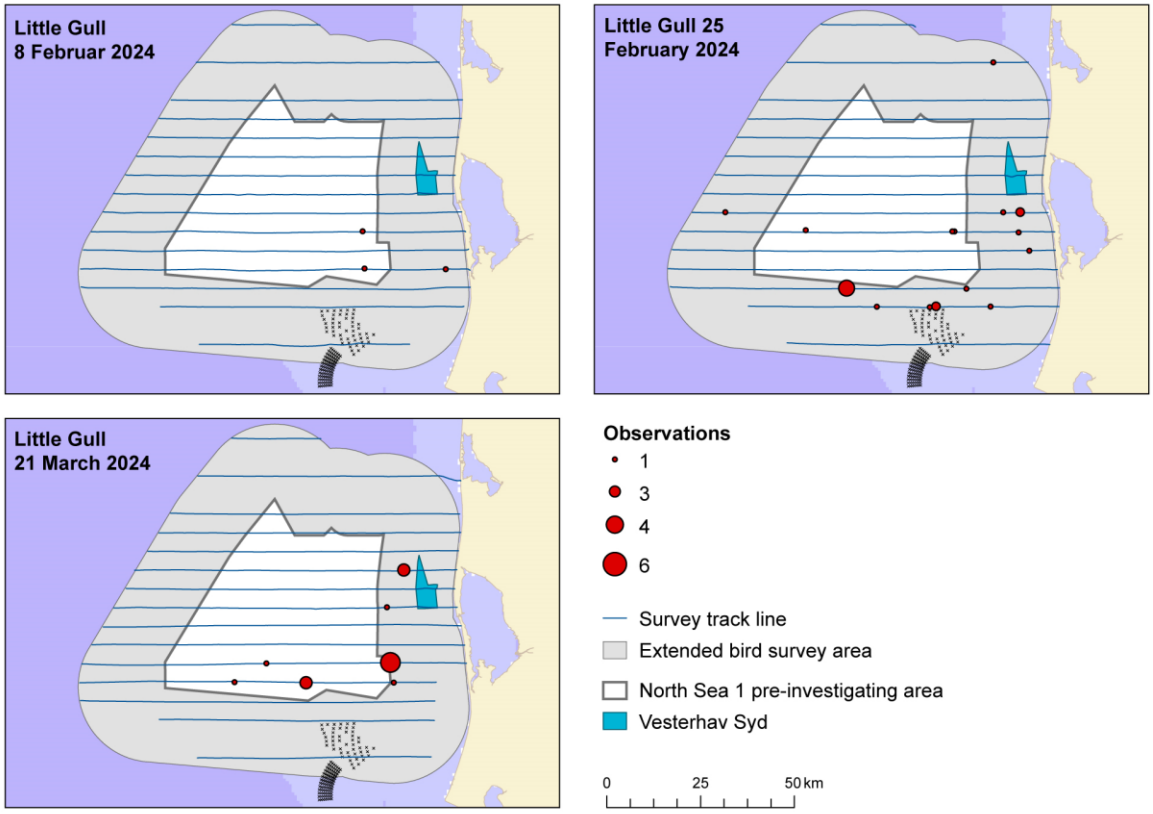

Figure 5.44 The numbers and distribution of little gulls observed during three surveys in 2024 in the North Sea I survey area.

5.1.7 Gull sp. (*Larus* sp.)

The gull group consisted of black-headed gulls, common gulls, European herring gulls, lesser black-backed gulls, great black-backed gulls, and gulls not identified to species (gull sp.). Within this group of gulls, a total of 1,928 records were made. The mean flock size was 2.35, and the maximum flock size recorded was 400 individuals. Two other gull species, black-legged kittiwake and little gull, are described individually above.

The European herring gull was the most numerously recorded species within this group, with 2,136 birds counted across the eight surveys. The corresponding number for gull sp. was 617 birds, 478 birds for common gull and 323 for lesser black-backed gull (Table 5.1).

European herring gull, common gull, great black-backed gull and gull sp. were all recorded during all eight surveys, while lesser black-backed and black-headed gull were absent over the winter. This group of gulls had the highest numbers in the eastern parts of the survey area, although smaller numbers were present across the survey area. In July 2023, a concentration of gulls was present in the central northern parts of the survey area (Figure 5.45 and Figure 5.46).

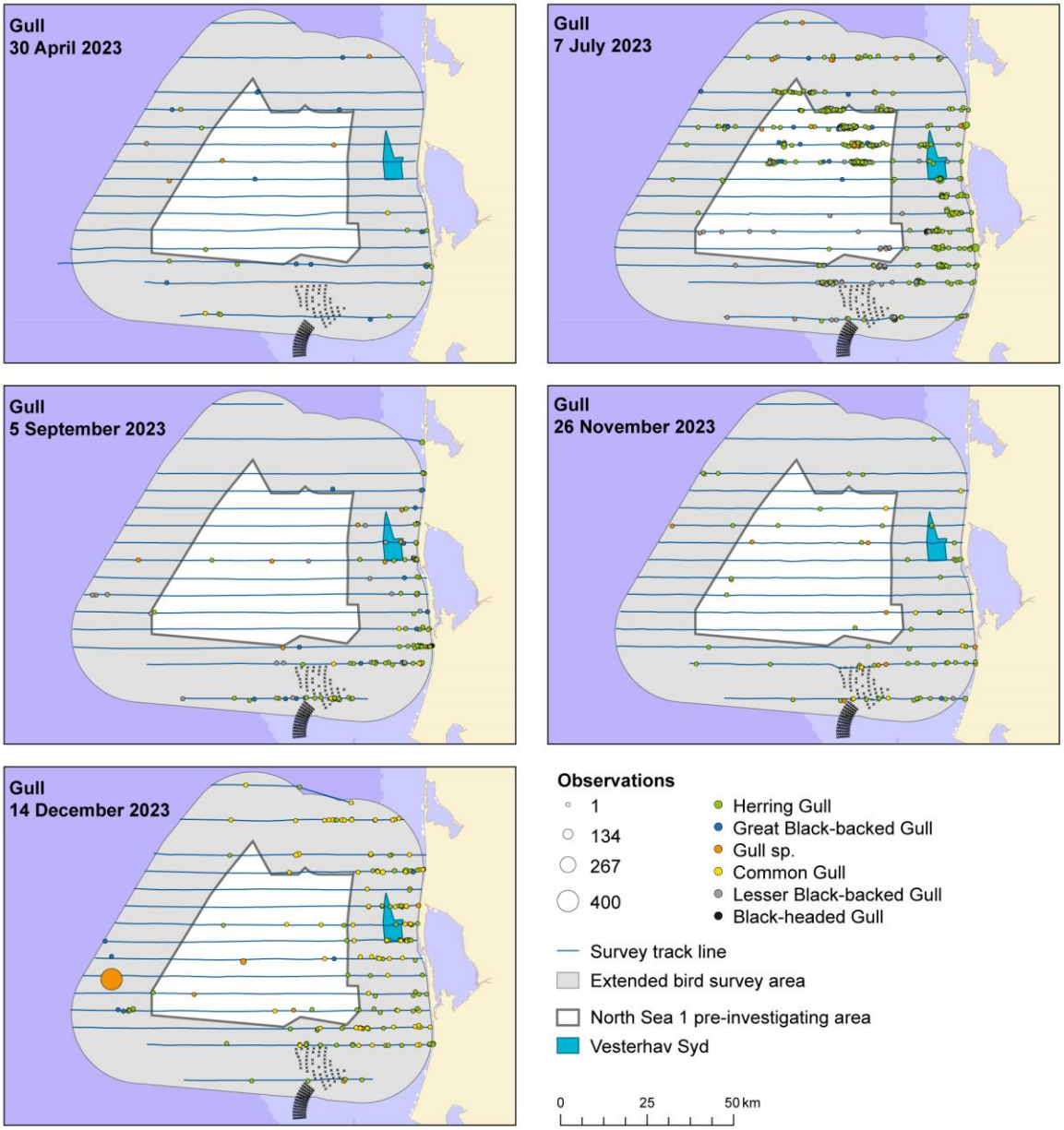

Figure 5.45 The numbers and distribution of European herring gull, great black-backed gull, common gull, lesser black-backed gull, black-headed gull and gull sp., observed during five surveys in 2023 in the North Sea I survey area.

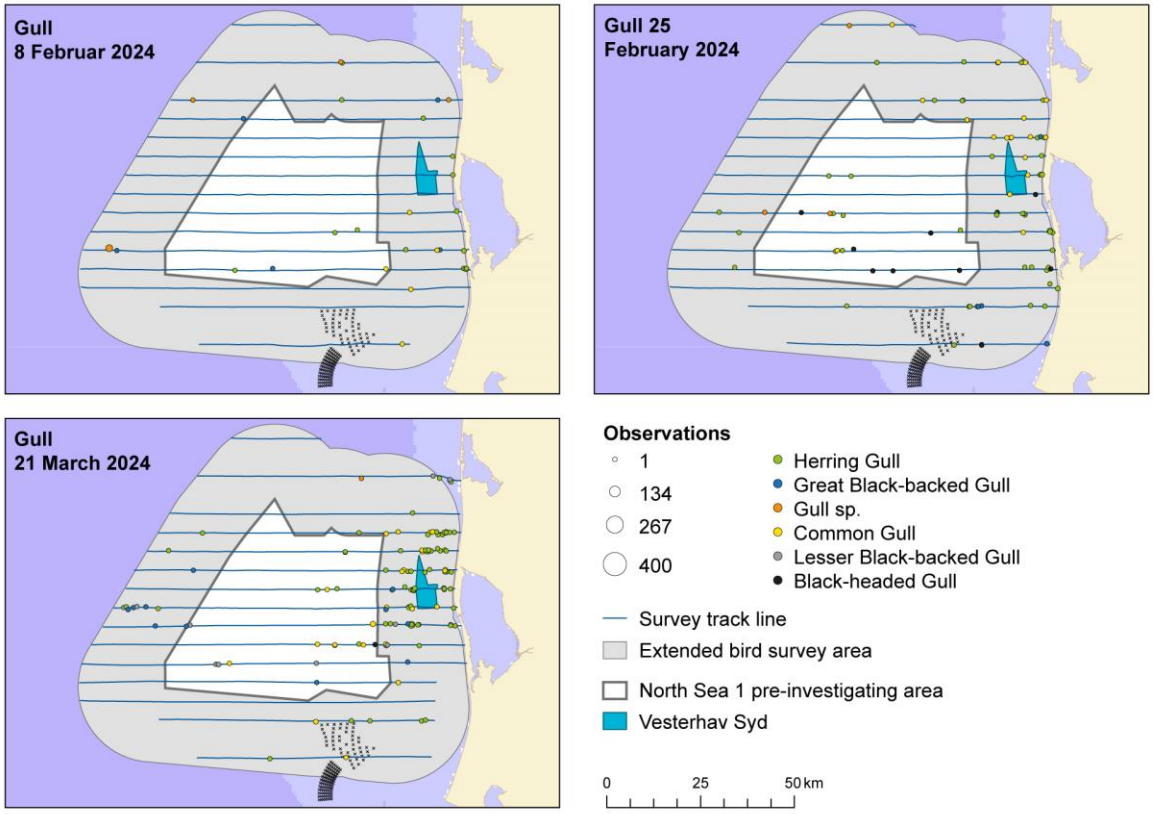

Figure 5.46 The numbers and distribution of European herring gull, great black-backed gull, common gull, lesser black-backed gull, black-headed gull and gull sp., observed during three surveys in 2024 in the North Sea I survey area.

The group gulls sp. data did not allow for the estimation of total abundances and distribution due to a low number of observations.

5.1.8 Terns (*Sterna* sp.)

The tern group consisted of common terns, Arctic/common terns, sandwich terns, and terns not identified to species (tern sp.). Within this group of terns, a total of 476 records were made. The mean flock size was 1.6, and the maximum flock site recorded was 25 individuals.

Most recorded terns (77%) were identified as Arctic/common terns. Almost 97% of the recorded terns were seen during the April 2023 survey, which is the migration time for Arctic and common terns (Table 5.1). Few terns were seen in July and September 2023 and in March 2024, and no terns were recorded during the November and December surveys of 2023 or the two February 2024 surveys (Table 5.1).

During the April 2023 survey, terns were mainly recorded in the central and western parts of the survey area. The remaining few observations were mainly recorded in the eastern parts (Figure 5.47 and Figure 5.48).

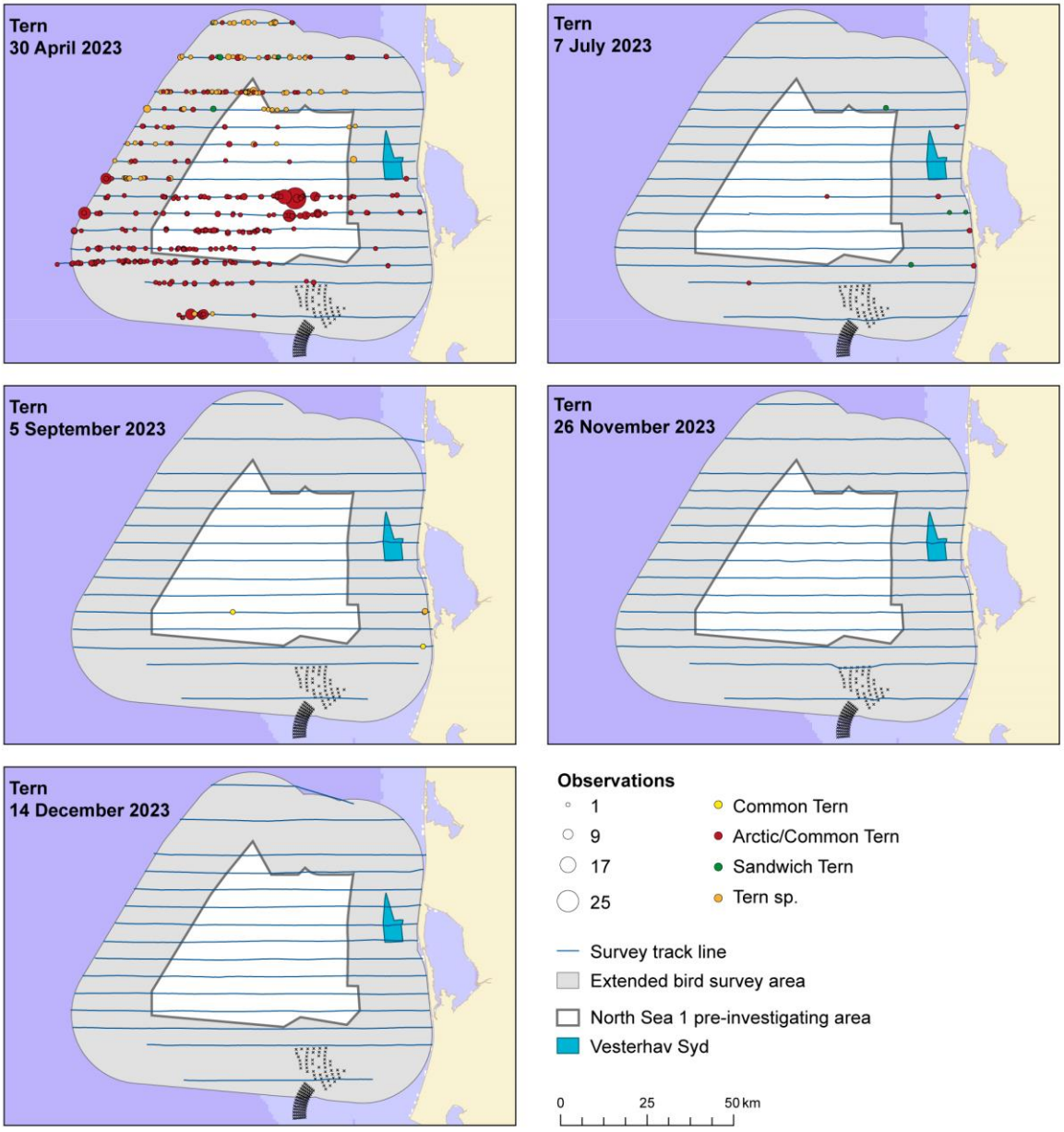

Figure 5.47 The numbers and distribution of common tern, Arctic/common tern, sandwich tern and unidentified terns (tern sp.), observed during five surveys in 2023 in the North Sea I survey area.

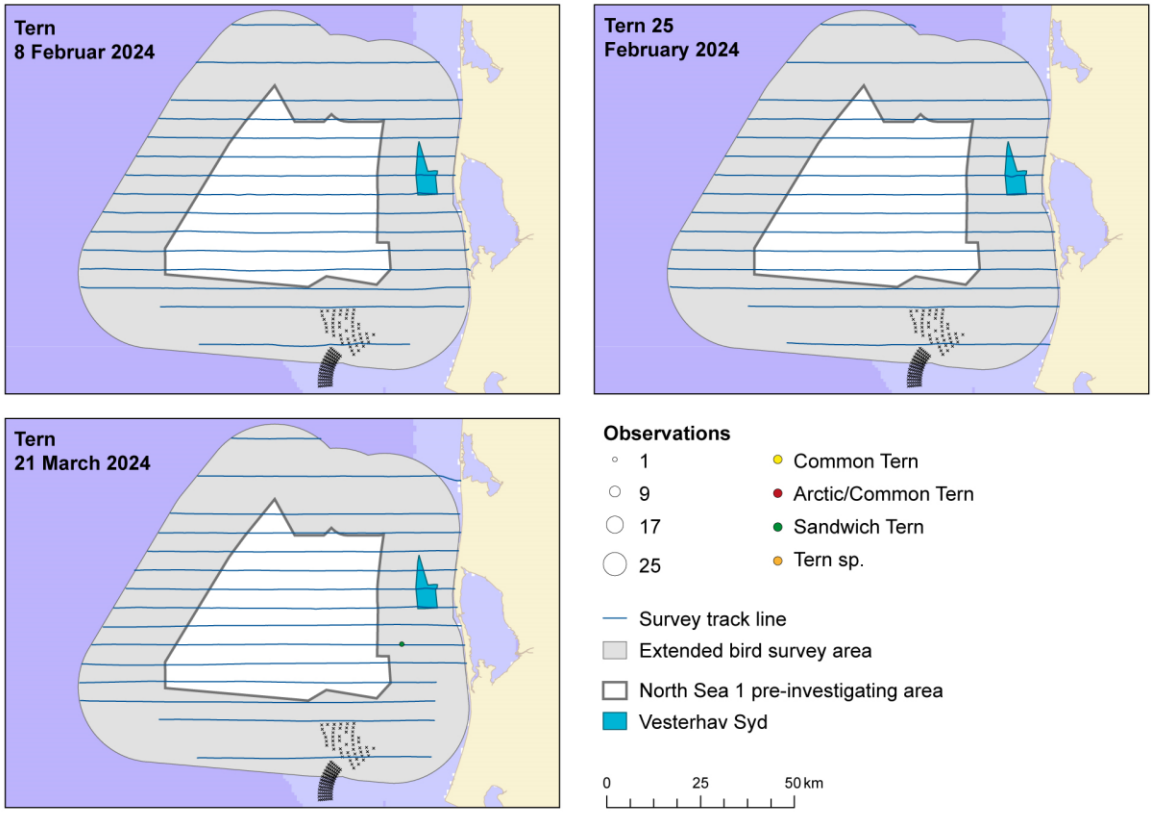

Figure 5.48 The numbers and distribution of common tern, Arctic/common tern, sandwich tern and unidentified terns (tern sp.), observed during three surveys in 2024 in the North Sea I survey area.

The tern data did not allow for the estimation of total abundances and distribution due to a low number of observations.

5.1.9 Razorbill/common guillemot (*Alca torda/Uria aalge*)

Razorbills/common guillemots were recorded during all eight surveys. A total of 3,120 birds were observed, 2,290 unidentified razorbills/common guillemots, 148 razorbills and 682 common guillemots summed for all eight surveys (Table 5.1). Thus, more than 73% of those were recorded as unidentified razorbills/common guillemots. 5% of the total numbers from this group were identified as razorbills, while 22% were identified as common guillemots. There were 1,629 records made within this group of species. The mean flock size was 1.9, and the maximum flock size recorded was 55 individuals.

Over half of the observed razorbills/common guillemots were recorded during the April 2024 survey. During that survey, most birds were seen in the central and northeastern parts of the survey area. During the remaining surveys, the species group was observed scattered over the survey area, with a tendency for fewer birds in the very easternmost and coastal parts (Figure 5.49 and Figure 5.50).

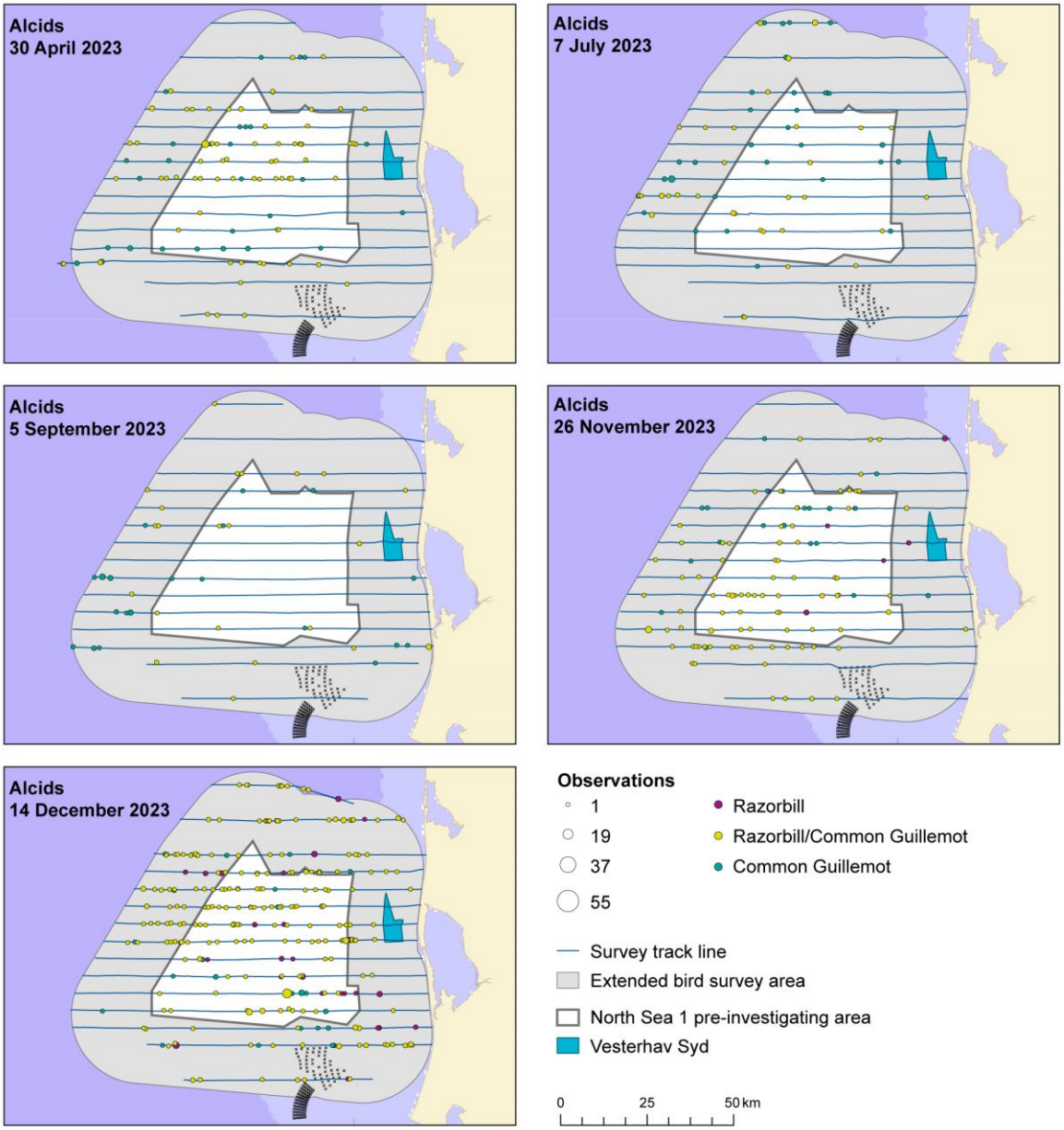

Figure 5.49 The numbers and distribution of razorbills, common guillemots and unidentified razorbills/common guillemots, observed during five surveys in 2023 in the North Sea I survey area.

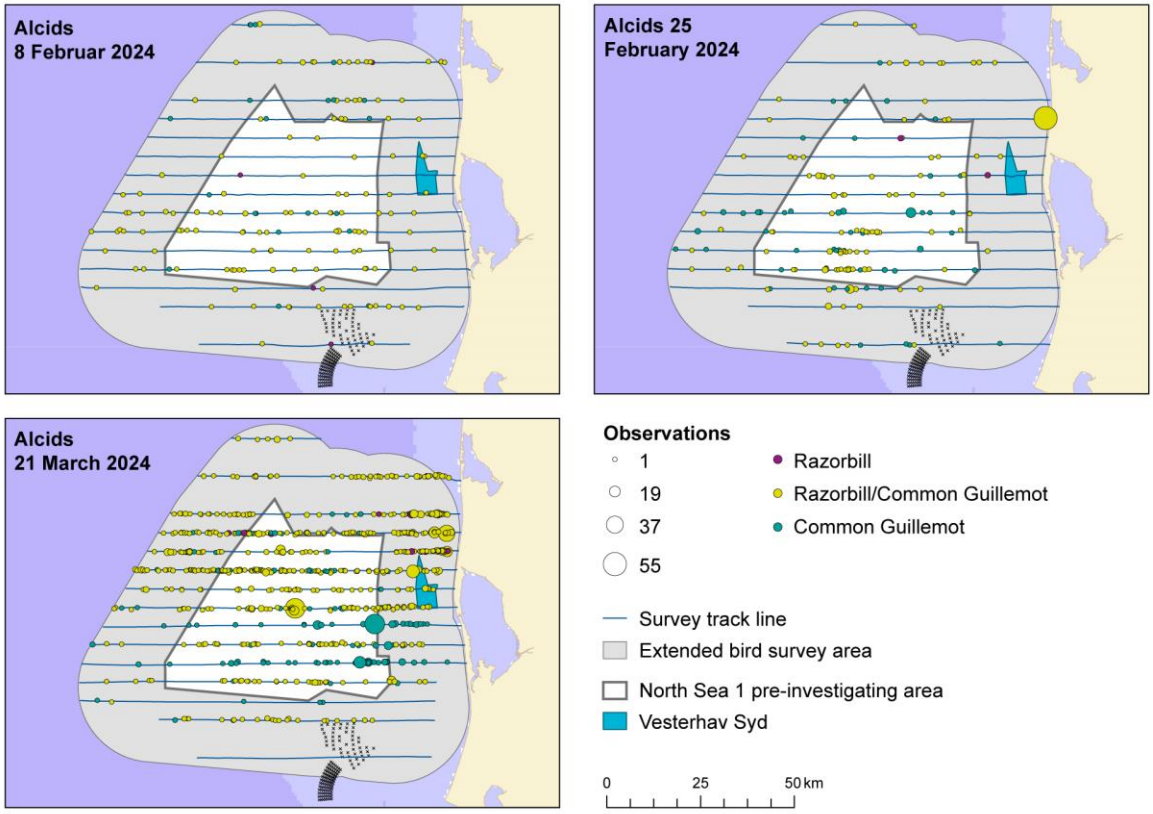

Figure 5.50 The numbers and distribution of razorbills, common guillemots and unidentified razorbills/common guillemots observed during three surveys in 2024 in the North Sea I survey area.

5.1.9.1 Distance analysis

The average probability of sighting razorbills/common guillemots was estimated to be 0.19 (CoV = 0.02). This probability was estimated using a hazard rate detection function and observer as a covariate (Figure 5.51).

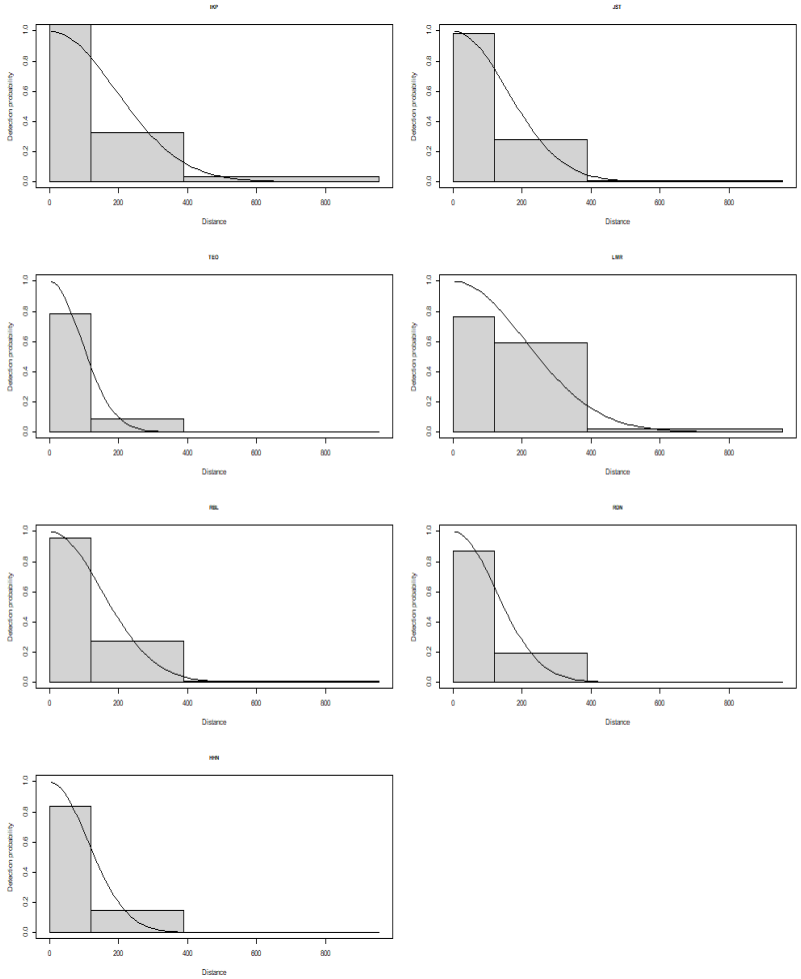

Figure 5.51 Figure showing the estimated detection function. The histograms represent the distances of the observed sightings for each of the seven observers.

5.1.9.2 Spatial analysis

Figure 5.52 shows the distribution of the distance corrected counts for each of the eight surveys.

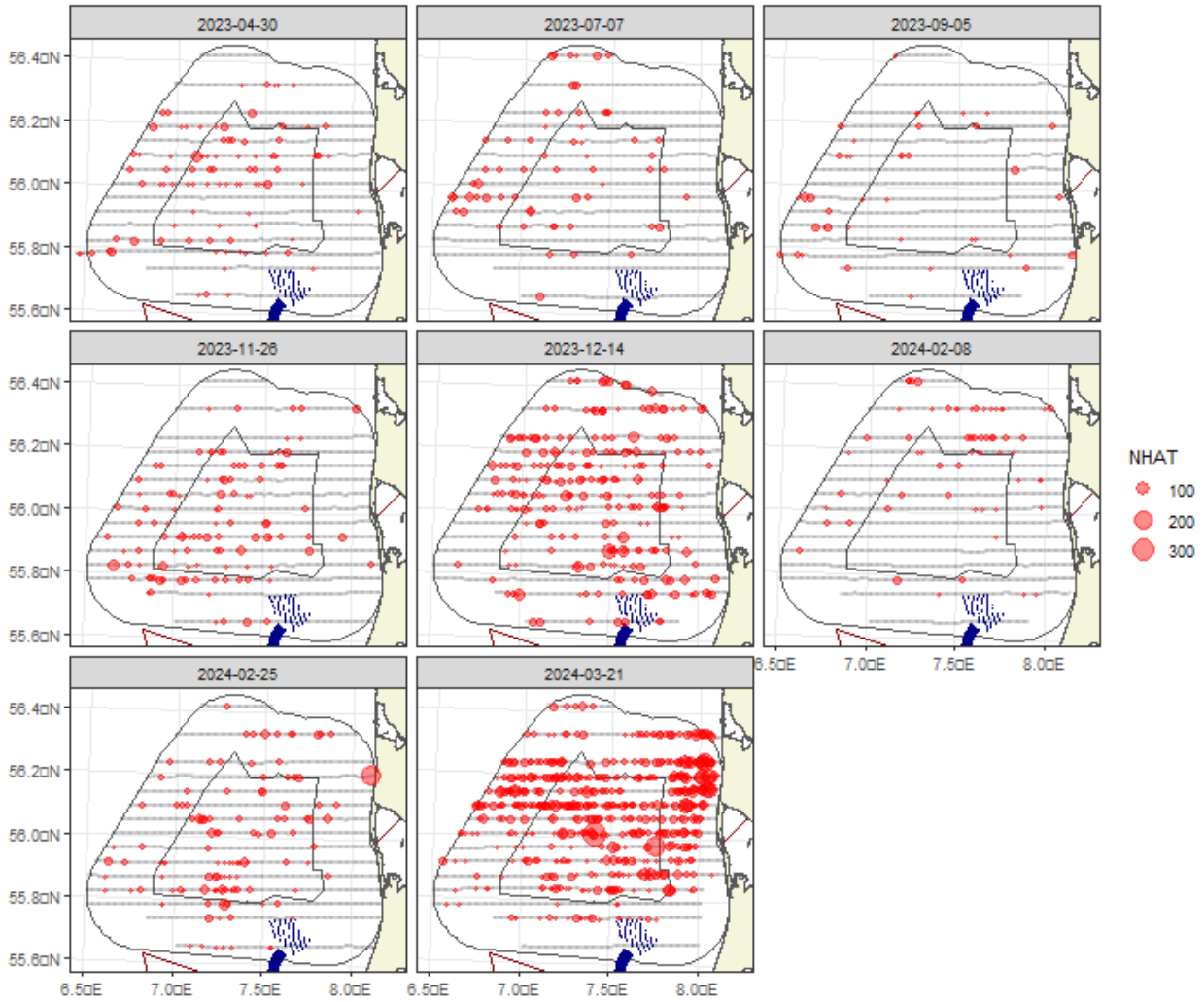

Figure 5.52 Distance-corrected counts for the razorbill/common guillemot species group across the eight surveys. The red circles indicate the distance-corrected counts along the transect lines. The grey dots are segments with a count of zero.

5.1.9.3 Model selection

For all but one survey, the models selected included a spatial term (of varying complexity). In contrast, the depth covariate (either as a linear or smooth term) was not selected for any surveys. The distance to the coast covariate was selected as a linear term for one model and as a smooth term for one model. This shows compelling evidence for non-uniform spatial patterns in almost all surveys. However, given these spatial patterns, there was no depth relationship and limited evidence for a distance to the coast relationship. The spatial surfaces selected ranged from 3 to 15 parameters for the spatial term (Table 5.8).

Table 5.8 Model selection results for razorbill/common guillemot for each survey. The model column represents the terms in the model.

Name	Model	Distribution	Variable 1D	Variable 2D	Number of parameters	Dispersion parameter	Tweedie parameter
2023-04-30	2D only	Tweedie	NA	s(x,y, df=5)	6	13.5	1.17
2023-07-07	2D only	Tweedie	NA	s(x,y, df=12)	13	9.6	1.20
2023-09-05	2D only	Tweedie	NA	s(x,y, df=10)	11	17.7	1.26

Name	Model	Distribution	Variable 1D	Variable 2D	Number of parameters	Dispersion parameter	Tweedie parameter
2023-11-26	Best 1D2D	Tweedie	distcoast, df=1	s(x,y, df=9)	11	17.8	1.26
2023-12-14	2D only	Tweedie	NA	s(x,y, df=4)	5	20.4	1.28
2024-02-08	2D only	quasipoisson	NA	s(x,y, df=9)	10	5.7	NA
2024-02-25	2D only	Tweedie	NA	s(x,y, df=5)	6	25.7	1.39
2024-03-21	2D only	Tweedie	NA	s(x,y, df=14)	15	15.5	1.42

The estimated abundances, densities and associated 95% confidence intervals for each month are given in Table 5.9 and Figure 5.53.The lowest estimated total number within the survey area was 971 birds in September 2023, while the highest number was 35,069 birds in March 2024. The estimated total number for March 2023 was almost a factor of 10 higher than for the other surveys.

Table 5.9 Estimated abundance and density of razorbill/common guillemot for each survey. The 95% CI is a percentile-based confidence interval.

Month	Area (km²)	Estimation type	Estimated count	95% CI count	Estimated density	95% CI density
2023-04-30	7,833	Spatial	3,365	(1,794, 6,785)	0.4	(0.2, 0.9)
2023-07-07	7,833	Spatial	2,064	(1,192, 3,929)	0.3	(0.2, 0.5)
2023-09-05	7,833	Spatial	971	(417, 2,634)	0.1	(0.1, 0.3)
2023-11-26	7,833	Spatial	2,974	(1,551, 7,037)	0.4	(0.2, 0.9)
2023-12-14	7,833	Spatial	9,474	(6,584, 13,888)	1.2	(0.8, 1.8)
2024-02-08	7,833	Spatial	2,617	(1,511, 5,105)	0.3	(0.2, 0.7)
2024-02-25	7,833	Spatial	5,839	(3,050, 12,141)	0.7	(0.4, 1.5)
2024-03-21	7,833	Spatial	35,069	(23,704, 53,636)	4.5	(3, 6.8)

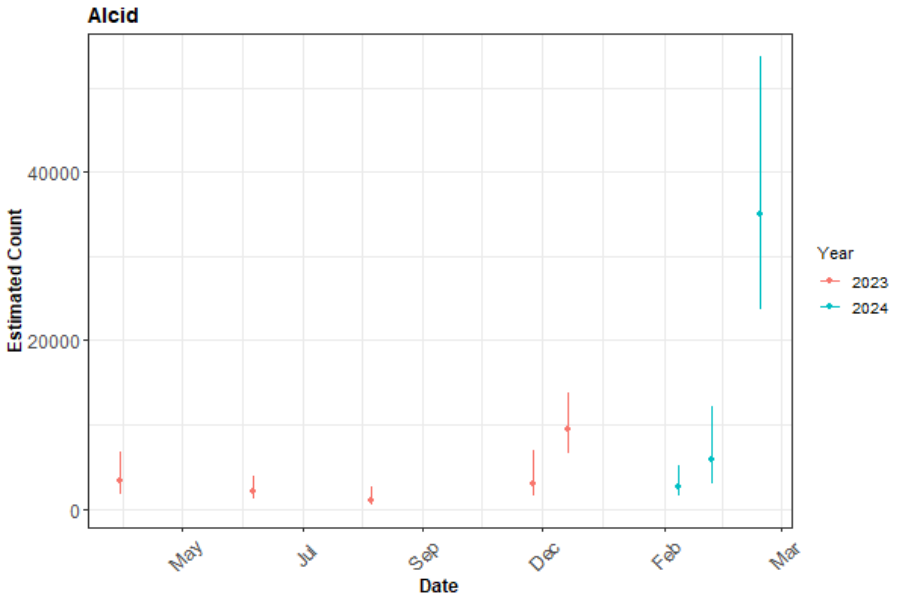

Figure 5.53 The estimated count of razorbill/common guillemot for each survey. The 95% CI are percentile-based confidence intervals are from a parametric bootstrap with 500 replicates.

5.1.9.4 Spatial results

Figure 5.54 and Figure 5.55 show the estimated razorbill/common guillemot counts in each 1 km^2 grid cell for each month. The first figure shows the surfaces on the same scale, which masks the patterns in all but one survey due to the large number of birds seen in the last survey. Figure 5.55 shows the estimated counts without the last survey included. Generally, the estimated abundances fitted well with the raw data, and there were no notable misalignments. In areas where the estimated counts were systematically higher, the abundances were also relatively high, and there were no areas with large, estimated abundances unsupported by the data.

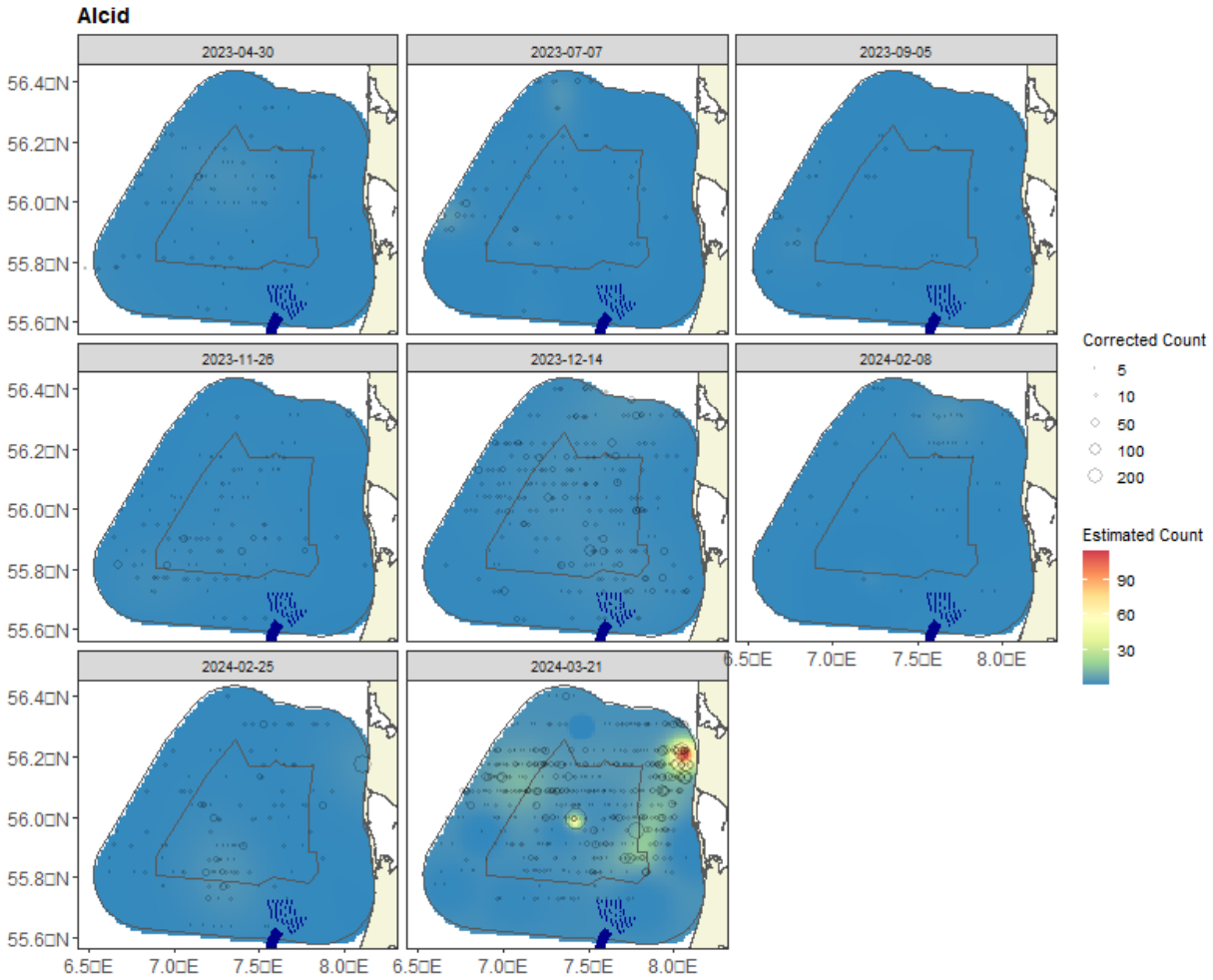

Figure 5.54 Figure showing the estimated razorbill/common guillemot abundance across the study site for each survey. The estimated counts are per 1 km x 1 km grid cell. The open circles show the corrected counts.

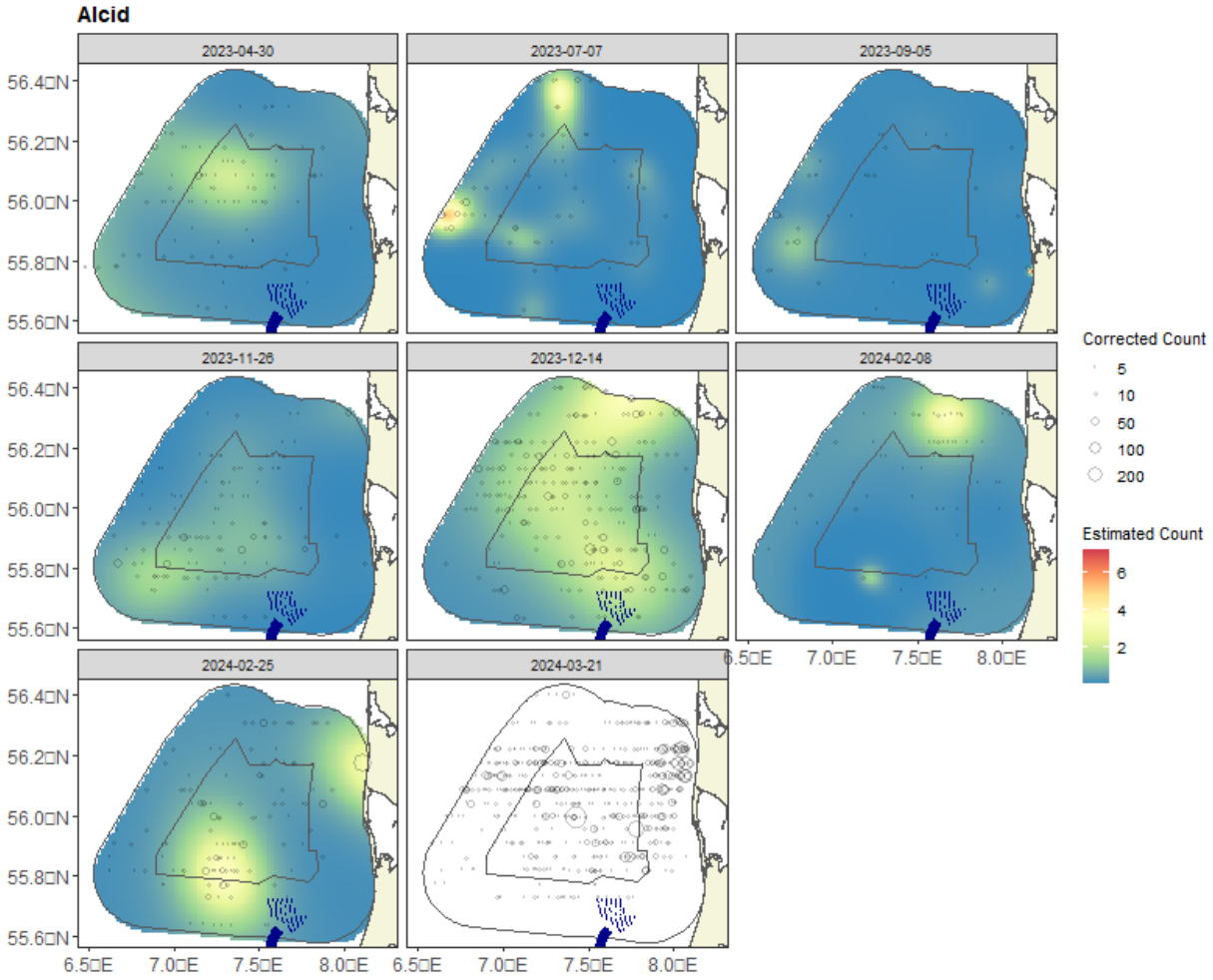

Figure 5.55 Figure showing the estimated razorbill/common guillemot abundance across the study site for each survey except the high abundance last one. The estimated counts are per 1 km x 1 km grid cell. The open circles show the corrected counts.

5.1.9.5 Uncertainty in spatial predictions

Broadly, the highest coefficient of variation (CoV) scores were associated with the `almost zero' predictions, and it is known that the CoV metric is highly sensitive to any uncertainty for very small predictions. There was no material over-lap between the high values of the CoV metric and the transect lines/locations with non-zero counts. Therefore, there were no concerns in this case (Figure 5.56).

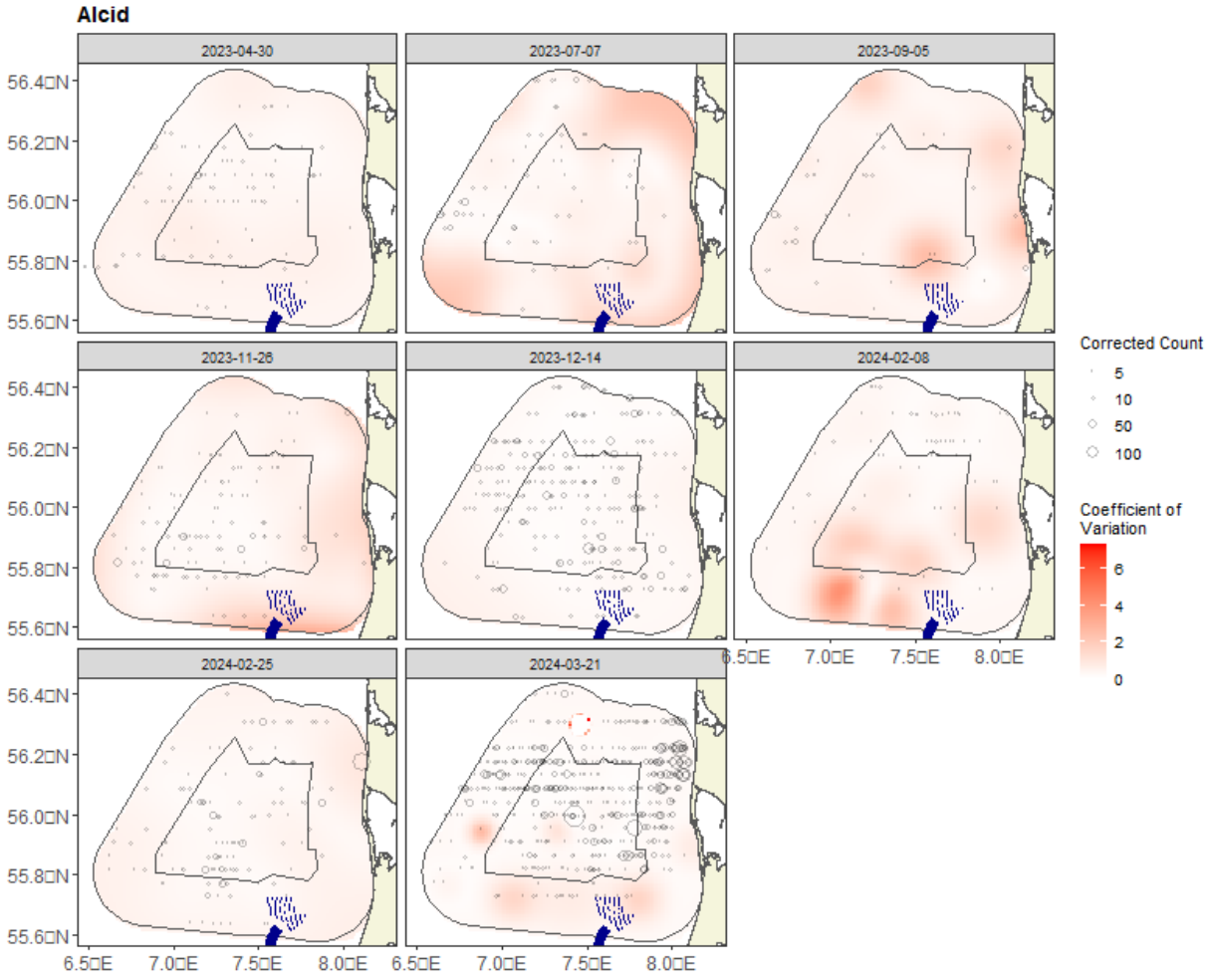

Figure 5.56 Figure showing the coefficient of variation (CoV) across the study region for each survey. The open circles show the distance corrected counts. The presence of dark red CoV scores in areas with virtually zero predictions is an artefact of the very small prediction rather than of any notable concern.

5.1.9.6 Model diagnostics

A blocking structure was used to account for potential residual non-independence for each model, and a robust standard error approach was based on unique transects. In each case, a reassuring decay to zero was seen (indicated by the red and grey lines Figure 5.57), implying that an appropriate blocking structure was used. All the plots in Figure 5.58 and Figure 5.59 are examples from the 8 razorbill/common guillemot models. A full set for all models is available on request.

The assumed mean-variance relationship was examined, and agreement was generally shown between the assumed (red) lines and the observed values. Figure 5.58 and Figure 5.59 show example relationships for a quasi-Poisson and Tweedie model. The example DHARMa diagnostic plots show that the distributional assumption for the model is appropriate and that the model is correctly specified.

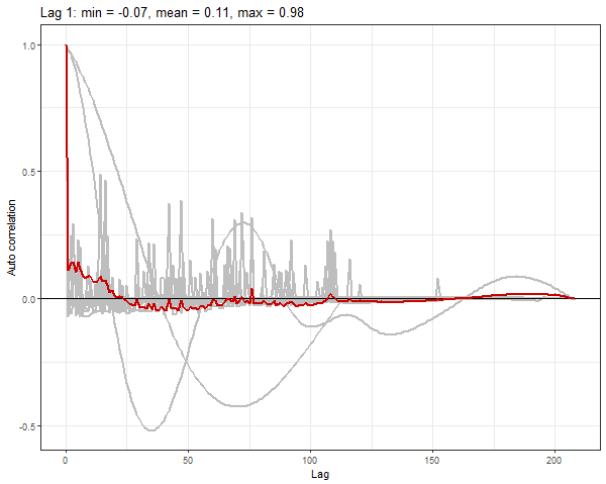

Figure 5.57 Example ACF plot. The grey lines represent the residual correlation observed in each transect, and the red line is the average of these values across transects.

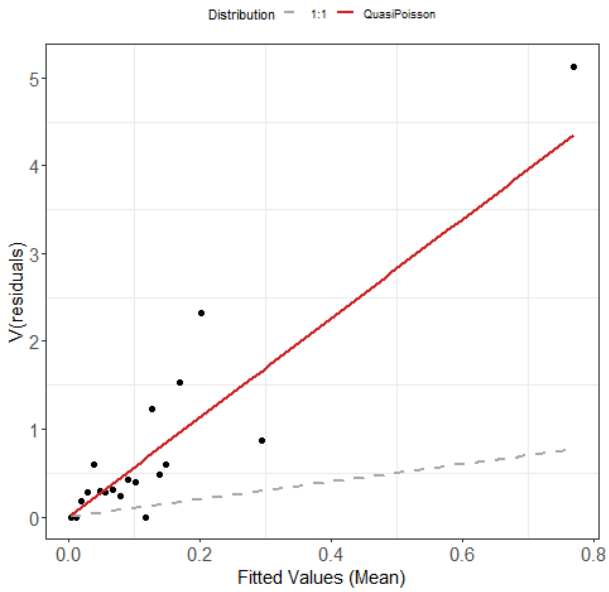

Figure 5.58 Example plot showing the estimated quasi-Poisson mean-variance relationship (red line) and actual (black dots). The black dots are based on 20 quantiles of the model residuals, and for reference, the grey dashed line shows the 1:1 relationship.

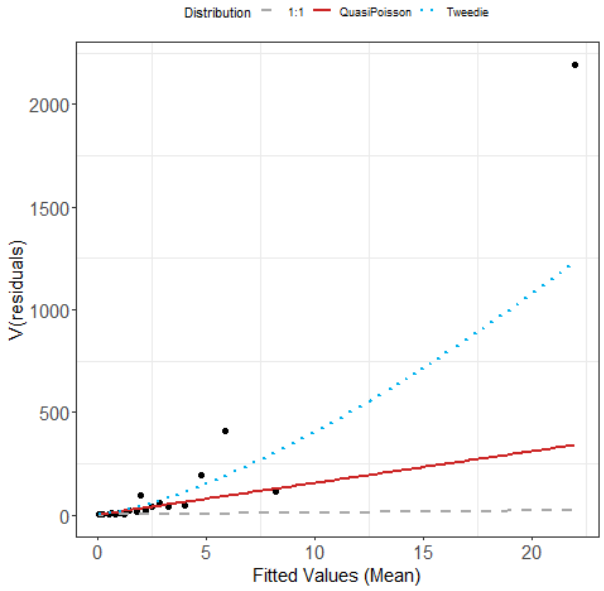

Figure 5.59 Example plot showing the estimated Tweedie mean-variance relationship (blue dashed line). The red line shows the V(μ)=ϕμ relationship, and the grey line shows the 1:1 relationship.

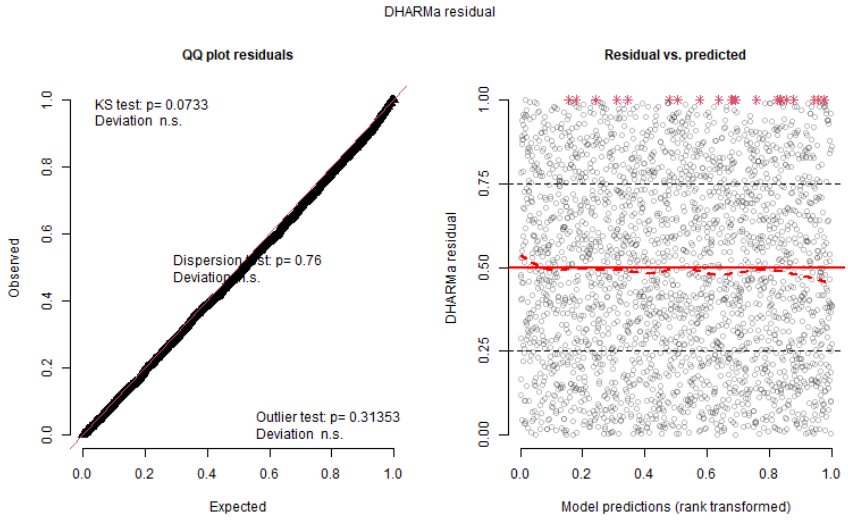

Figure 5.60 Example diagnostics. QQplot and residuals against predicted values. The red stars are outliers and the red line is a smooth spline around the mean of the residuals.

5.1.9.7 Areas of persistence

Across the eight surveys, there is moderate to low persistence for razorbills/common guillemots across the survey area (Figure 5.61). The highest persistence (~46%) occurs in the central and northern parts of the study area. The distribution of razorbills/common guillemots can vary considerably between surveys. Therefore, the persistence in spatial distribution across more surveys indicate that the birds do not select for any highly specific parts of the survey area.

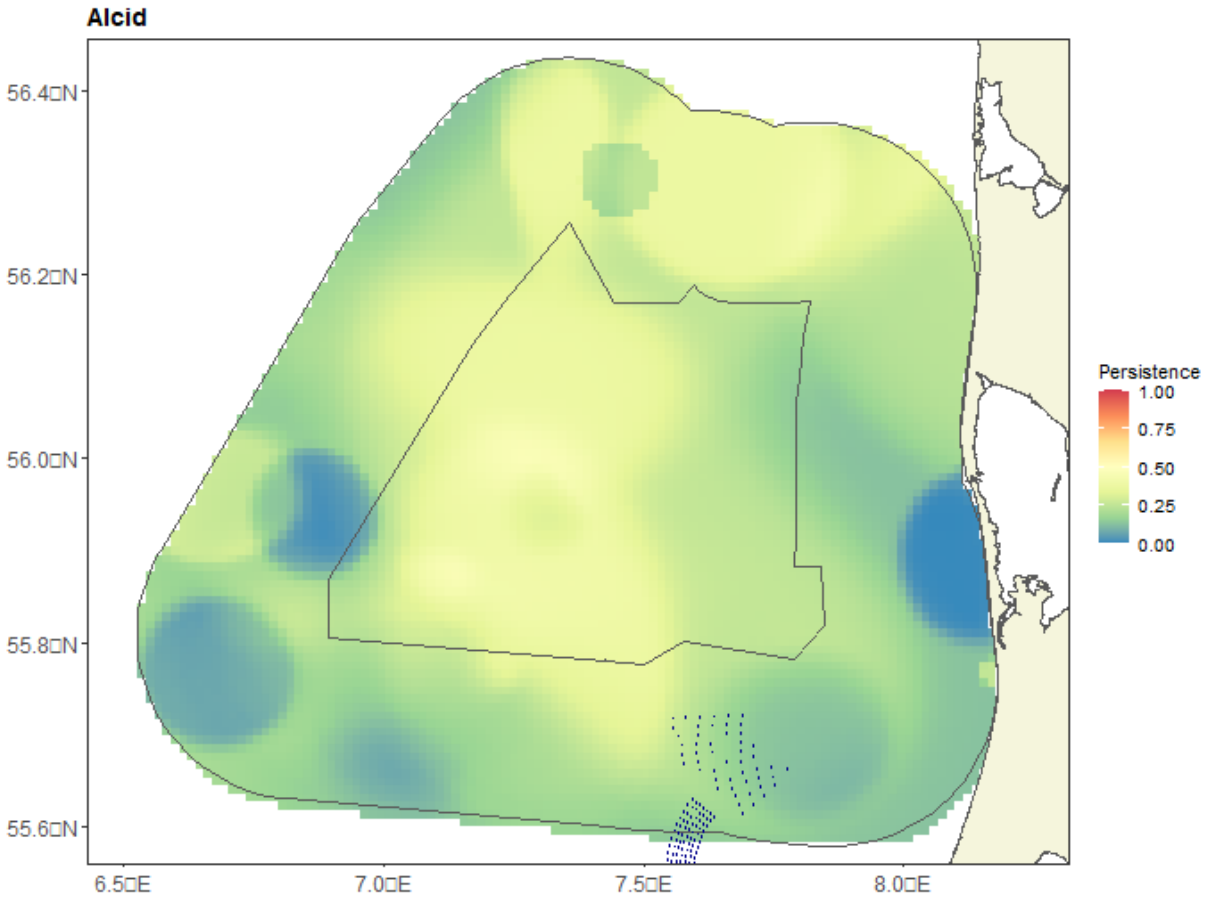

Figure 5.61 Persistence scores for razorbill/common guillemot across the eight surveys. The polygon represents the pre-investigation area (black line).

5.2 Ship-based surveys

The eight ship-based surveys in the North Sea I pre-investigation area resulted in 3,445 observations and 3,206 flight altitude recordings of 8,070 individuals and 94 species or species groups (Table 5.10). On average, each survey resulted in 430.6 (± 53.5) observations of 1,008.8 (± 189.2) individuals and 31.6 (± 4.9) species or species groups. Furthermore, flight altitude was, on average, recorded for 400.8 (± 50.2) observations during each survey. A comprehensive list of all species observed during ship-based surveys is provided in Appendix Table 8.8.

Table 5.10 Results of the eight ship-based surveys conducted in the North Sea I pre-investigation area. The table shows the number of observations (N = 3,445) and flight altitude recordings (N = 3,206) made, as well as the number of individuals (N = 8,070) and species (N = 94) observed.

Survey ID	Observations	Altitude recordings	Individuals	Species
S1	638	620	1418	39
S2	394	357	751	47
S3	465	427	790	20
S4	492	430	1480	28
S5	579	533	1194	50
S6	292	281	433	38

Survey ID	Observations	Altitude recordings	Individuals	Species
S7	418	398	1755	16
S8	167	160	249	15

Surveys at each observation position resulted in approximately an equal number of observations (Appendix Table 8.4), flight altitude recordings (Appendix Table 8.5), and an equal number of individuals (Appendix Table 8.6) and species (Appendix Table 8.7) observed. Each survey resulted in, on average, 154.6 (± 27.3), 146.4 (± 27.7), and 187.5 (± 43.4) observations and 122.9 (± 21.6), 122.8 (± 21.6), and 155.4 (± 40.3) flight altitude recordings from the North, Southeast, and Southwest observation positions, respectively. Similarly, each survey resulted in, on average, 287 (± 80.4), 372 (± 158.0), and 364.5 (± 108.4) individuals and 18.3 (± 3.9), 18.9 (± 3.5), and 19.5 (± 4.4) species observed from the North, Southeast, and Southwest observation positions, respectively. Overall, 31.1%, 29.7% and 39.2% of the observations, and 30.7%, 30.6% and 38.8% of the flight altitude recordings were made at the North, Southeast and Southwest observation positions, respectively. Furthermore, 28.1%, 36.4% and 35.6% of the individuals and 66.3%, 61.1% and 65.3% of the species were observed at the North, Southeast and Southwest observation positions, respectively.

5.2.1 Bird flight altitude

This chapter presents the flight altitude distribution of bird species observed during the ship-based surveys across altitude intervals ranging from 0 to 250 m above sea level. During the ship-based surveys, observers recorded 3,170 flight altitudes of the selected species and species groups. Of these altitude recordings, 229 were measurements (7.2%), whereas 2,941 were estimates (92.8%).

Observed birds showed a pronounced preference for lower flight altitudes, with 84% of all birds recorded within the 0-25 m altitude interval (Table 5.11). For example, northern fulmars and common scoters were all observed flying within the lowest altitude interval. While some species, such as gulls, waders and skuas, displayed a more varied flight altitude distribution, the numbers of birds flying above 100 m remained relatively small. Consequently, observations above this altitude accounted for less than 1% of the total. The subsequent subchapters provide a detailed analysis of the flight altitude distribution for the most observed species and species groups.

Table 5.11 Flight altitudes of species and species groups observed during the eight ship-based surveys conducted in the North Sea I pre-investigation area. The table shows the number of observed individuals within each 25 m flight altitude interval (N = 3,170).

Species	Altitude interval (m)										Total
	0-25	26-50	51-75	76-100	101-125	126-150	151-175	176-200	201-225	226-250	
Auks	470	1	0	0	0	0	0	0	0	0	471
Divers	77	17	2	0	0	0	0	0	0	0	96
Great black-backed gull	72	27	12	2	0	2	0	0	0	0	115
Lesser black-backed gull	525	214	50	15	4	1	0	0	0	0	809
Northern fulmar	153	0	0	0	0	0	0	0	0	0	153
Petrels	12	0	0	0	0	0	0	0	0	0	12
Terns	952	25	5	0	0	0	0	0	0	0	982
Common gull	219	30	6	3	0	1	0	0	0	0	259
European herring gull	161	69	14	6	0	4	0	0	0	0	254
Ducks	65	24	0	0	0	0	0	0	0	0	89
Passerines	571	144	3	6	0	0	0	0	0	0	724
Waders	230	4	8	0	6	1	0	0	0	0	249

Common scoter	206	0	0	0	0	0	0	0	0	0	206
Northern gannet	415	43	5	0	0	0	0	0	0	0	463
Black-legged kittiwake	301	31	5	3	2	0	0	0	0	0	342
Gulls	49	23	12	8	0	0	0	1	1	1	95
Skuas	17	2	0	2	0	0	0	0	0	1	22
Total (individuals)	**4,495**	**654**	**122**	**45**	**12**	**9**	**0**	**1**	**1**	**2**	**5,341**
Total (proportion %)	**84.16**	**12.24**	**2.28**	**0.84**	**0.22**	**0.17**	**0.00**	**0.02**	**0.002**	**0.004**	

5.2.1.1 Auks

Auk flight altitudes were analysed by pooling observations of common guillemots, black guillemots and razorbills. In total, flight altitude was recorded during 324 observations, encompassing 471 individuals. Auks were predominantly observed flying alone (79.9%) or in pairs (10.2%), resulting in an average flock size of 1.5 (± 0.1) individuals. The largest flock of auks observed consisted of 20 common guillemots. Auks flew almost exclusively at altitudes below 25 m (99.8%), with the highest recorded flight altitude being a common guillemot at 30 m (Table 5.10; Figure 5.62).

Table 5.12 Auk flight altitudes recorded during the eight ship-based surveys conducted in the North Sea I pre-investigation area. The table shows the number and proportion of observations (N = 324) and individuals (N = 471) within each 25 m flight altitude interval.

Altitude interval (m)	Observations		Individuals	
	Total	Proportion	Total	Proportion
0-25	323	0.997	470	0.998
26-50	1	0.003	1	0.002
51-75	0	0.000	0	0.000
76-100	0	0.000	0	0.000
101-125	0	0.000	0	0.000
126-150	0	0.000	0	0.000
151-175	0	0.000	0	0.000
176-200	0	0.000	0	0.000
201-225	0	0.000	0	0.000
226-250	0	0.000	0	0.000

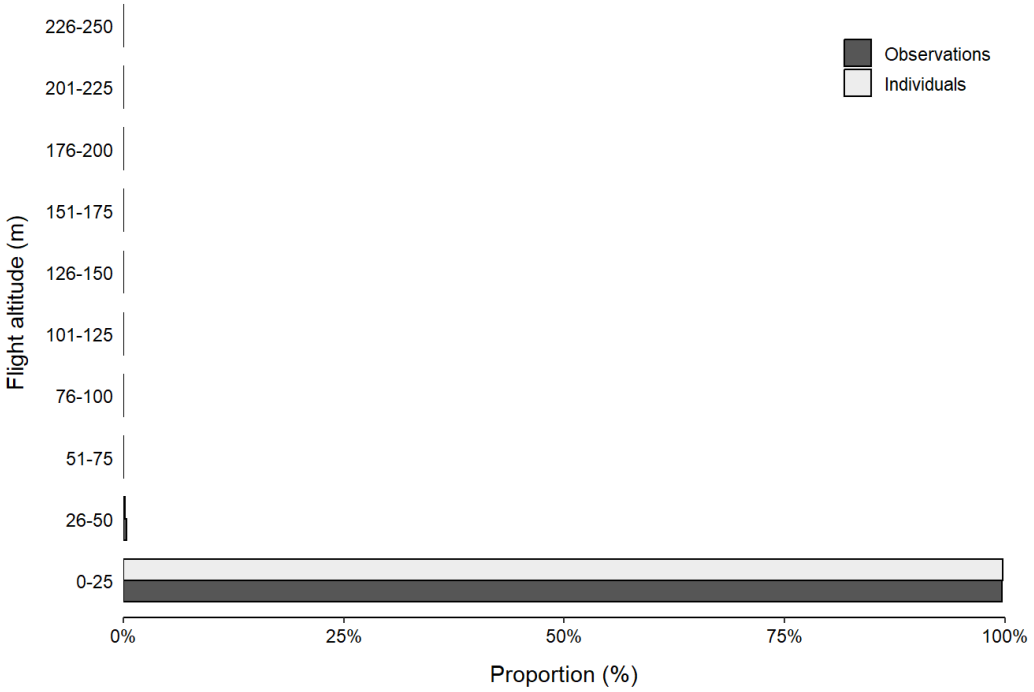

Figure 5.62 Auk flight altitudes recorded during the eight ship-based surveys conducted in the North Sea I pre-investigation area. The figure shows the proportion of observations (N = 324) and individuals (N = 471) within each 25 m flight altitude interval.

5.2.1.2 Divers

Diver flight altitudes were analysed by pooling observations of black-throated, red-throated, and unidentified divers (diver sp.). In total, flight altitude was recorded during 71 observations, encompassing 96 individuals. Divers were predominantly observed flying alone (78.9%) or in pairs (14.1%), with an average flock size of 1.4 (± 0.1) individuals. The largest diver flock observed consisted of 5 red-throated divers. Divers flew predominantly at altitudes below 50 m (97.9%), with most individuals flying below 25 m (80.2%) (Table 5.13; Figure 5.63). The highest recorded flight altitude was a red-throated diver at 70 m.

Table 5.13 Diver flight altitudes recorded during the eight ship-based surveys conducted in the North Sea I pre-investigation area. The table shows the number and proportion of observations (N = 71) and individuals (N = 96) within each 25 m flight altitude interval.

Altitude interval (m)	Observations		Individuals	
	Total	Proportion	Total	Proportion
0-25	60	0.845	77	0.802
26-50	10	0.141	17	0.177
51-75	1	0.014	2	0.021
76-100	0	0.000	0	0.000
101-125	0	0.000	0	0.000
126-150	0	0.000	0	0.000
151-175	0	0.000	0	0.000
176-200	0	0.000	0	0.000
201-225	0	0.000	0	0.000
226-250	0	0.000	0	0.000

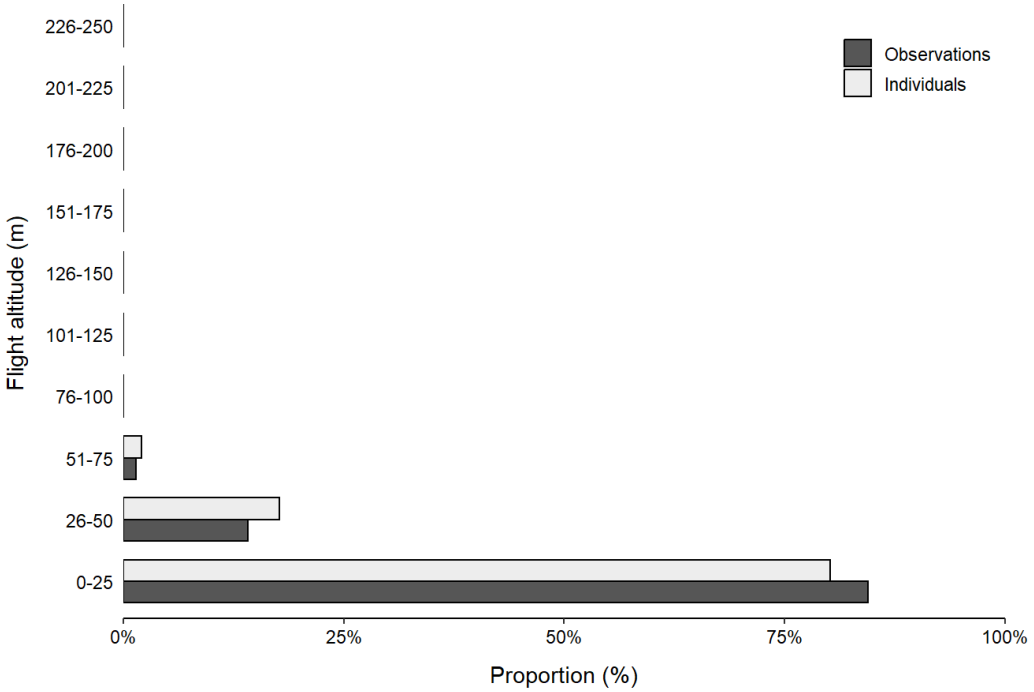

Figure 5.63. Diver flight altitudes recorded during the eight ship-based surveys conducted in the North Sea I pre-investigation area. The figure shows the proportion of observations (N = 71) and individuals (N = 96) within each 25 m flight altitude interval.

5.2.1.3 Great black-backed gull

In total, flight altitude was recorded for 101 observations of great black-backed gulls, encompassing 115 individuals. Great black-backed gulls were predominantly observed flying alone (90.1%) or in pairs (7.9%), resulting in an average flock size of 1.1 (± 0.1) individuals. The largest great black-backed gull flock observed consisted of five individuals. Great black-backed gulls predominantly flew at altitudes below 50 m (86.1%), with a small number of individuals flying between 51-150 m (Table 5.14; Figure 5.64). The highest recorded great black-backed gull flight altitude was 130 m.

Table 5.14. Great black-backed gull flight altitudes recorded during the eight ship-based surveys conducted in the North Sea I pre-investigation area. The table shows the number and proportion of observations (N = 101) and individuals (N = 115) within each 25 m flight altitude interval.

Altitude interval (m)	Observations		Individuals	
	Total	Proportion	Total	Proportion
0-25	61	0.604	72	0.626
26-50	26	0.257	27	0.235
51-75	11	0.109	12	0.104
76-100	2	0.020	2	0.017
101-125	0	0.000	0	0.000
126-150	1	0.010	2	0.017
151-175	0	0.000	0	0.000
176-200	0	0.000	0	0.000

201-225	0	0.000	0	0.000
226-250	0	0.000	0	0.000

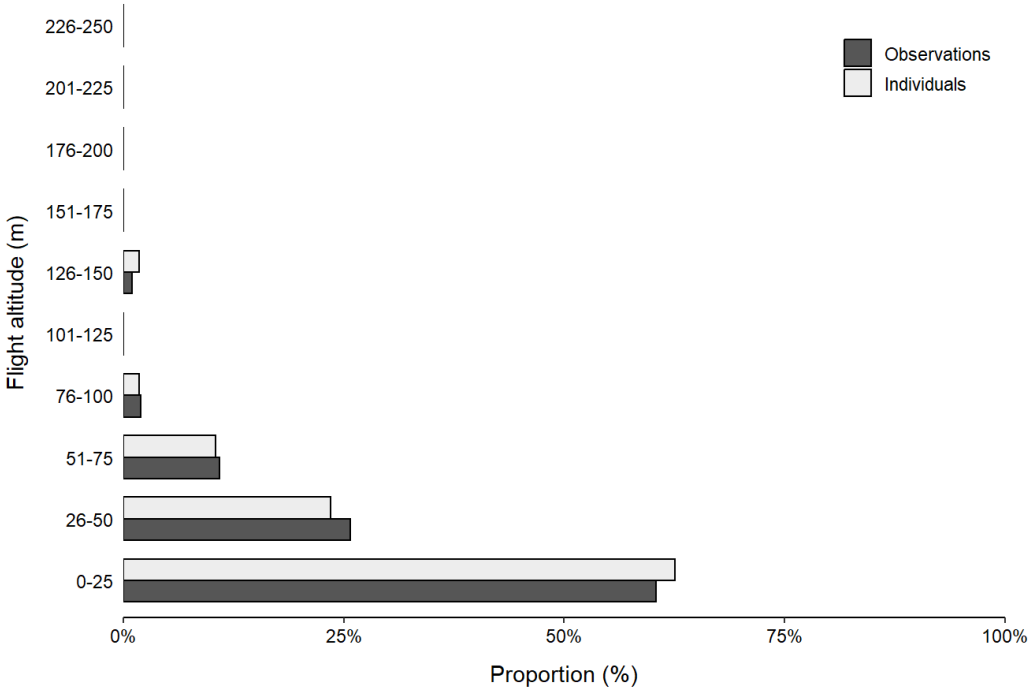

Figure 5.64. Great black-backed gull flight altitudes recorded during the eight ship-based surveys conducted in the North Sea I pre-investigation area. The figure shows the proportion of observations (N = 101) and individuals (N = 115) within each 25 m flight altitude interval.

5.2.1.4 Lesser black-backed gull

In total, flight altitude was recorded during 589 observations of lesser black-backed gulls, encompassing 809 individuals. Lesser black-backed gulls were predominantly observed flying alone (87.3%), in pairs (6.6%) or small flocks, with an average flock size of 1.4 (± 0.1) individuals. The largest lesser black-backed gull flock observed consisted of 37 individuals. Lesser black-backed gulls flew predominantly at altitudes below 50 m (91.4%), with a small number of individuals flying between 51-150 m (Table 5.15; Figure 5.65). The highest recorded Lesser Black-backed Gull flight altitude was 150 m.

Table 5.15 Lesser black-backed gull flight altitudes recorded during the eight ship-based surveys conducted in the North Sea I pre-investigation area. The table shows the number and proportion of observations (N = 589) and individuals (N = 809) within each 25 m flight altitude interval.

Altitude interval (m)	Observations		Individuals	
	Total	Proportion	Total	Proportion
0-25	331	0.562	525	0.649
26-50	200	0.340	214	0.265
51-75	38	0.065	50	0.062
76-100	15	0.025	15	0.019

101-125	4	0.007	4	0.005
126-150	1	0.002	1	0.001
151-175	0	0.000	0	0.000
176-200	0	0.000	0	0.000
201-225	0	0.000	0	0.000
226-250	0	0.000	0	0.000

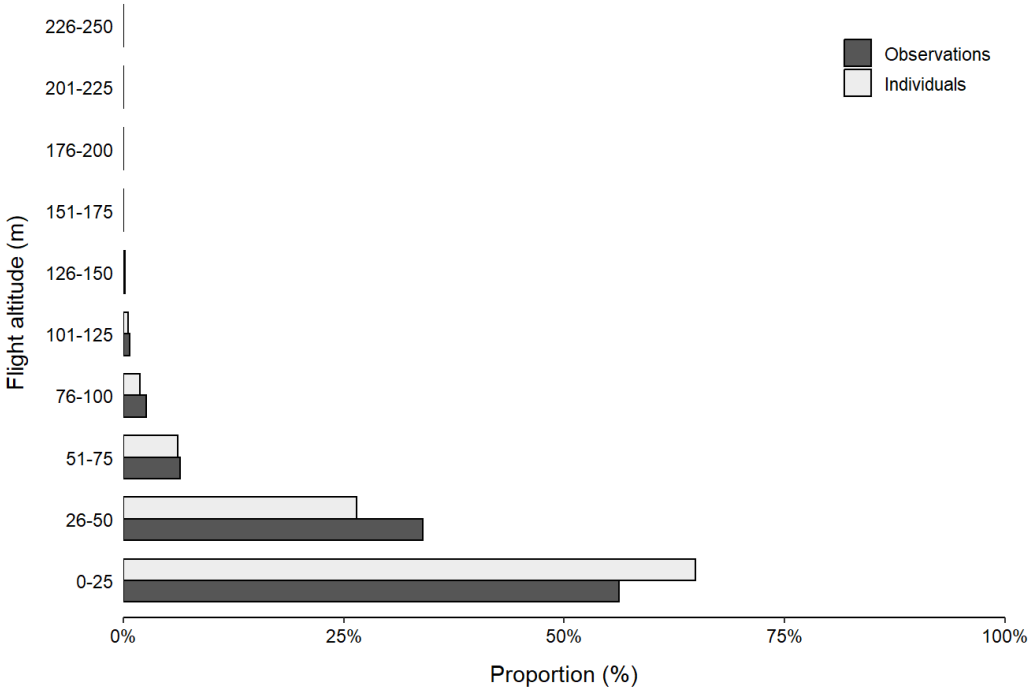

Figure 5.65 Lesser black-backed gull flight altitudes recorded during the eight ship-based surveys conducted in the North Sea I pre-investigation area. The figure shows the proportion of observations (N = 589) and individuals (N = 809) within each 25 m flight altitude interval.

5.2.1.5 Northern fulmar

In total, flight altitude was recorded for 146 observations of northern fulmars, encompassing 153 individuals. Northern fulmars were almost exclusively observed flying alone (96.6%), with the largest flock observed consisting of 4 individuals. Northern fulmars were predominantly observed flying close to the sea surface and solely flew at altitudes below 25 m, with the highest recorded flight altitude being 15 m (Table 5.16; Figure 5.66).

Table 5.16. Northern fulmar flight altitudes recorded during the eight ship-based surveys conducted in the North Sea I pre-investigation area. The table shows the number and proportion of observations (N = 146) and individuals (N = 153) within each 25 m flight altitude interval.

Altitude interval (m)	Observations		Individuals	
	Total	Proportion	Total	Proportion
0-25	146	1.000	153	1.000
26-50	0	0.000	0	0.000

51-75	0	0.000	0	0.000
76-100	0	0.000	0	0.000
101-125	0	0.000	0	0.000
126-150	0	0.000	0	0.000
151-175	0	0.000	0	0.000
176-200	0	0.000	0	0.000
201-225	0	0.000	0	0.000
226-250	0	0.000	0	0.000

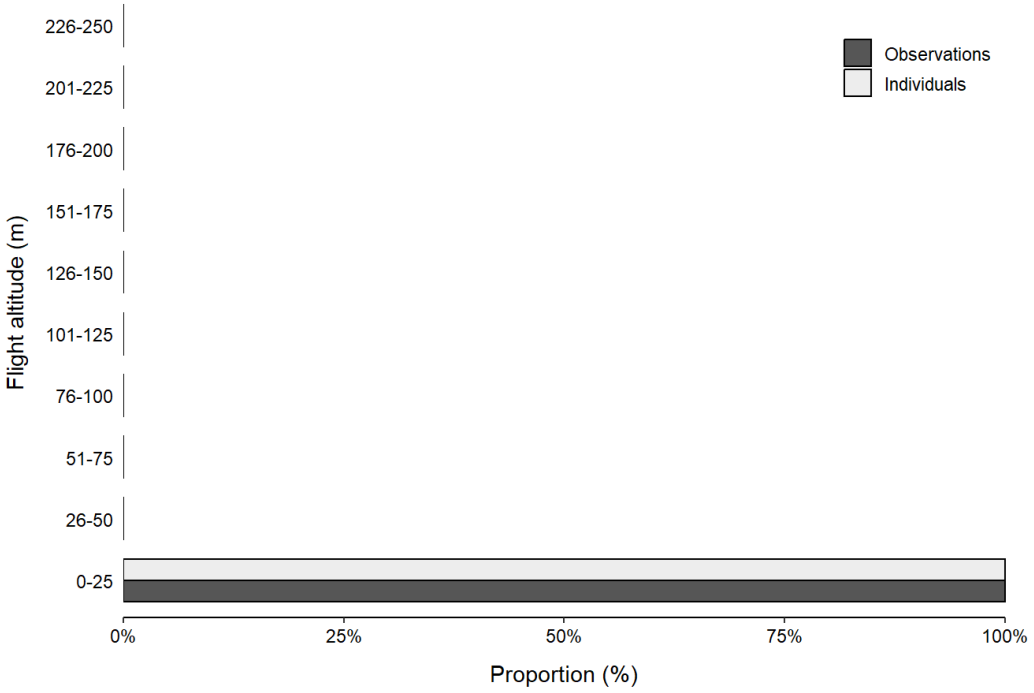

Figure 5.66 Northern fulmar flight altitudes recorded during the eight ship-based surveys conducted in the North Sea I pre-investigation area. The figure shows the proportion of observations (N = 146) and individuals (N = 153) within each 25 m flight altitude interval.

5.2.1.6 Petrels

Petrel flight altitudes were analysed by pooling observations of storm petrels, great shearwaters, sooty shearwaters and unidentified petrels (petrel sp.). Northern fulmars were analysed separately. In total, flight altitude was recorded during 12 observations of 12 individuals. Petrels were exclusively observed flying alone. Petrels were predominantly observed flying close to the sea surface and exclusively flew at altitudes below 25 m, with the highest recorded flight altitude being a sooty shearwater at 15 m (Table 5.17; Figure 5.67).

Table 5.17 Petrel (excluding northern fulmar) flight altitudes recorded during the eight ship-based surveys conducted in the North Sea I pre-investigation area. The table shows the number and proportion of observations (N = 12) and individuals (N = 12) within each 25 m flight altitude interval.

Altitude interval (m)	Observations		Individuals	

	Total	Proportion	Total	Proportion
0-25	12	1.000	12	1.000
26-50	0	0.000	0	0.000
51-75	0	0.000	0	0.000
76-100	0	0.000	0	0.000
101-125	0	0.000	0	0.000
126-150	0	0.000	0	0.000
151-175	0	0.000	0	0.000
176-200	0	0.000	0	0.000
201-225	0	0.000	0	0.000
226-250	0	0.000	0	0.000

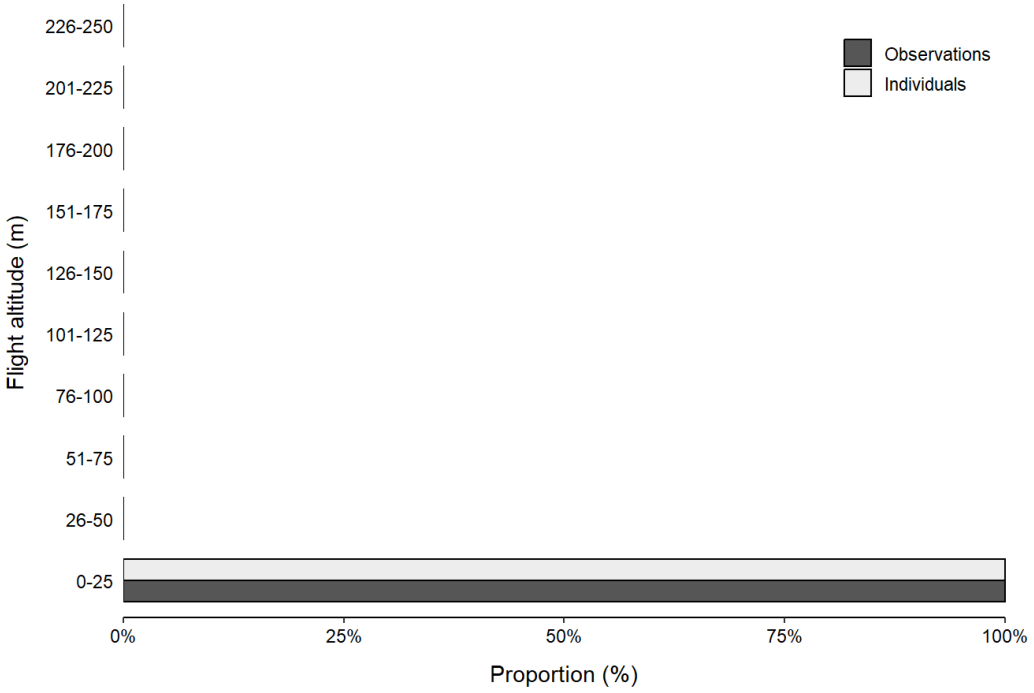

Figure 5.67 Petrel (excluding northern fulmar) flight altitudes recorded during the eight ship-based surveys conducted in the North Sea I pre-investigation area. The figure shows the proportion of observations (N = 12) and individuals (N = 12) within each 25 m flight altitude interval.

5.2.1.7 Terns

Tern flight altitudes were analysed by pooling observations of Arctic, black, common, and sandwich terns. In total, flight altitude was recorded during 375 observations, encompassing 982 individuals. Terns were predominantly observed flying alone (51.7%), in pairs (16.5%) or in small flocks, with an average flock size of 2.6 (± 0.1) individuals. The largest tern flock observed consisted of 19 common/Artic terns. Terns predominantly flew at altitudes below 25 m (96.9%), with the highest recorded flight altitude being 70 m for a sandwich tern (Table 5.18; Figure 5.68).

Table 5.18. Tern flight altitudes recorded during the eight ship-based surveys conducted in the North Sea I pre-investigation area. The table shows the number and proportion of observations (N = 375) and individuals (N = 982) within each 25 m flight altitude interval.

Altitude interval (m)	Observations		Individuals	
	Total	Proportion	Total	Proportion
0-25	365	0.973	952	0.969
26-50	8	0.021	25	0.025
51-75	2	0.005	5	0.005
76-100	0	0.000	0	0.000
101-125	0	0.000	0	0.000
126-150	0	0.000	0	0.000
151-175	0	0.000	0	0.000
176-200	0	0.000	0	0.000
201-225	0	0.000	0	0.000
226-250	0	0.000	0	0.000

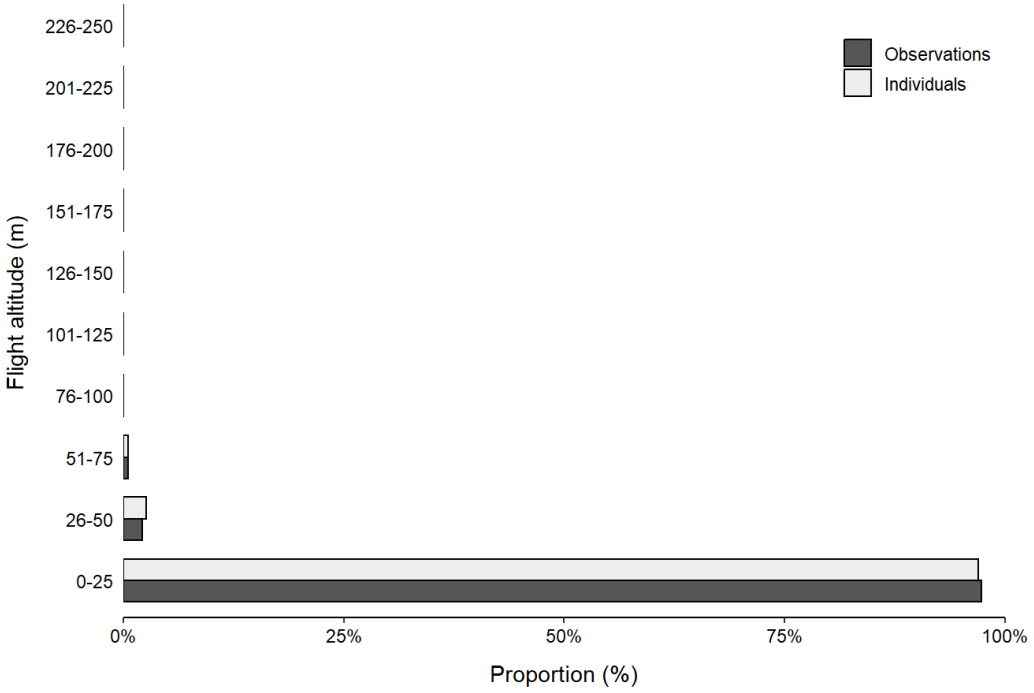

Figure 5.68 Tern flight altitudes recorded during the eight ship-based surveys conducted in the North Sea I pre-investigation area. The figure shows the proportion of observations (N = 375) and individuals (N = 982) within each 25 m flight altitude interval.

5.2.1.8 Common gull

In total, flight altitude was recorded during 181 observations of common gulls, encompassing 259 individuals. Common gulls were predominantly observed flying alone (81.8%) or in pairs (10.5%), with an average flock size of 1.4 (± 0.1) individuals. The largest common gull flock observed consisted of 13 individuals. Common gulls flew predominantly at altitudes below 50 m (96.2%), with most individuals flying below 25 m (84.6%) (Table 5.19; Figure 5.69). The highest recorded common gull flight altitude was 130 m.

Table 5.19 Common gull flight altitudes recorded during the eight ship-based surveys conducted in the North Sea I pre-investigation area. The table shows the number and proportion of observations (N = 181) and individuals (N = 259) within each 25 m flight altitude interval.

Altitude interval (m)	Observations		Individuals	
	Total	Proportion	Total	Proportion
0-25	147	0.812	219	0.846
26-50	26	0.144	30	0.116
51-75	4	0.022	6	0.023
76-100	3	0.017	3	0.012
101-125	0	0.000	0	0.000
126-150	1	0.006	1	0.004
151-175	0	0.000	0	0.000
176-200	0	0.000	0	0.000
201-225	0	0.000	0	0.000
226-250	0	0.000	0	0.000

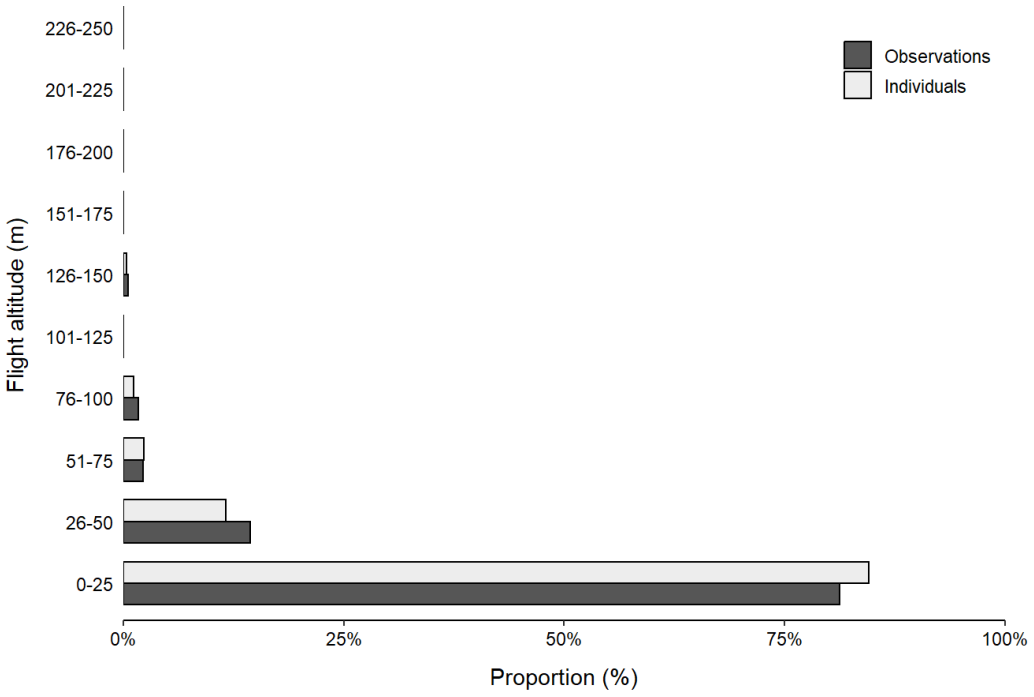

Figure 5.69 Common gull flight altitudes recorded during the eight ship-based surveys conducted in the North Sea I pre-investigation area. The figure shows the proportion of observations (N = 181) and individuals (N = 259) within each 25 m flight altitude interval.

5.2.1.9 European herring gull

In total, flight altitude was recorded during 205 observations of European herring gulls, encompassing 254 individuals. European herring gulls were predominantly observed flying alone (89.8%) or in small flocks, with an average flock size of 1.2 (± 0.1) individuals. The largest European herring gull flock observed consisted of eight individuals. European

herring gulls flew predominantly at altitudes below 50 m (90.6%), with most individuals flying below 25 m (63.4%) (Table 5.20; Figure 5.70). The highest recorded European herring gull flight altitude was 150 m.

Table 5.20 European herring gull flight altitudes recorded during the eight ship-based surveys conducted in the North Sea I pre-investigation area. The table shows the number and proportion of observations (N = 205) and individuals (N = 254) within each 25 m flight altitude interval.

Altitude interval (m)	Observations		Individuals	
	Total	Proportion	Total	Proportion
0-25	123	0.600	161	0.634
26-50	61	0.298	69	0.272
51-75	13	0.063	14	0.055
76-100	6	0.029	6	0.024
101-125	0	0.000	0	0.000
126-150	2	0.010	4	0.016
151-175	0	0.000	0	0.000
176-200	0	0.000	0	0.000
201-225	0	0.000	0	0.000
226-250	0	0.000	0	0.000

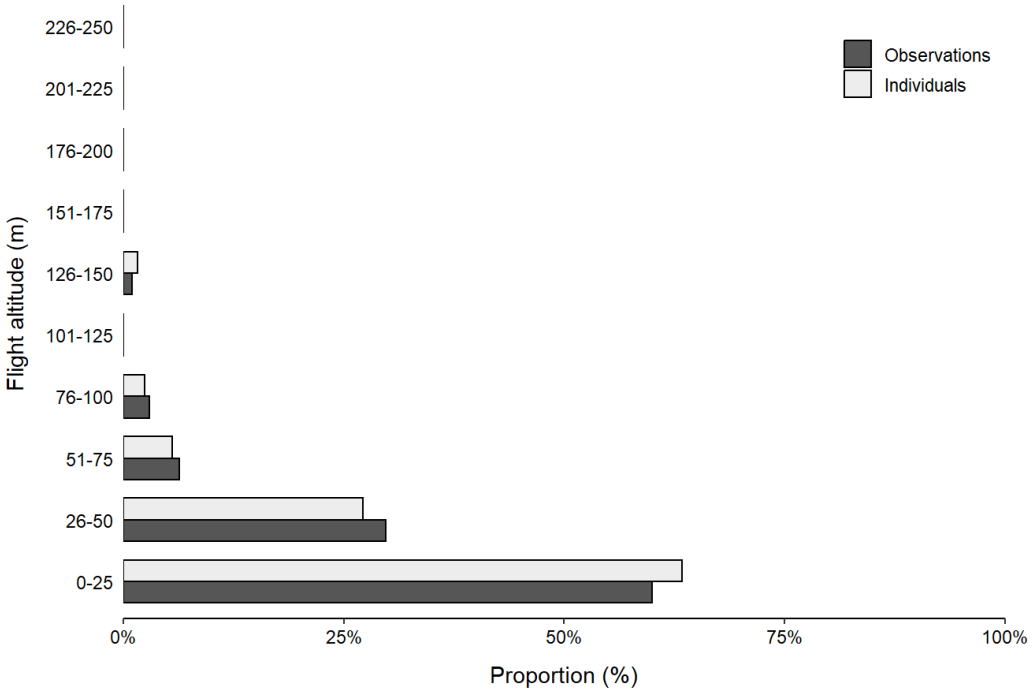

Figure 5.70 European herring gull flight altitudes recorded during the eight ship-based surveys conducted in the North Sea I pre-investigation area. The figure shows the proportion of observations (N = 205) and individuals (N = 254) within each 25 m flight altitude interval.

5.2.1.10 Ducks

Duck flight altitudes were analysed by pooling observations of northern pintails, northern shovelers, Eurasian teals, Eurasian wigeons, greater scaups and unidentified dabbling ducks (dabbling duck sp.). Common scoters were analysed separately. In total, flight altitude was recorded during 22 observations of 89 individuals. Ducks were mainly observed flying alone (45.5%) or in smaller flocks, with an average flock size of 4.0 (± 0.8) individuals. The largest duck flock observed consisted of 15 individuals of an unidentified species of dabbling duck. Ducks were predominantly observed flying at altitudes below 25 m (73%), with a small number of individuals flying at altitudes between 26-50 m (Table 5.21; Figure 5.71). The highest recorded flight altitude was an unidentified dabbling duck species flying at 50 m.

Table 5.21. Duck (excluding common scoter) flight altitudes recorded during the eight ship-based surveys conducted in the North Sea I pre-investigation area. The table shows the number and proportion of observations (N = 22) and individuals (N = 89) within each 25 m flight altitude interval.

Altitude interval (m)	Observations		Individuals	
	Total	Proportion	Total	Proportion
0-25	18	0.818	65	0.73
26-50	4	0.182	24	0.27
51-75	0	0.000	0	0.000
76-100	0	0.000	0	0.000
101-125	0	0.000	0	0.000
126-150	0	0.000	0	0.000
151-175	0	0.000	0	0.000
176-200	0	0.000	0	0.000
201-225	0	0.000	0	0.000
226-250	0	0.000	0	0.000

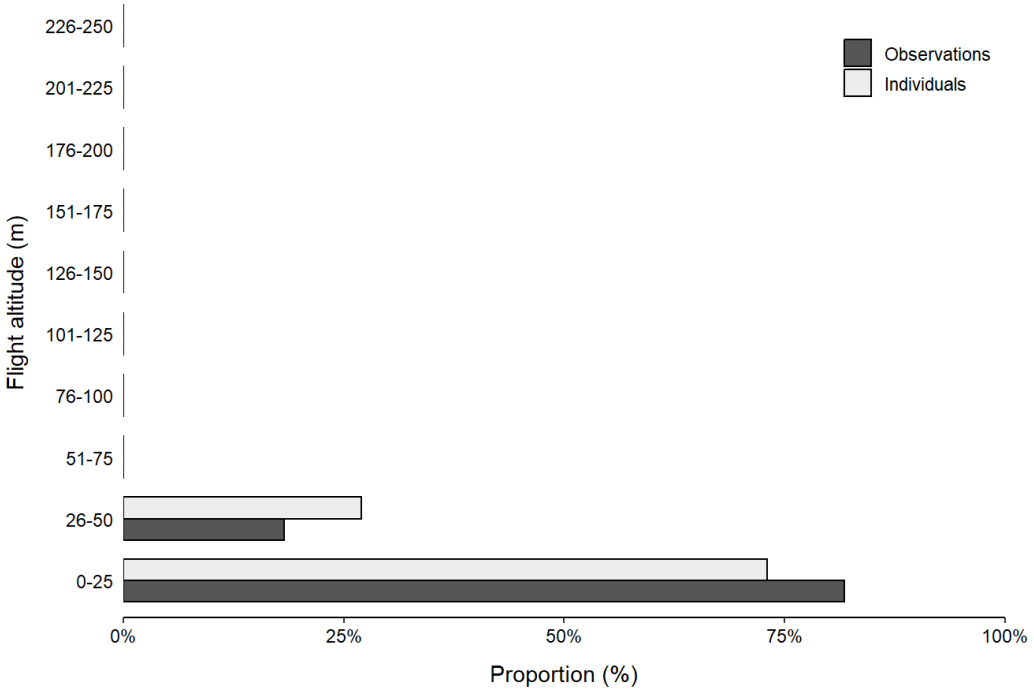

Figure 5.71. Duck (excluding common scoter) flight altitudes recorded during the eight ship-based surveys conducted in the North Sea I pre-investigation area. The figure shows the proportion of observations (N = 22) and individuals (N = 89) within each 25 m flight altitude interval.

5.2.1.11 Passerines (Passeriformes)

Passerines were the largest species group pooled during the flight altitude analyses. Passerine flight altitudes were analysed by pooling observations of lesser redpolls, Eurasian skylarks, European rock pipits, meadow pipits, western house martins, European robins, Eurasian chaffinches, bramblings, barn swallows, pied wagtails, grey wagtails, western yellow wagtails, northern wheatears, black redstarts, common redstarts, willow warblers, goldcrest, common starlings, Eurasian blackcaps, Eurasian wrens, redwings, song thrushes, fieldfares, mistle thrushes, and unidentified species of thrushes (thrush sp.), barn swallows (swallow sp.), warblers (warbler sp.) and passerines (passerine sp.). In total, flight altitude was recorded during 219 observations of 724 individuals. Passerines were mainly observed flying alone (55.3%) or in pairs (13.7%), resulting in an average flock size of 3.3 (± 0.4) individuals. The largest passerine flock observed consisted of 16 Starlings. Passerines were predominantly observed flying at altitudes below 50 m (98.8%), with the majority flying at altitudes below 25 m (78.9%) (Table 5.22; Figure 5.72). The highest recorded flight altitude was a western house martin flying at 100 m.

Table 5.22 Passerine flight altitudes recorded during the eight ship-based surveys conducted in the North Sea I pre-investigation area. The table shows the number and proportion of observations (N = 219) and individuals (N = 724) within each 25 m flight altitude interval.

Altitude interval (m)	Observations		Individuals	
	Total	Proportion	Total	Proportion
0-25	191	0.872	571	0.789
26-50	23	0.105	144	0.199
51-75	3	0.014	3	0.004
76-100	2	0.009	6	0.008

101-125	0	0.000	0	0.000
126-150	0	0.000	0	0.000
151-175	0	0.000	0	0.000
176-200	0	0.000	0	0.000
201-225	0	0.000	0	0.000
226-250	0	0.000	0	0.000

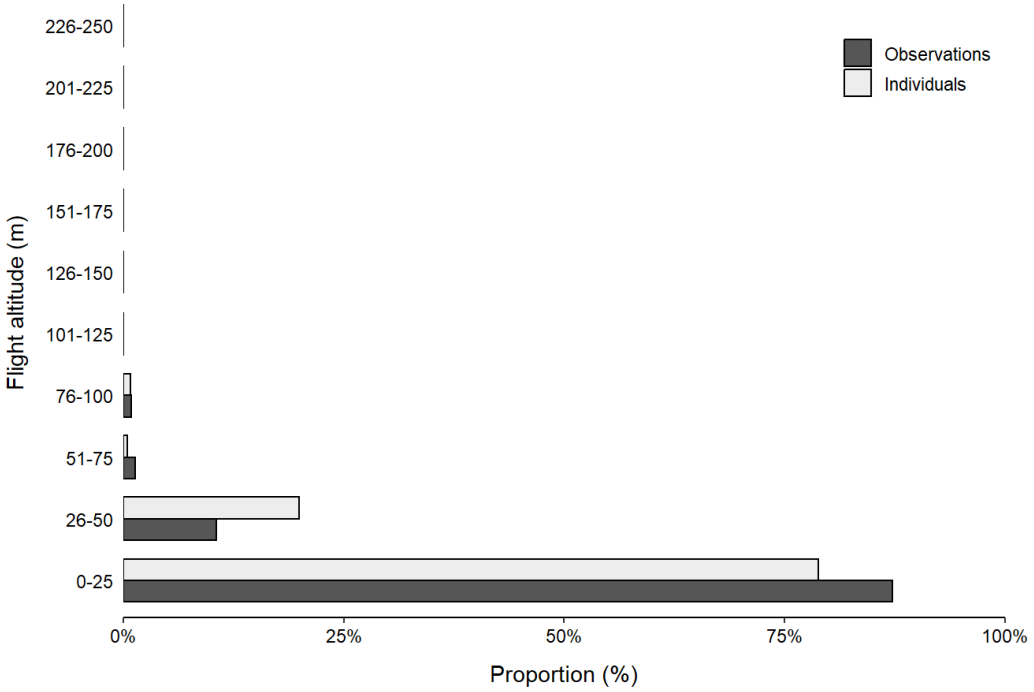

Figure 5.72 Passerine flight altitudes recorded during the eight ship-based surveys conducted in the North Sea I pre-investigation area. The figure shows the proportion of observations (N = 219) and individuals (N = 724) within each 25 m flight altitude interval.

5.2.1.12 Waders (Charadriiformes)

Wader flight altitudes were analysed by pooling observations of dunlins, European golden plovers, common sandpipers, ruddy turnstones, red knots, common ringed plovers, common snipes, Eurasian curlews, whimbrels, grey plovers, common redshanks, and unidentified species of curlews (curlew sp.) and waders (wader sp.). In total, flight altitude was recorded during 73 observations of 249 individuals. Waders were mainly observed flying alone (43.8%), in pairs (17.8%) or in small flocks with an average flock size of 3.4 (± 0.5) individuals. The largest wader flock observed consisted of 25 dunlins. Waders were predominantly observed flying at altitudes below 25 m (92.4%), with a small number of individuals flying at altitudes between 26-150 m (Table 5.23; Figure 5.73). The highest recorded flight altitude was an unidentified curlew species flying at 150 m.

Table 5.23 Wader flight altitudes recorded during the eight ship-based surveys conducted in the North Sea I pre-investigation area. The table shows the number and proportion of observations (N = 73) and individuals (N = 249) within each 25 m flight altitude interval.

Altitude interval (m)	Observations	Individuals

	Total	Proportion	Total	Proportion
0-25	65	0.890	230	0.924
26-50	4	0.055	4	0.016
51-75	2	0.027	8	0.032
76-100	0	0.000	0	0.000
101-125	1	0.014	6	0.024
126-150	1	0.014	1	0.004
151-175	0	0.000	0	0.000
176-200	0	0.000	0	0.000
201-225	0	0.000	0	0.000
226-250	0	0.000	0	0.000

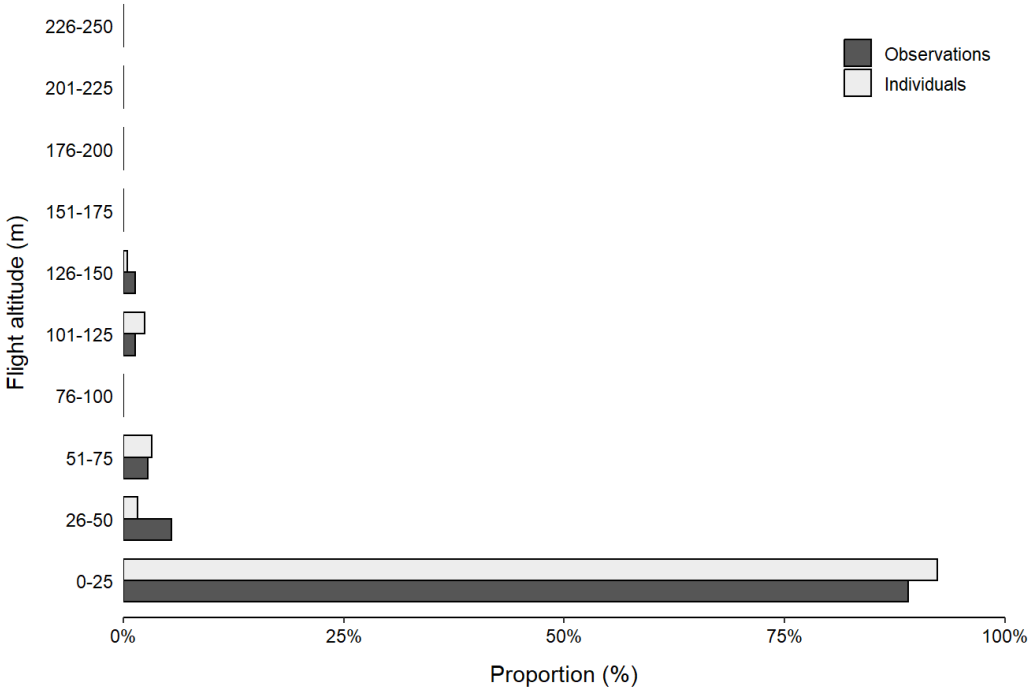

Figure 5.73. Wader flight altitudes recorded during the eight ship-based surveys conducted in the North Sea I pre-investigation area. The figure shows the proportion of observations (N = 73) and individuals (N = 249) within each 25 m flight altitude interval.

5.2.1.13 Common scoter

In total, flight altitude was recorded during 47 observations of common scoters, encompassing 206 individuals. Common scoters were often observed flying alone (27.7%) or in pairs (27.7%). However, common scoters were observed flying in flocks of up to 39 individuals, with an average flock size of 4.4 (± 0.9) individuals. Common scoters exclusively flew at altitudes below 25 m (90.6%), with the highest recorded flight altitude being 25 m (Table 5.24; Figure 5.74).

Table 5.24. Common scoter flight altitudes recorded during the eight ship-based surveys conducted in the North Sea I pre-investigation area. The table shows the number and proportion of observations (N = 47) and individuals (N = 206) within each 25 m flight altitude interval.

Altitude interval (m)	Observations		Individuals	
	Total	Proportion	Total	Proportion
0-25	47	1.000	206	1.000
26-50	0	0.000	0	0.000
51-75	0	0.000	0	0.000
76-100	0	0.000	0	0.000
101-125	0	0.000	0	0.000
126-150	0	0.000	0	0.000
151-175	0	0.000	0	0.000
176-200	0	0.000	0	0.000
201-225	0	0.000	0	0.000
226-250	0	0.000	0	0.000

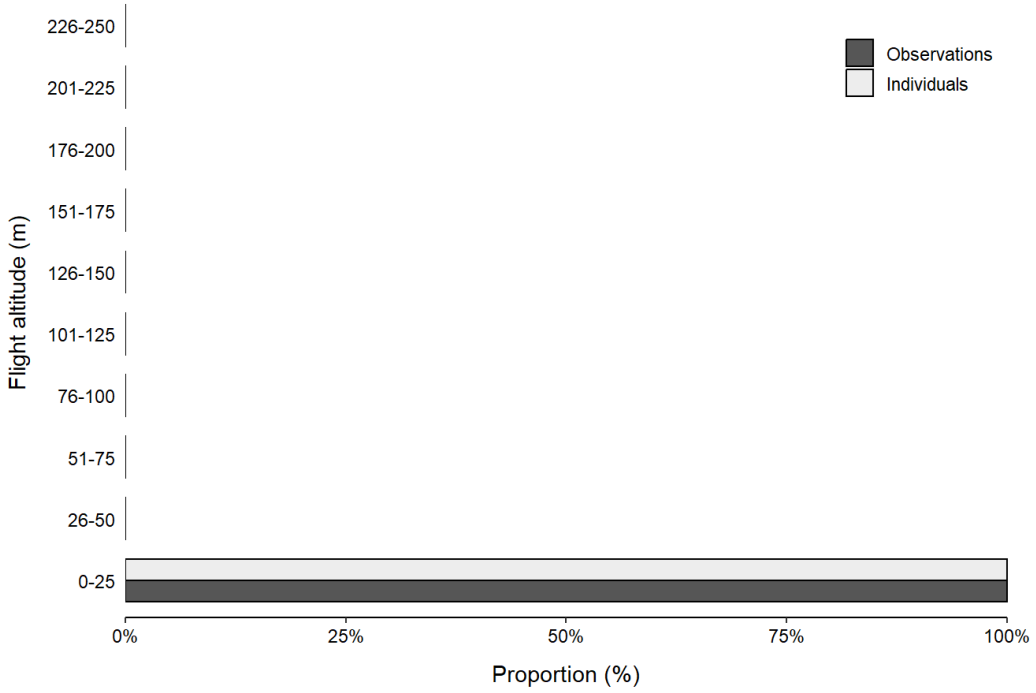

Figure 5.74 Common scoter flight altitudes recorded during the eight ship-based surveys conducted in the North Sea I pre-investigation area. The figure shows the proportion of observations (N = 47) and individuals (N = 206) within each 25 m flight altitude interval.

5.2.1.14 Northern gannet

In total, flight altitude was recorded during 418 observations of northern gannets, encompassing 463 individuals. Northern gannets were predominantly observed flying alone (94.7%), with an average flock size of 1.1 (± 0.1) individuals. The largest northern gannet flock observed consisted of 21 individuals. Northern gannets flew predominantly at altitudes below 25 m (89.6%), with a small number of individuals flying at altitudes between 26-75 m (Table 5.25; Figure 5.75). The highest recorded northern gannet flight altitude was 75 m.

Table 5.25 Northern gannet flight altitudes recorded during the eight ship-based surveys conducted in the North Sea I pre-investigation area. The table shows the number and proportion of observations (N = 418) and individuals (N = 463) within each 25 m flight altitude interval.

Altitude interval (m)	Observations		Individuals	
	Total	Proportion	Total	Proportion
0-25	374	0.895	415	0.896
26-50	39	0.093	43	0.093
51-75	5	0.012	5	0.011
76-100	0	0.000	0	0.000
101-125	0	0.000	0	0.000
126-150	0	0.000	0	0.000
151-175	0	0.000	0	0.000
176-200	0	0.000	0	0.000
201-225	0	0.000	0	0.000
226-250	0	0.000	0	0.000

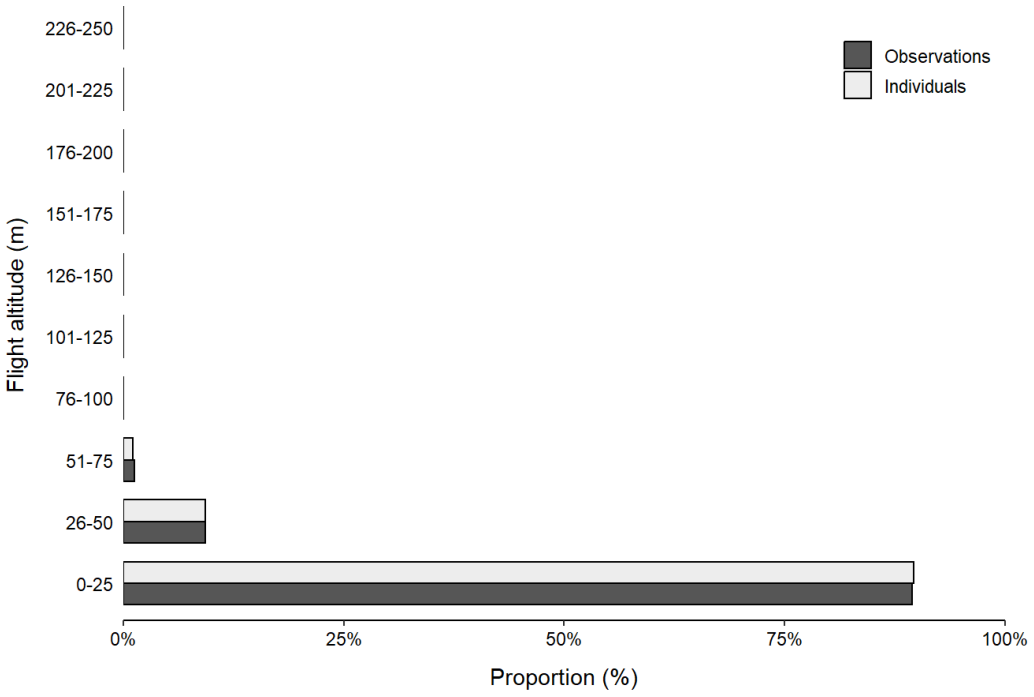

Figure 5.75 Northern gannet flight altitudes recorded during the eight ship-based surveys conducted in the North Sea I pre-investigation area. The figure shows the proportion of observations (N = 418) and individuals (N = 463) within each 25 m flight altitude interval.

5.2.1.15 Black-legged kittiwake

In total, flight altitude was recorded during 278 observations of black-legged kittiwakes, encompassing 342 individuals. Black-legged kittiwakes were predominantly observed flying alone (86%) or in pairs (10.1%), with an average flock size of 1.2 (± 0.0) individuals. The largest black-legged kittiwake flock observed consisted of eight individuals. Black-legged kittiwakes flew predominantly at altitudes below 25 m (88%) (Table 5.26; Figure 5.76). However, the highest recorded black-legged kittiwake flight altitude was 120 m.

Table 5.26 Black-legged kittiwake flight altitudes recorded during the eight ship-based surveys conducted in the North Sea I pre-investigation area. The table shows the number and proportion of observations (N = 278) and individuals (N = 342) within each 25 m flight altitude interval.

Altitude interval (m)	Observations		Individuals	
	Total	Proportion	Total	Proportion
0-25	237	0.853	301	0.880
26-50	31	0.112	31	0.091
51-75	5	0.018	5	0.015
76-100	3	0.011	3	0.009
101-125	2	0.007	2	0.006
126-150	0	0.000	0	0.000
151-175	0	0.000	0	0.000
176-200	0	0.000	0	0.000
201-225	0	0.000	0	0.000
226-250	0	0.000	0	0.000

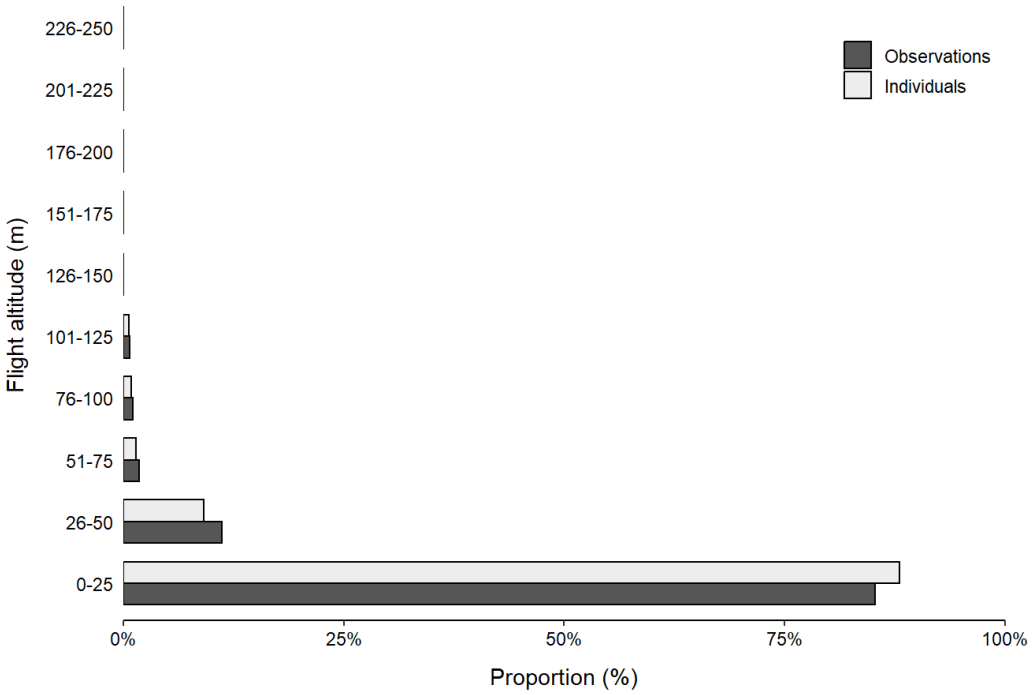

Figure 5.76 Black-legged kittiwake flight altitudes recorded during the eight ship-based surveys conducted in the North Sea I pre-investigation area. The figure shows the proportion of observations (N = 278) and individuals (N = 342) within each 25 m flight altitude interval.

5.2.1.16 Gulls (Laridae)

Gull flight altitudes were analysed by pooling observations of Caspian gulls, little gulls, black-headed gulls, and unidentified gull species (gull sp.). Black-legged kittiwakes, lesser black-backed gulls, European herring gulls, common gulls and great black-backed gulls were analysed separately. In total, flight altitude was recorded during 87 observations comprising 95 individuals. Gulls were mainly observed flying alone (92%), with an average flock size of 1.1 (± 0.0) individuals. The largest gull flock observed consisted of three black-headed gulls. Gulls were predominantly observed flying at altitudes below 50 m (75.8%) (Table 5.27; Figure 5.77). However, they generally flew at higher altitudes than other species, with individuals flying as high as 250 m, the highest recorded flight altitude in the analysis.

Table 5.27 Gull flight altitudes recorded during the eight ship-based surveys conducted in the North Sea I pre-investigation area. The table shows the number and proportion of observations (N = 87) and individuals (N = 95) within each 25 m flight altitude interval.

Altitude interval (m)	Observations		Individuals	
	Total	Proportion	Total	Proportion
0-25	42	0.483	49	0.516
26-50	22	0.253	23	0.242
51-75	12	0.138	12	0.126
76-100	8	0.092	8	0.084
101-125	0	0.000	0	0.000
126-150	0	0.000	0	0.000
151-175	0	0.000	0	0.000
176-200	1	0.011	1	0.011
201-225	1	0.011	1	0.011
226-250	1	0.011	1	0.011

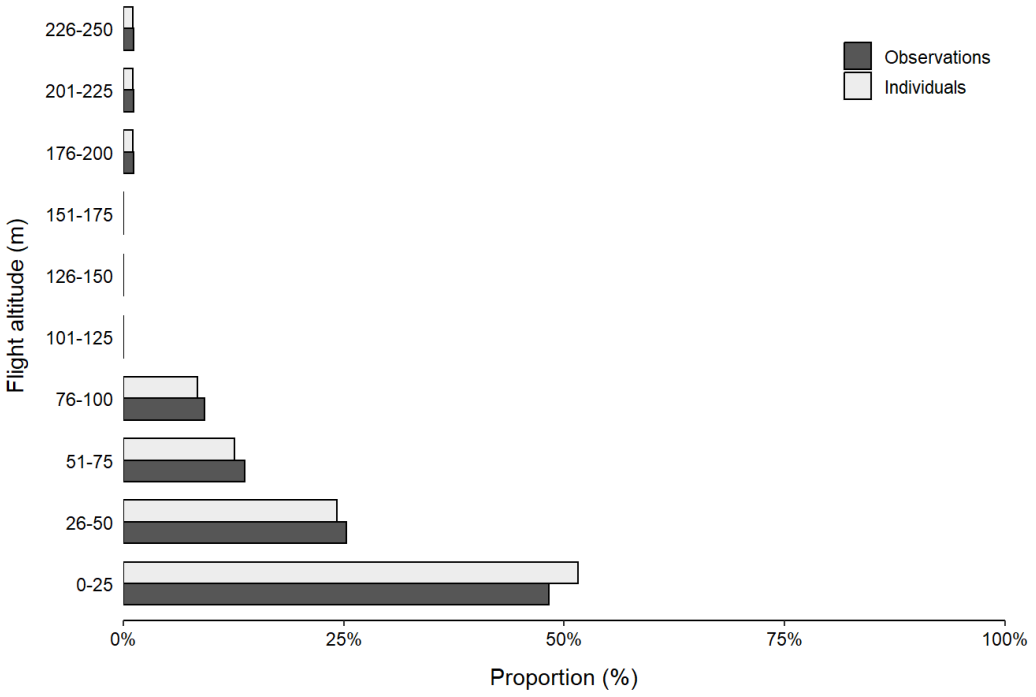

Figure 5.77 Gull flight altitudes recorded during the eight ship-based surveys conducted in the North Sea I pre-investigation area. The figure shows the proportion of observations (N = 87) and individuals (N = 95) within each 25 m flight altitude interval.

5.2.1.17 Skuas (Stercorariidae)

Skua flight altitudes were analysed by pooling observations of Arctic skuas, long-tailed, great, and unidentified skuas (skua sp.). In total, flight altitude was recorded during 22 observations of 22 individuals. Skuas were exclusively observed flying alone. Skuas were predominantly observed flying at altitudes below 50 m (86.4%) (Table 5.28 and Figure 5.78). However, they were observed flying as high as 250 m, the highest recorded flight altitude in the analysis.

Table 5.28 Skua flight altitudes recorded during the eight ship-based surveys conducted in the North Sea I pre-investigation area. The table shows the number and proportion of observations (N = 22) and individuals (N = 22) within each 25 m flight altitude interval.

Altitude interval (m)	Observations		Individuals	
	Total	Proportion	Total	Proportion
0-25	17	0.773	17	0.773
26-50	2	0.091	2	0.091
51-75	0	0.000	0	0.000
76-100	2	0.091	2	0.091
101-125	0	0.000	0	0.000
126-150	0	0.000	0	0.000
151-175	0	0.000	0	0.000
176-200	0	0.000	0	0.000
201-225	0	0.000	0	0.000
226-250	1	0.045	1	0.045

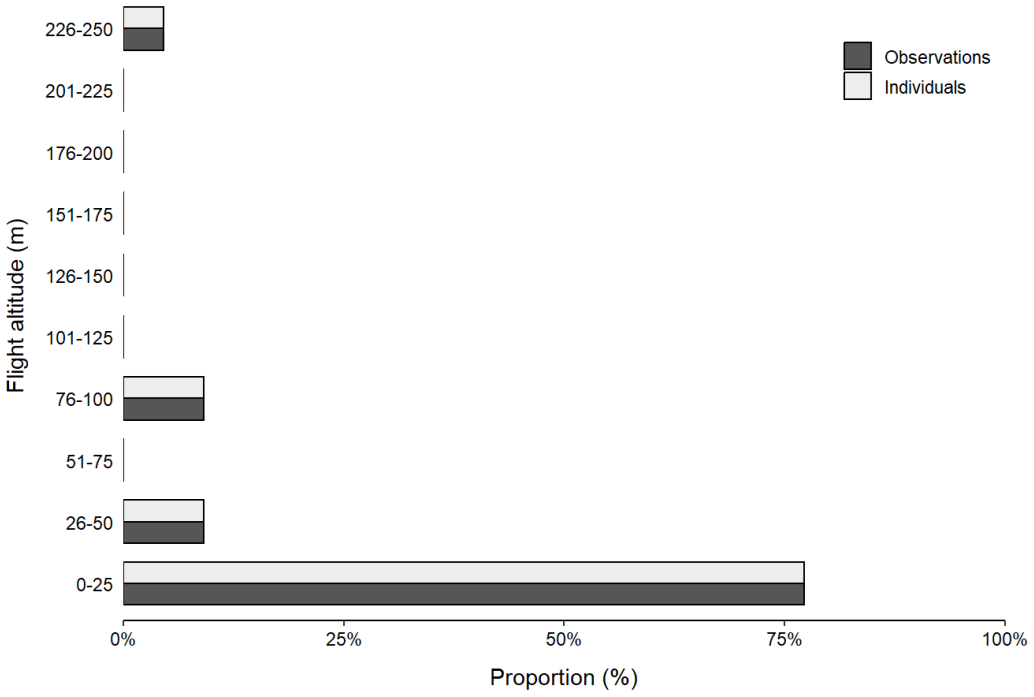

Figure 5.78. Skua flight altitudes recorded during the eight ship-based surveys conducted in the North Sea I pre-investigation area. The figure shows the proportion of observations (N = 22) and individuals (N = 22) within each 25 m flight altitude interval.

5.2.2 Species composition

For each of the eight surveys, species ratios were analysed for divers, gulls (excluding black-headed gulls and black-legged kittiwakes), terns, and auks (common guillemots, black guillemots, and razorbills). Only observations of individuals identified to species were included.

5.2.2.1 Auks

The species composition of auks was analysed by pooling observations of common guillemots, razorbills and black guillemots. In total, the auk species composition was analysed based on 170 observations of 248 individuals (Table 5.29). Of these individuals, 56.5% were common guillemots, whereas 43.1% were razorbills. Only one black guillemot was observed during the ship-based surveys.

Table 5.29 Species composition of auks observed during the eight ship-based surveys conducted in the North Sea I pre-investigation area. The table shows the number and proportion of observations (N = 170) and individuals (N = 248) of each species.

Species	Observations		Individuals	
	Total	Proportion	Total	Proportion
Black guillemot	1	0.006	1	0.004
Common guillemot	108	0.635	140	0.565
Razorbill	61	0.359	107	0.431

The proportion of common guillemots relative to razorbills varied greatly depending on the survey (Figure 5.79). For example, all auks observed during the August survey (S4) were identified as common guillemots. In contrast, razorbills

were the most abundant auk species observed during the September (S5) and December surveys (S7). The single black guillemot was observed during the April survey (S1).

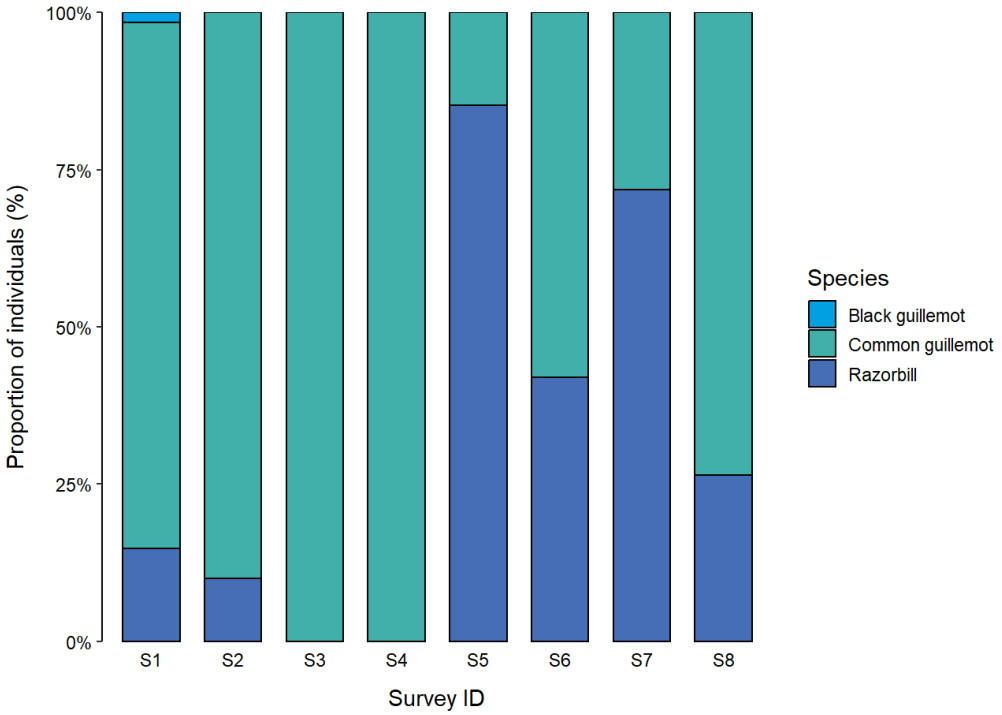

Figure 5.79 Species composition of auks observed during the eight ship-based surveys conducted in the North Sea I pre-investigation area. The figure shows the proportion of individuals of each species (N = 248).

5.2.2.2 Divers

The species composition of divers was analysed by pooling observations of red-throated and black-throated divers. In total, the diver species composition was analysed based on 66 observations of 89 individuals (Table 5.30). Of these individuals, 98.9% were red-throated divers, whereas only one black-throated diver was observed during the ship-based surveys.

Table 5.30 Species composition of divers observed during the eight ship-based surveys conducted in the North Sea I pre-investigation area. The table shows the number and proportion of observations (N = 66) and individuals (N = 89) of each species.

Species	Observations		Individuals	
	Total	Proportion	Total	Proportion
Black-throated diver	1	0.015	1	0.011
Red-throated diver	65	0.985	88	0.989

Divers were only observed during the April (S1), May (S2), June (S3), September (S5) and October (S6) surveys, where almost all divers observed were identified as red-throated divers (Figure 5.80). The single black-throated diver was observed during the May survey (S2).

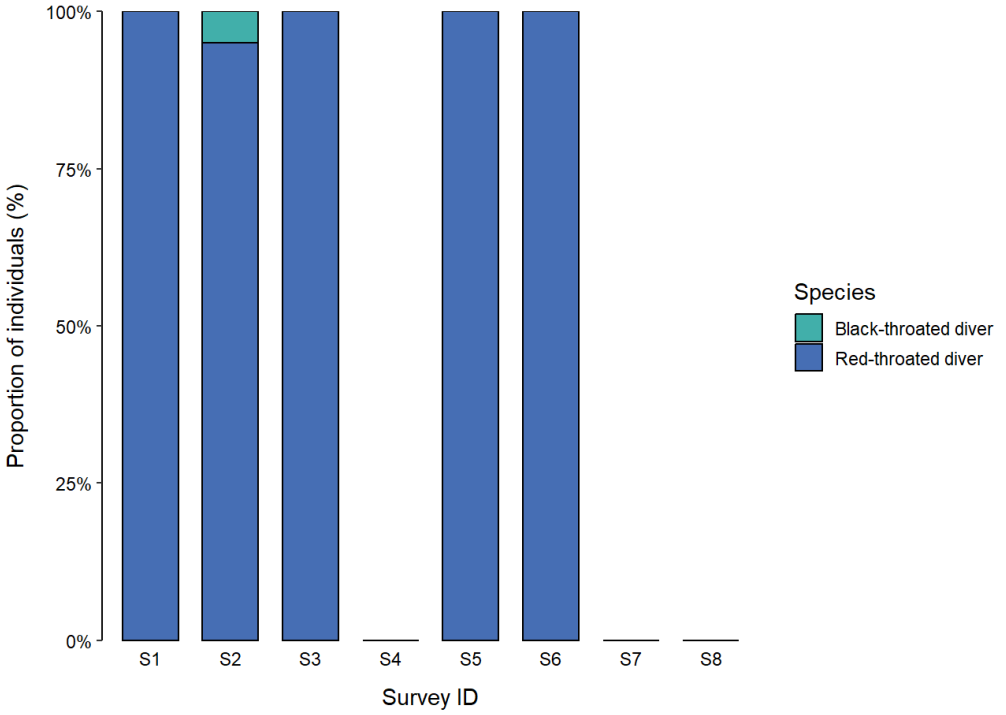

Figure 5.80 Species composition of divers observed during the eight ship-based surveys conducted in the North Sea I pre-investigation area. The figure shows the proportion of individuals of each species (N = 89).

5.2.2.3 Terns

The species composition of terns was analysed by pooling observations of Arctic, black, common, and sandwich terns. In total, the tern species composition was analysed based on 245 observations of 594 individuals (Table 5.31). Of these individuals, 47.1% were Arctic terns, 42.3% were common terns, and 10.3% were sandwich terns. Only one black tern was observed during the ship-based surveys.

Table 5.31 Species ratios of terns observed during the eight ship-based surveys conducted in the North Sea I pre-investigation area. The table shows the number and proportion of observations (N = 245) and individuals (N = 594) of each species.

Species	Observations		Individuals	
	Total	Proportion	Total	Proportion
Arctic Tern	89	0.363	280	0.471
Black Tern	1	0.004	2	0.003
Common Tern	128	0.522	251	0.423
Sandwich Tern	27	0.110	61	0.103

Terns were only observed during the April (S1), May (S2), June (S3), August (S4) and September (S5) surveys. However, the proportion of Artic, common, and sandwich terns varied greatly depending on the survey (Figure 5.81). For example, all terns observed during the June survey (S3) were sandwich terns. In contrast, Arctic terns were the most observed terns during the May survey (S2), whereas common terns were the most observed terns in the August (S4) and September (S5) surveys. The single black tern was observed during the May survey (S2).

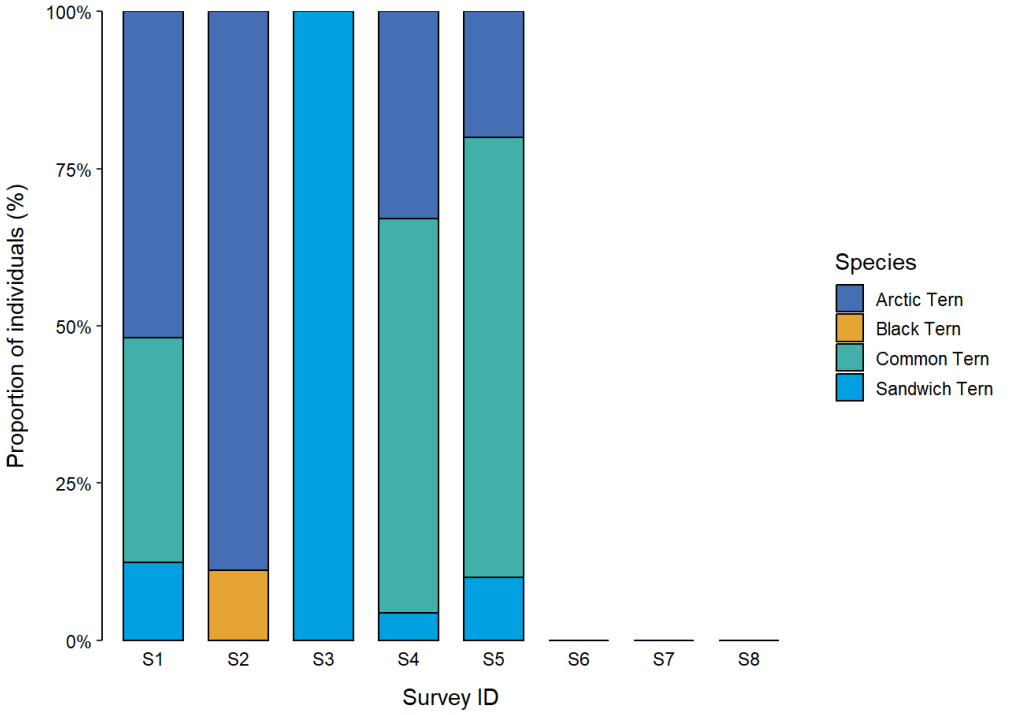

Figure 5.81 Species ratios of terns observed during the eight ship-based surveys conducted in the North Sea I pre-investigation area. The figure shows the proportion of individuals of each species (N = 594).

5.2.2.4 Gulls

The species composition of gulls was analysed by pooling observations of Caspian, little, common, lesser black-backed, great black-backed, and European herring gulls. Black-headed gulls and black-legged kittiwakes were not included, as these were identifiable during aerial surveys. Gull species composition was analysed using 1,255 observations of 4,025 individuals (Table 5.32). Of these individuals, most were lesser black-backed gulls (48.1%) and common gulls (36.9%). In contrast, only 9.2% were European herring gulls, 5.3% were great black-backed gulls, 0.3% were little gulls, and 0.2% were Caspian gulls.

Table 5.32 Species composition of gulls (excluding black-headed gulls and black-legged kittiwakes) observed during the eight ship-based surveys conducted in the North Sea I pre-investigation area. The table shows the number and proportion of observations (N = 1,255) and individuals (N = 4,025) of each species.

Species	Observations		Individuals	
	Total	Proportion	Total	Proportion
Caspian Gull	7	0.006	7	0.002
Common Gull	204	0.163	1484	0.369
Great Black-backed Gull	139	0.111	215	0.053
Herring Gull	236	0.188	369	0.092
Lesser Black-backed Gull	660	0.526	1938	0.481
Little Gull	9	0.007	12	0.003

Gulls were observed during all surveys. However, the proportion of the different species varied greatly depending on the survey (Figure 5.82). For example, no lesser black-backed gulls were observed during the December (S7) and February (S8) surveys, where common gulls were the most frequently observed. In contrast, European herring gulls and great black-backed gulls were observed during all surveys. Caspian gulls were observed during the April (S1), September (S5), December (S7) and February (S8) surveys. However, they were observed only in very low numbers. Little gull was the least frequently observed gull and was only observed during the September (S5) and December (S7) surveys.

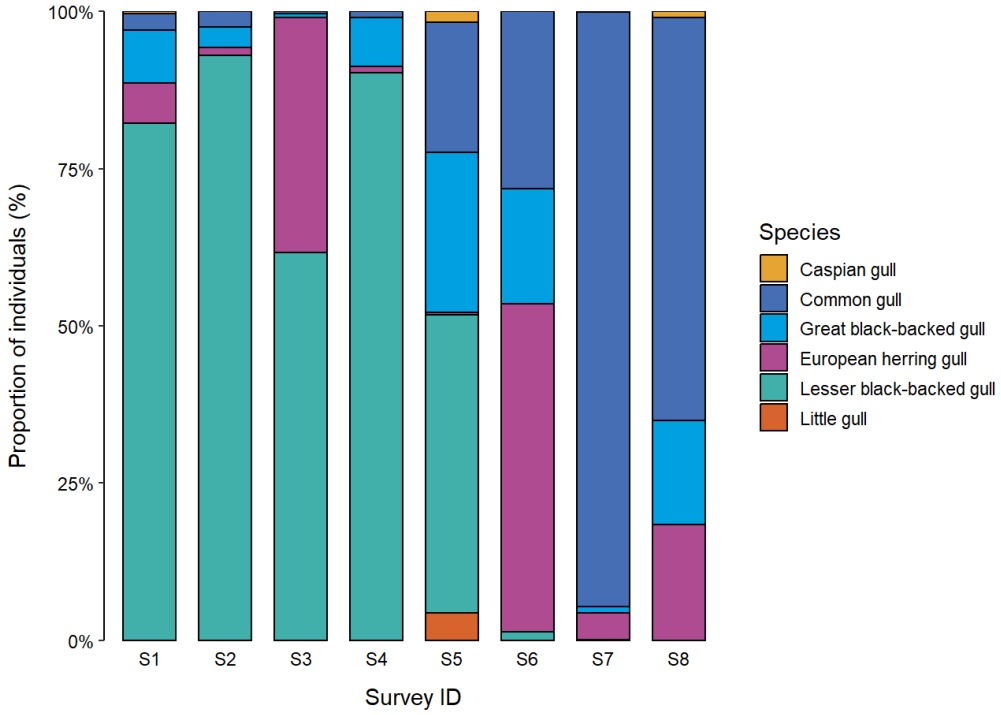

Figure 5.82 Species composition of gulls (excluding black-headed gulls and black-legged kittiwakes) observed during the eight ship-based surveys conducted in the North Sea I pre-investigation area. The figure shows the proportion of individuals of each species (N = 4025).

5.2.3 Vertical radar

Predictions were made successfully for August, September, October and December. However, in June, the noise level exceeded the threshold in all hours of the survey, which may have been related to poor weather or the use of a medium pulse setting on the radar. Temporal analyses are presented with the annotations and ComputerVision (CV) predictions, while spatial analyses use only the CV predictions. This is because the CV algorithm is necessary to extract the horizon angles from images and obtain a corrected location for each bird. Furthermore, the December session was excluded from the spatial analyses because the entire right side of the scan area showed a high prevalence of artefacts in that survey.

5.2.3.1 Bird numbers in time

The putative bird counts from the CV algorithm matched the counts from annotations very well in October, the month from which the training subset was derived, and quite well in August and December (Figure 5.83). In October, the annotations from the two observers were very closely matched. October had the most bird traffic, followed by September and August. Furthermore, most of the counts in October were concentrated on a single night on October 7, with bird counts peaking at nearly 1,500 objects per hour (~1,500 objects across 30 radar sweeps).

Analysis of bird counts across diel periods revealed that counts were generally highest between dusk and dawn, especially in October when bird counts were the highest (Figure 5.84). However, September presented an interesting exception, with relatively high counts during the day.

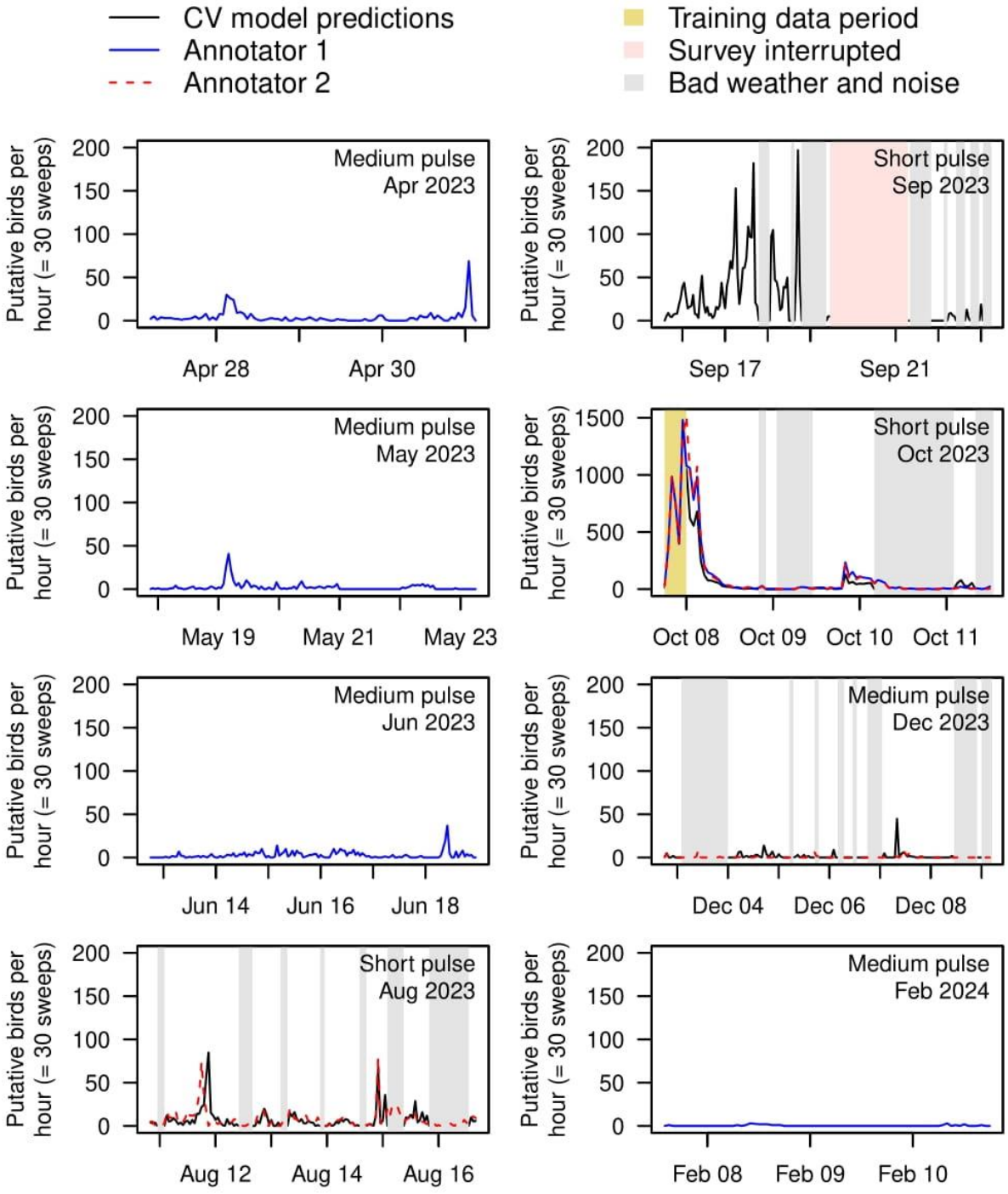

Figure 5.83 Putative bird counts across days during the eight survey sessions, expressed as the number of bird detections per hour (i.e. summed across 30 sweeps). Note that the y-axis is rescaled for October, which is the month with the highest bird traffic. Solid black lines represent the predicted counts from a computer vision (CV) algorithm, while solid blue and dashed red lines represent counts from Annotator 1 (TOE) and Annotator 2 (RDN), respectively. Grey areas represent periods where there was too much noise or bad

weather to get reliable predictions from the CV algorithm. The yellow area represents the period from which the training subset was taken. The pink area represents a sampling hiatus.

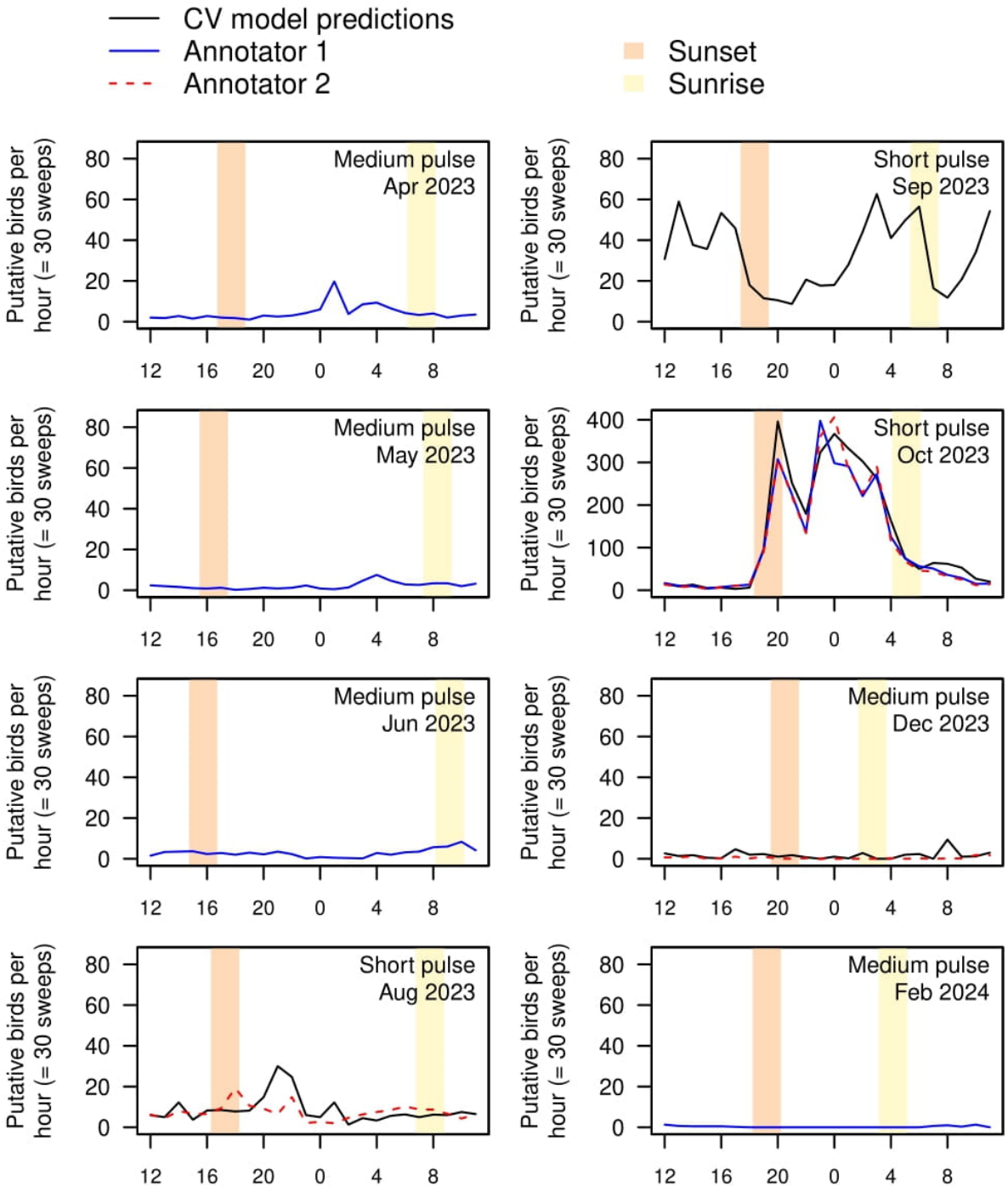

Figure 5.84 Putative bird counts across hours during the eight survey sessions, expressed as the number of bird detections per hour (i.e. summed across 30 sweeps). Note that the y-axis is rescaled for October, which is the month with the highest bird traffic. Solid black lines represent the predicted counts from a computer vision (CV) algorithm, while solid blue and dashed red lines represent counts from Annotator 1 (TOE) and Annotator 2 (RDN), respectively. The orange areas represent dusk periods, while light yellow areas represent dawn periods.

5.2.3.2 *Bird densities in space*

Estimates of bird densities in the August, September and October surveys were strongly affected by distance from the radar sensor, with low densities very close to, or far away from, the vessel (Figure 5.85). After accounting for this effect, altitude significantly affected the density of putative birds. Densities peaked at the lowest observable altitude range of 50-100 m, steadily declining to a third of the peak at 300 m above sea level (Figure 5.86). The densities above 300 m became quite stable, with increasing uncertainty levels due to a reduced scan area at these altitudes.

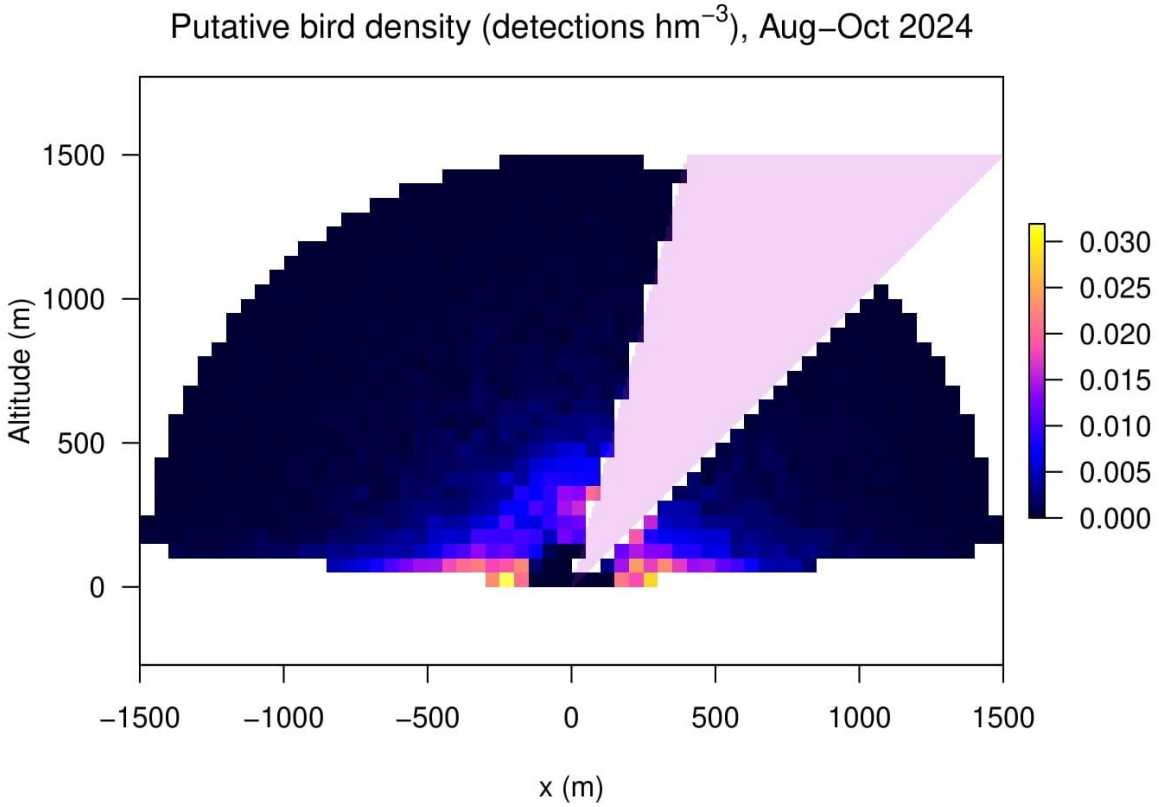

Figure 5.85 Putative bird densities (hm^{-3}) across 50 × 50 m grid cells of the radar scan area during three radar recording sessions in August, September and October 2024. Putative bird densities are derived from a computer vision algorithm. Grid cells with >50 % area within 5° of the horizon or a zone from 15 to 45° with a high frequency of artefacts in August and October are excluded.

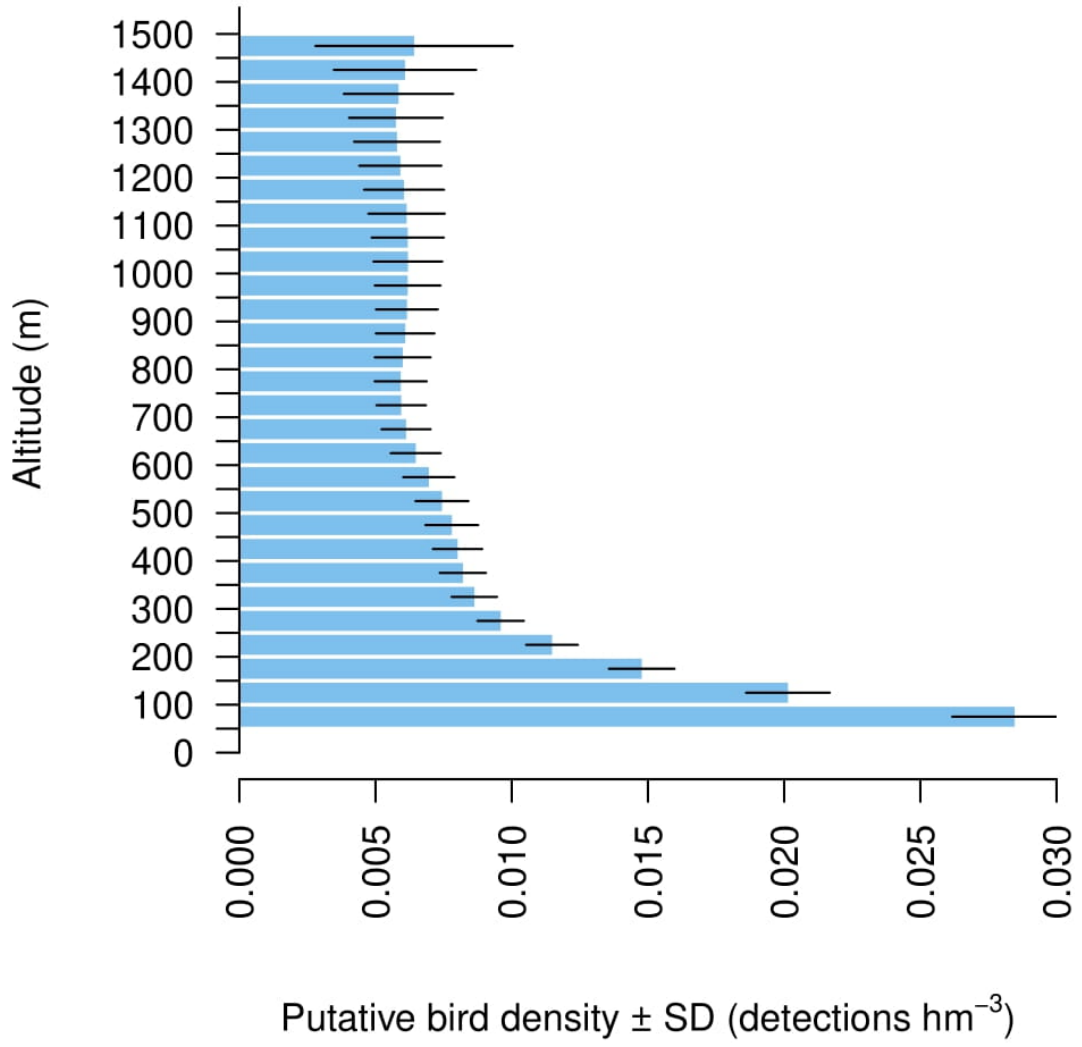

Figure 5.86 Predicted putative bird density at 50 m intervals from 50-1500 m above sea level. Predictions were made using a generalised additive model, capturing the effect of altitude on putative bird density while accounting for a nonlinear effect of distance from the sensor. Putative bird densities were, in turn, derived using a computer vision algorithm. Confidence intervals represent the prediction ± 2× standard error of the prediction.

5.2.3.3 Model accuracy

A pipeline that accelerates the extraction of putative birds from vertical radar images was created. Trained over several days using a laptop computer, the CV algorithm takes less than 10 seconds to generate horizon angles, a noise indicator, and putative bird detections for a radar image. The model generates putative bird detections within a training period that match observed annotations with almost 90% accuracy. Furthermore, outside of the training period, putative bird counts over time match counts from annotations well (Figure 5.83), especially during October and other sessions which used similar radar recording settings. Above all, the CV algorithm can extract the horizon from radar images, calculating the true locations of birds with respect to the sea level. This demonstrates that bird traffic is highest at low altitudes, even after accounting for non-linear variation in the detectability of birds with distance from the radar sensor.

While the CV algorithm has proven fit for rapidly generating a spatiotemporal analysis of bird activity, this approach still has clear limitations. Chief among these is the variation in imagery between recording sessions, owing to natural atmospheric variations and variations in recording apparatus and software settings. The model was ineffective in detecting birds in April and May due to resolution issues, in June due to a high prevalence of artefacts and a medium pulse radar setting, or in February due to technical issues and a shift in the colour domain of the images. These variations represent a major challenge for the CV algorithm approach and can only be tackled in one of two ways:

1. The data collection environment, apparatus and software are consistent.
2. More annotations are generated as conditions change, and the model is updated and retrained to cope with changing conditions.

While the first way may be a suitable solution in the short term, it has proven difficult during this project. For example, software updates are necessary for the functioning of the equipment for data capture but lead to inconsistency of screen contents and hinder automated processing. As such, the second way will likely be a better long-term solution. To that end, it is important to recognise the value of manual annotations to expand the possible training domain for CV and machine learning models to detect birds under a wider range of imaging conditions. Furthermore, the manual review of images was crucial to capturing issues related to image quality. For example, a manual review of images in June, August, October and December provided an early warning that artefacts were prevalent in all or parts of the images. This information was crucial to post-process bird detections to ensure sensible conclusions were reached (see blocked-out angles in Figure 5.85, for example).

Similar to previous work using vertical radars to detect birds on land, the continuous nature of the data capture was found to be a crucial strength. Most bird detections throughout the 2023 surveys were observed during a single night on 7 October. Recording for many days at a time and throughout the entire day-night cycle, was crucial so as not to miss important ecological events – in this case, the migration of large numbers of birds, many at low altitudes, across the North Sea in a single night. The development of vertical radar technology and the automated analysis of resulting data will be crucial to understanding the risks of offshore developments for biodiversity in the future.

6. Data and knowledge gaps

The data collected from the eight aerial surveys, which assessed bird abundances and distributions across the survey area, and eight ship-based surveys, which provided information on flight magnitude, altitude, and species composition, are deemed to be of sufficient quality to meet the objectives outlined in the North Sea I, year one bird program.

6.1 Bird abundance and distribution

Surveys of resting and staging birds in the study area were conducted by human observers from aircraft. Initially, under the North Sea Energy Island project, the plan was to use digital orthophotos instead of human observers, a decision that was abandoned before it was set in force. In order to ensure data compatibility between the NSI and the North Sea Energy Island aerial survey data, it was decided to use human-based observers for the aerial suveys at the NSI site. Although the data from human observer-based surveys have been adequate for this task, the data quality could be improved using a digital monitoring method. Using a digital method would allow for bird density estimates without introducing the distance sampling detection function, which is expected to reduce the confidence intervals for density estimates. While this improvement is not essential for the current project, it could enable more precise statistical comparisons of bird densities before and after future wind energy developments.

6.2 Bird flight data

Bird flight magnitude, altitude, and species composition data were collected from eight ship-based surveys across the annual cycle. Initially, it was planned that a 3D radar placed at HR3 OWF would provide continuous and very precise data for that purpose. This idea was abandoned due to time constraints and logistical challenges with installing the radar on an appropriate offshore installation. However, the available data on bird flight magnitude and altitude was considered sufficient with the data collection protocol used in this project.

Continuous data collection on flight altitudes concerning land-based wind farm projects is well established. However, logistical challenges limit data collection in the open sea. With the presence of the HR3 OWF, the Vesterhav Syd OWF, and, within a short time, the Thor OWF, options for overcoming these logistical challenges are present. Therefore, using a 3D radar could be reconsidered for future investigations concerning wind energy development in the area.

Information on birds' reactions to wind turbines is important when estimating the collision risk for birds in the marine environment. While some bird species may avoid the structures, others may be attracted to them. Information on this issue could be gained by introducing a 3D radar at the HR3 or the upcoming Thor OWF.

7. Discussion and conclusion

The abundances and spatial distributions of bird species in the survey area were investigated by conducting eight aerial surveys across an annual cycle from April 2023 to March 2024. While the temporal survey coverage was good during winter and spring, the temporal coverage across summer and autumn was poorer. The results in this report indicate that general bird abundance in the study area is higher in winter and spring than in summer and autumn. This is true for divers, common scoters, black-legged kittiwakes and razorbills/common guillemots. The present annual spread of surveys is, therefore, seen as giving an optimal dataset for the objectives of this project.

Within the survey area, several anthropogenic activities may influence the distribution of birds. The HR3 OWF is situated in the southern part of the survey area. The Vesterhav Syd OWF was operational in the spring and summer of 2024. Moreover, activities related to the Thor OWF in the northern part of the survey area and activities related to the present project were ongoing during the survey period. These activities may have influenced the abundance and distribution of some bird species. The potential impact of those activities on bird abundance and distribution could not be quantified.

Marine birds respond to human activities at sea (Fox & Petersen, 2019). When considering the impact on the distribution of birds, shipping activity has been shown to have species-specific effects on birds (Garthe & Hüppop, 2004; Fliessbach, et al., 2019). Diver species and common scoter are classified as species with a high impact from such activities, whereas, for instance, gull species are less sensitive. Comparisons of before and after construction distribution of common scoters and long-tailed ducks in Danish waters showed marked displacement effects (Petersen, MacKenzie, Rexsted, Wisz, & Fox, 2011; Petersen, Nielsen, & Mackenzie, 2014; Petersen, Mackenzie, & Scott-Hayward, 2018). Data from these analyses also indicated a distribution effect on red-throated divers, though this was not then believed to be an effect of the presence of the wind farms. Analyses of the distribution of red-throated divers in the German Bight concluded a marked displacement of this species from the wind farms (Mendel, et al., 2019). Common guillemots were shown to be displaced up to considerable distances from offshore wind farms in the German Bight (Peschko, et al., 2024). A project initiated by Energinet is currently investigating the long-term effects of wind farms at Horns Rev on red-throated divers and common scoters. The results will be available in autumn 2024.

The avifauna of the bird survey area were predominantly composed of marine species. True marine species such as northern fulmars, northern gannets, black-legged kittiwakes, and razorbills/common guillemots comprised most of the

bird population. However, groups like common scoter, divers, gulls, and terns were also present in significant numbers.

The razorbill/common guillemot group was estimated to be the most numerous, with over 35,000 individuals present in the survey area in March 2024. This made it the most abundant species group. Additionally, black-legged kittiwakes, northern gannets, and divers were other significant groups for which total abundance and distribution data were available. In March 2024, an estimated 7,548 divers and 2,642 northern gannets were present. The lowest numbers of divers and black-legged kittiwakes were recorded in July and September 2023, while northern gannets had their lowest numbers in November and December 2023 and early February 2024.

Existing data from April and May 2019 covering the entire Danish North Sea indicated the presence of an estimated 22,648 divers, primarily red-throated divers, mostly found in the southeastern parts of the Danish North Sea, with higher numbers extending northwards along the west coast of Jutland. Additionally, April and May 2019 data estimated populations of 46,437 northern fulmars, 31,723 northern gannets, 4,472 black-legged kittiwakes and 89,681 razorbills/common guillemots in the Danish North Sea. In the North Sea Energy Island area, situated further offshore to the northwest of the North Sea I area and covering ca. 60% of the survey area of the NSI area, common scoters and red-throated divers were less abundant. There, bird species with a more pelagic distribution, such as razorbills/guillemots, northern fulmars and northern gannets were more abundant. Razorbill/common guillemot abundances in the North Sea Energy Island area were estimated to count ca. 14,000 individuals in March 2023 and 25,000 birds in April 2023. Northern gannets were estimated at 2,500 to 3,800 birds in early and late April 2022, and reduced to 24 and 668 in March and April 2023 (Petersen, et al., 2024).

Razorbills, common guillemots, black-legged kittiwakes and fulmars are offshore species. They primarily feed on small fish and invertebrates by pursue-diving or surface feeding. These species are, therefore, mainly found in the deeper, central and western parts of the survey area. Common scoters primarily feed on benthic bivalves, and due to energetic constraints, they select water depths of up to 20 m. Therefore, this species occurs along the coast or at Horns Rev. Red-throated divers feed on small fish species, primarily benthic species. The species can dive deeper than common scoter and are generally found in water depths out to more than 30 m. Divers are, therefore, primarily found in the eastern parts of the survey area. The divers primarily occur in the survey area in winter and spring, from November/December until late April or early May. Common scoters occur in the area most of the year, though with much higher numbers in late winter and early spring. Black-legged kittiwakes occur primarily in winter, and razorbill/common guillemot peaked in abundance in late winter/early spring.

Furthermore, another study component described the flight patterns of birds in the North Sea I area using data from ship-based surveys, focusing on flight altitude distribution and species composition. Nearly all individuals of some species groups, such as auks, petrels and terns, were recorded flying very low over the sea surface (0-25 m). Similarly, over 85% of northern fulmars, common scoters and northern gannets were recorded flying at altitudes below 25 m. In contrast, gulls and skuas were generally recorded flying at higher altitudes than most other species observed, flying as high as 250 m above the sea surface.

Observations from ship-based surveys also provided valuable insights into the species composition of birds that are challenging to identify from aerial surveys. For example, divers were almost exclusively red-throated divers (99%), while auks comprised 43.1% razorbills, 56.5% common guillemots, and 0.4% black guillemots, with notable seasonal variations in their composition.

8. References

Buckland, S. T., Anderson, D. R., Burnham, K. P., Laake, J. L., Borchers, D. L., & and Thomas, L. (2001). *Introduction to Distance Sampling.* Oxford: Oxford University Press.

Buckland, S., Rexstad, E., Marques, T., & Oedekoven, C. (2015). *Distance sampling: methods and applications.* Switzerland: Springer International Publishing.

Fliessbach, K., Borkenhagen, K., Guse, N., Markones, N., Schwemmer, P., & Garthe, S. (2019). A ship traffic disturbance vulnerability index for Northwest European seabirds as a tool for marine spatial planning. *Frontiers in Marine Science, 6*, 192. doi:10.3389/fmars.2019.00192

Fox, A., & Petersen, I. (2019). Offshore wind farms and their effects on birds. *Dansk Ornitologisk Forenings Tidsskrift, 113*, 86-101. Hentet fra https://pub.dof.dk/publikationer/144

Garthe, S., & Hüppop, O. (2004). Scaling possible adverse effects of marine wind farms on seabirds: developing and applying a vulnerability index. *Journal of Applied Ecology, 41*, 724-734. doi:10.1111/j.0021-8901.2004.00918.x

Laursen, K., Pihl, S., Durinck, J., Hansen, M., Skov, H., Frikke, J., & Danielsen, F. (1997). Numbers and distribution of waterbirds in Denmark 1987-1989. *Danish Review of Game Biology, 14*(1), 1-184.

Leys, C., Ley, C., Klein, O., Bernard, P., & Licata, L. (2013). Detecting outliers: do not use standard deviation around the mean, use absolute deviation around the median. *Journal of Experimental Social Psychology, 49*(4), 764-766.

Marques, F. F., & Buckland, S. T. (2004). Covariate models for the detection function. I *Advanced Distance Sampling* (s. 31-47). Oxford: Oxford University Press.

Marques, T. A., Thomas, L., Fancy, S. G., & Buckland, S. T. (2007). Improving estimates of bird densities using multiple covariate distance sampling. *The Auk*, 1229-1243.

Mendel, B., Schwemmer, P., Peschko, V., Müller, S., Schwemmer, H., Mercker, M., & Garthe, S. (2019). Operational offshore wind farms and associated ship traffic cause profound changes in distribution patterns of Loons (Gavia spp.). *Journal of Environmental Management, 231*, 429-438. doi:10.1016/j.jenvman.2018.10.053

Nielsen, R., & Petersen, I. (2014). *Abundance and distribution of birds and marine mammals in Jammerbugten in 2012 and 2013. Report commissioned by the Environmental Group under the Danish Environmental Monitoring Programme through contract with Vattenfall.* DCE - Danish Centre for Environment and Energy. Aarhus University.

Peschko, V., Schwemmer, H., Mercker, M., Markones, N., Borkenhagen, K., & Garthe, S. (2024). Cumulative effects of offshore wind farms on common guillemots (Uria aalge) in the southern North Sea - climate versus biodiversity? *Biodiversity and Conservation, 33*, 949-970. doi:10.1007/s10531-023-02759-9

Petersen, I. K., Mackenzie, M. L., & Scott-Hayward, L. A. (2018). *Long-term impacts on Long-tailed Duck distributions resulting from the construction of the Rødsand II and Nysted offshore wind farms, Denmark.* Aarhus, Denmark: DCE – Danish Centre for Environment and Energy, Aarhus University.

Petersen, I. K., MacKenzie, M. L., Rexsted, E., Wisz, M. S., & Fox, A. D. (2011). *Comparing pre- and post-construction distributions of long-tailed ducks Clangula hyemalis in and around the Nysted offshore wind farm, Denmark : a quasi-designed experiment accounting for imperfect detection, local surface features and autocorrelation.* St. Andrews, UK: University of St. Andrews. Hentet fra https://hdl.handle.net/10023/2008

Petersen, I. K., Thomsen, H. M., Lindesay, S., Isojuuno, S., McKencie, M., Pedersen, C., . . . Nielsen, R. S. (2024). *North Sea Energy Island, Technical Report, Birds.* Aarhus: NIRAS & Aathus University.

Petersen, I., & Sterup, J. (2019). *Number and distribution of birds in and around two potential offshore wind farm areas in the Danish North Sea and Kattegat. Scientific report no. 327.* DCE - Danish Centre for Environment and Energy. Aarhus University.

Petersen, I., Nielsen, R., & Clausen, P. (2016). *Vurdering af IBA'er (Important Bird Areas) i relation til fuglebeskyttelsesområder - med særligt henblik på marine arter og områder. Tenisk rapport nr. 202.* DCE - Nationalt Center for Miljø og Energi. Aarhus Universitet.

Petersen, I., Nielsen, R., & Clausen, P. (2019). *Opdateret vurdering af IBA udpegninger i relation til otte specifikke marine områder. Teknisk rapport nr. 203.* DCE - Nationalt Center for Miljø og Energi. Aarhus Universitet.

Petersen, I., Nielsen, R., & Mackenzie, M. (2014). *Post-construction evaluation of bird abundances and distributions in the Horns Rev 2 offshore wind farm area, 2011 and 2012.* Kalø, Denmark: Danish Centre for Environment and Energy, Aarhus University.

Scott-Hayward, L. A., Mackenzie, M. L., & Walker, C. G. (2023). MRSea R package (V1.5.0): spatially adaptive uni and bi-variate regression splines using SALSA.

Scott-Hayward, L. A., Mackenzie, M. L., Donovan, C. R., Walker, C. G., & Ashe, E. (2014). Complex Region Spatial Smoother (CReSS). *Journal of Computational and Graphical Statistics*, *23*(2), 340-360.

Skov, H., Durinck, J., Leopold, M. F., & Tasker, M. L. (1995). *Important bird areas in the North Sea, including the Channel and the Kattegat.* Cambridge: BirdLife International.

Stone, C., Webb, A., Barton, C., Ratcliffe, N., Reed, T., Tasker, M., . . . Pienkowski, M. (1995). *An atlas of seabird distribution in north-west European waters.* Peterborough: Joint Nature Conservation Committee.

Tasker, M., Webb, A., Hall, A., Pienkowski, M., & Langslow, D. (1987). *Seabirds in the North Sea.* Nature Conservancy Council.

Walker, C., Mackenzie, M., Donovan, C., & O'Sullivan, M. (2010). SALSA - a Spatially Adaptive Local Smoothing Algorithm. *Journal of Statistical Computation and Simulation*, *81*(2), 179-191.

Appendix 1

Ship-based survey effort at observation positions

Observation days

Table 8.1 The number of observation days spent at each observation position during the eight ship-based surveys conducted in the North Sea I pre-investigation area (N = 40).

Survey ID	Observation days		
	North	Southeast	Southwest
S1	0	2	2
S2	2	1	2
S3	2	2	2
S4	2	2	2
S5	3	2	2
S6	2	1	0
S7	2	2	2
S8	2	0	1

Observation hours

Table 8.2 The number of observation hours spent at each observation position during the eight ship-based bird surveys conducted in the North Sea I pre-investigation area (N = 477.5).

Survey ID	Observation hours		
	North	Southeast	Southwest
S1	0	29.5	30
S2	32.3	16.2	32.2
S3	34	34.5	34
S4	30	30	21.1
S5	22.8	14	24.9
S6	21.5	10.8	0
S7	13.5	13.8	14
S8	9.8	0	8.7

Appendix 2

Aerial survey modelling methods

Detailed summary of bird density modelling methods

Distance sampling analysis

Distance sampling analyses were conducted for each species or species group by pooling the information across all surveys. When fitting detection functions, the effects of covariates, other than perpendicular distance, are incorporated into the detection function model directly (Multiple Covariate Distance Sampling, MCDS) (Marques & Buckland, 2004; Marques, Thomas, Fancy, & Buckland, 2007; Buckland, et al., 2001). In these cases, the probability of detection becomes a multivariate function, representing the probability of detection at perpendicular distance and covariates, where Q is the number of covariates. In this study, using a half-normal detection function $e^{-\left(\frac{y^2}{\sigma^2}\right)}$ the covariates were incorporated via the scale term, σ, where for sighting j, σ has the form:

$$\sigma_j = \exp\left(\beta_0 + \sum_{q=1}^{Q}(\beta_q v_{jq}\right)$$

where β_0 and β_q $(q = 1, \dots, Q)$ are parameters to be estimated (Buckland, et al., 2001). Half-normal and hazard rate detection functions were fitted with BIC (Bayesian Information Criterion) to choose between the models. The candidate variables trialled as covariates were bird group size, behaviour, observer, glare and sea state as the incorporation of these variables are often seen to improve the model (Table 4.2). There were too few observations for some observers, so in those cases, the observers' observations were combined with the observer with the next smallest number of observations. Observations with a sea state greater than four were removed from the analysis. Sea state is a measure of wave activity, and the more wave activity the more difficult it becomes to detect birds with increased distance away from the survey track line.

Table 8.3 Table detailing the covariates used in the detection function fitting.

Covariates	Values
Behaviour	S (sitting or diving) and F (flying or flushing)
Observer	7 Observers
Glare	1 (full sun), 2, 3 (cloudy), 9 (changeable)
Sea state	0, 0.5, 1, 1.5, 2, 2.5, 3, 3.5 (calm to rough)

Mitigating the effects of glare

Sighting conditions, such as sun glare and sea state, can influence the detection of sea birds from aerial surveys. Data to describe sighting conditions is usually collected in situ. However, when this is absent, alternative methods are required to identify (and adjust for) heterogeneity in the detection probability. Accounting for such heterogeneity is particularly important for distance sampling, where near-perfect detection at the track line is often a required assumption.

Detection information from band A was used for the left-hand and right-hand sides of the aircraft to identify transect lines with likely poor sighting conditions. For all species except flying northern gannets and black-legged kittiwakes, which are much easier to see even when glare is present, the identified transects removed observations from the affected side and reduced the coverage to one side (i.e., returning a one-sided transect).

The effects of glare and any mitigations, as a result, were approached using a dedicated analysis. The analysis was designed to quantify the extent to which directional sun glare can lead to left-hand or right-hand side bias in counts within a single transect line with the same direction of travel. Specifically, it was assumed that the proportion of left or right sightings in band A should be 0.5 and follow a binomial distribution. The proportions for each transect were then compared to a critical value calculated as the quantile of the binomial $(n, p = 0.5)$ distribution at three standard

errors greater than the mean and where n equals the number of observations on the transect. This is a common measure in extreme value theory (Leys, Ley, Klein, Bernard, & Licata, 2013). Any transects with values greater than the critical value had the observations from the smaller side removed and the coverage reduced to a single side.

Spatial analysis framework

The following sections describe the modelling methods employed for this analysis and the following outputs. For a high-level executive summary of the methods, see Appendix 2.

Model framework

The response variable for the spatial models under analysis here are bird counts in a small area (segment) corrected for detectability. This response was modelled using a Tweedie framework, which includes an estimated dispersion parameter (ϕ) and Poisson-Gamma mixing parameter (ξ) to return an appropriate mean-variance relationship in each case. The mixing parameter takes on values from 1 (equivalent to quasi-Poisson) and 2 (equivalent to Gamma). If the estimated parameter was close to 1, the models were considered quasi-Poisson.

A set of candidate explanatory variables were associated with each segment to model the signal, and in this study, each of the 12 surveys was analysed separately, including covariate selection. The candidate environmental covariates were water depth and distance from the coast (DC). As a one-dimensional term, DC was considered in each model in the unlikely case that there was compelling evidence for consistent spatial patterns with DC, which were the same in all directions. Additionally, a spatial surface was fitted to each model to account for more realistic (and localised) surface patterns potentially due to unmeasured covariates. Specifically, a two-dimensional CReSS-based (Complex Region Spatial Smoother) surface using a Gaussian radial basis function was included in the model (Scott-Hayward, Mackenzie, Donovan, Walker, & Ashe, 2014).

As an illustration, the following equation represents an example of a Tweedie model with a log link function and fitted with a one-dimensional smooth term (e.g., bathymetry) alongside a two-dimensional spatial smooth:

$$y_{ij} \sim Tw(\mu_{ij}, \phi, \xi)$$

$$\mu_{ij} = e^{\left(\beta_0 + s_1\left(\text{Bathymetry}_{ij}\right) + s_2\left(\text{XPos}_{ij}, \text{YPos}_{ij}\right)\right)}$$

where y_{ij} is the estimated count for transect i segment j and s_1 represents either a quadratic B-spline or a natural cubic spline smooth of depth. Here, s_2 is a two-dimensional smooth of space (with coordinates XPos and YPos in UTMs). Implicit in this model are also coefficients for the intercept (β_0) and any spline-based coefficients associated with the smooth terms. The effort associated with each observation varied depending on the associated segment area, so the segment area was included as an offset term (on the log scale).

A globally applicable depth or distance to the coast term and a more flexible spatial term were trialled for inclusion in each model to indicate how best to model spatial patterns in each case. In particular, this quantifies if any spatial patterns are sufficiently described by the one-dimensional covariates (which apply the same across the surface) or if a more considered approach to spatial patterns was required for each survey. For example, if the depth was selected and a two-dimensional spatial element was not deemed necessary (as determined by the model selection procedure governed by objective fit criteria), then this signals that any spatial patterns are primarily a function of the depth, regardless of the geographical location of this depth in the survey area.

If the two-dimensional spatial term was selected for inclusion in a model, then the spatial density patterns (over and above any environment-related terms) were accommodated using a spatially adaptive term which permits different amounts of flexibility across the surface in a targeted and parsimonious way. Consequently, relatively complex spatial patterns can be accommodated with few parameters.

Selection between competing models was undertaken using a 5-fold cross-validation metric while preserving any within-transect correlation via the appropriate blocking structures.

Model specification, selection and fitting

Spatially adaptive generalised additive models, with targeted flexibility, were fitted to data from each survey to allow for non-linear relationships between the one-dimensional and two-dimensional covariates and the response (Scott-Hayward, Mackenzie, Donovan, Walker, & Ashe, 2014; Scott-Hayward, Mackenzie, & Walker, 2023; Walker, Mackenzie, Donovan, & O'Sullivan, 2010).

All covariates were permitted to have a linear or nonlinear relationship with the response. When a smooth term was included in a model, it was specified to be either a quadratic (degree 2) *B*-spline (df = 3, 4, 5) or a natural cubic spline (df = 2, 3, 4). However, in cases where these degrees of freedom boundaries were reached, a broader range of parameters was trialled instead. The degrees of freedom for these terms determine the flexibility of these smooth (and nonlinear) relationships - the more degrees of freedom, the more flexible the relationship can be.

The location of this flexibility (along the x-axis) in these terms (e.g., depth) was also determined as part of the model selection process. This permitted the relationship in some areas of the covariate range to be relatively complex (e.g., in shallow waters) and in other areas (e.g., in deep waters) to be relatively simple. Both smooth types permitted a maximum of three internal knots and a specific spline number of boundary knots. An objective fit criterion determined the number and location of knots.

The spatial patterns in each analysis were based on a two-dimensional spatial term (of variable complexity). The flexibility of the spatial element constituted part of the model selection procedure and was determined for each survey using a Spatially Adaptive Local Smoothing Algorithm (SALSA). While this model selection element technically occurred between limits (df = [2, 100]), the flexibility chosen in each case was not bounded in practice by those values since the selection procedure occurred well within the bounds of the specified range.

The `MRSea` `R` package, designed to fit both CReSS- and SALSA-type models, was used for model fitting, and a five-fold cross-validation procedure was used to govern all model selection elements (Scott-Hayward, Mackenzie, & Walker, 2023). The cross-validation procedure attempts to balance the fit to data unseen by the model while minimising the number of parameters (parsimony). It was used here to select terms and the extent of their flexibility in each model. Note that this cross-validation was predicated on preserving correlated blocks of survey data (transect lines) so that any residual autocorrelation present was not disrupted when choosing folds. This was considered necessary to ensure independent sampling units under the scheme.

Parameter inference

The response data were collected along survey lines in sequence, so consecutive observations are likely to be correlated in space and time (i.e., points close together in space and/or time are likely to be more similar than points distant in time and/or space). Further, the covariates included in the model are unlikely to fully explain these patterns, so some elements will likely remain in model residuals. These patterns violate residual independence (which underpins traditional model approaches such as Generalised Additive Models). Thus, robust standard errors were routinely used in the `MRSea` modelling framework to account for residual auto-correlation.

Due to the nature of the survey procedure, uncertainty about model parameter estimates proceeded via robust standard errors. These essentially work by inflating the standard errors (normally obtained under traditional approaches) concerning the positive correlation observed within pre-specified blocks of residuals. In cases where this residual correlation is minimal, the adjustments are small, and when the correlation is more extreme, the inflation is larger.

A transect-based blocking structure was used to reflect potential correlation within blocks while independence (i.e., no correlation) between blocks was assumed. To ensure this assumption was realistic, the decay of any residual correlation to zero (i.e., independence) with the distance between points (within blocks along transects) was assessed visually. Specifically, transects in each survey were used as the blocking structure, and an Auto Correlation Function (ACF) plot was used to check the suitability of this blocking structure via a 'decay to zero trend' within blocks.

Modelling diagnostics

Diagnostic measures were used to assess the adequacy of the model fit in each case. The assumed mean-variance relationship under the model was assessed visually using plots of the model's fitted values against the residuals' variance. In this analysis, Tweedie models were employed, which assume a nonlinear mean-variance relationship

$$Var(y) = V(\mu)\phi = \mu^{\xi}\phi$$

where ϕ is the dispersion parameter. The dispersion parameter was estimated for each model, and this estimate was used in the visual assessment of the mean-variance relationship that was assumed to hold under the model. ξ is the power parameter and is estimated prior to the model fitting by using a maximum likelihood profile approach. Based on the nature of the response data, the values of ξ were permitted between 1 (Quasi-Poisson) and 2 (Gamma).

QQ plots and residuals against predicted values plots were assessed to ascertain the level of agreement between the data and the model. These plots were created using the ***DHARMa R*** package and using simulated residuals.

Regarding interpretation, the left panel is a uniform QQ plot, and the right panel shows the residuals against predicted values, with outliers highlighted in red. Given these outputs, we would expect that a correctly specified model shows:

a) A straight 1-1 line and no compelling evidence against the null hypothesis of a correct overall residual distribution, as indicated by the *p*-values for the associated tests in the QQ plot.
b) Visual homogeneity of residuals in vertical and horizontal directions in the residuals against the predictor plot.

Pearson residuals for each model were also spatially visualised to ensure no areas of consistent bias across the survey area. Clusters of negative or positive residuals in spatially similar locations would indicate this.

Residual independence was not assumed to hold under the model. Instead, model inference proceeded under robust standard errors. As described, Auto Correlation Function (ACF) plots were instead used to check the suitability of this blocking structure via a 'decay to zero' trend within blocks.

Model predictions and estimates of uncertainty

Based on each selected model, predictions of counts were made to a grid of points (each point representing a 1 km^2 grid cell) across the survey area. Additionally, abundances within the survey-based prediction region were obtained by summing the grid cell counts across the relevant areas.

The uncertainty in the detection function was reflected using a parametric bootstrap ($n = 500$) of the fitted distance sampling model. This generated new estimated counts for each segment. The selected spatial model was then re-fitted to each of the new datasets to obtain a new set of parameter estimates for the model. The final output of this process was a parametric bootstrap procedure using the robust variance-covariance matrix from each parametric bootstrap model. These were used to calculate 500 sets of model predictions, which generated 95% percentile-based intervals and allowed for calculating a coefficient of variation for each grid cell. If it was impossible to fit a spatial model to the data, the abundance estimates for the survey were calculated from the distance analysis parametric bootstraps.

A calculation of 'persistence' was also undertaken across the two data types using the geo-referenced estimates of density (abundance/associated area) across the survey area. Persistence scores were calculated for every grid cell in the following way. Each bootstrap replicate was allocated a binary value based on whether or not the estimate in each location was above the mean estimated density (1) throughout the survey area or below this mean estimated density (0). This was performed for all 500 sets of plausible predictions in each grid cell (based on the bootstrap replicates), and the proportion of these bootstrap predictions above the mean (indicated by the value of 1) was calculated for each grid cell to give a persistence score for that location. A persistence score of 1 indicates that the density in that grid cell was estimated to be above average in every bootstrap replicate in every survey (so uniformly above the mean; high persistence), while a value of 0.1 indicates that just 10% of the estimates were above the estimated mean, and thus indicates low persistence in that location.

Appendix 3

Vertical radar computer vision pipeline

Executive summary

Scan area detection

Inputs: one representative radar image; scan area colour parameters (determined manually).

Outputs: centre coordinates and radius of scan circle; eccentricity to convert to ellipse.

Screen grabs contain information outside of the radar scan area that is distracting for detecting birds (Figure 8.1). To isolate the scan area of images, we:

- Pixels in the image that meet specific colour criteria are selected.
- Only edge pixels using a 1-pixel erosion are selected.
- The minimum bounding circle of those pixels is found using the 'miniball' Python package.
- These are converted to an ellipse by comparing the height and width of the scan area.

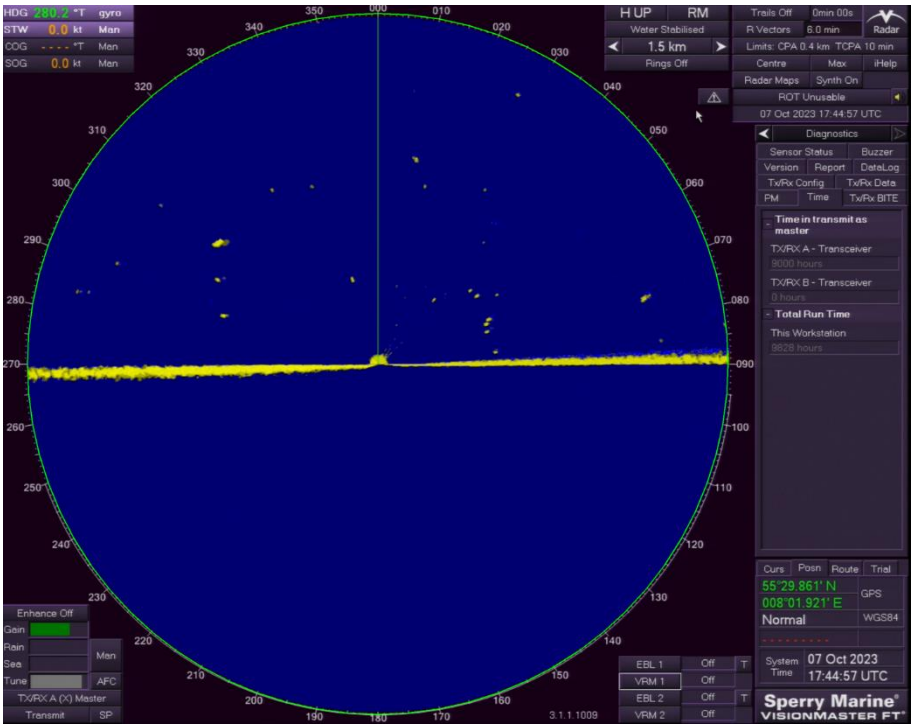

Figure 8.1 An example of a screen grab from the October session. The green line depicts the scan circle before conversion to an ellipse.

Foreground segmentation

Inputs: input image (RGB), foreground hue +/- range; minimum saturation.

Outputs: foreground mask.

To capture the yellow areas of the scan, including birds, artefacts, the water's surface, and some features of the graphical interface (Figure 8.2):

- The image is converted from RGB to HSV space.
- Pixels with hues falling within a range around a specific value are extracted, while regions of low saturation are excluded.

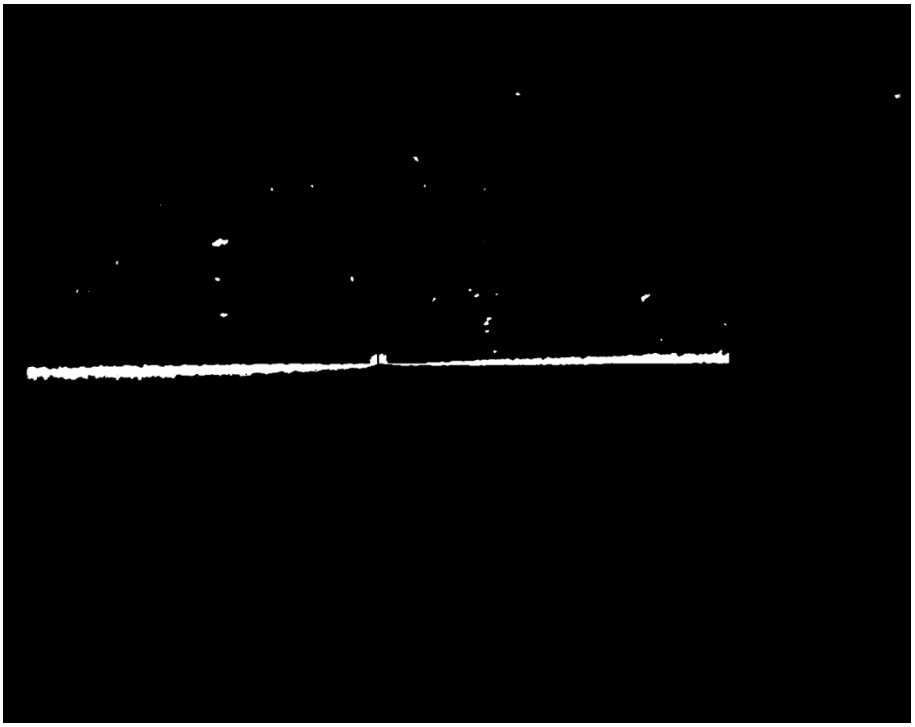

Figure 8.2 The foreground mask derived from the same image as in Figure 8.1.

Horizon detection

Inputs: scan area ellipse parameters, foreground mask, minimum horizon strength, horizon buffer angle, minimum radial artefact strength.

Outputs: Left and right horizon angles, radial artefact angles, above horizon foreground mask.

To detect the horizon lines and isolate a search area above the horizon:

- The foreground mask is cropped to the scan area.
- The average pixel value (yellowness) in the foreground mask along radial lines at 0.5-degree intervals is recorded.
- The uppermost lines with the yellowness is taken above a certain threshold on the left and right half of the ellipse as the left and right horizons, respectively (the brightest red on each side in Figure 8.3).
- The foreground mask is cropped to exclude areas within a buffer angle of each horizon line (Figure 8.4).
- The angles of those radial lines with yellowness above a certain threshold are retained to eliminate some radial artefacts.

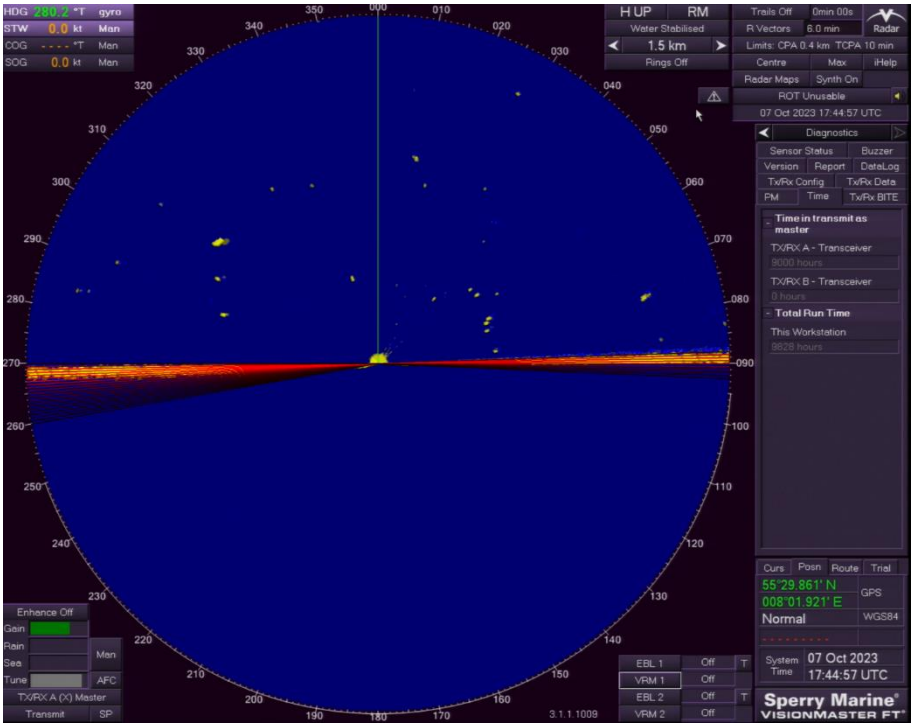

Figure 8.3 Candidate horizon lines for the image in Figure 8.1, based on the foreground mask in Figure 8.2

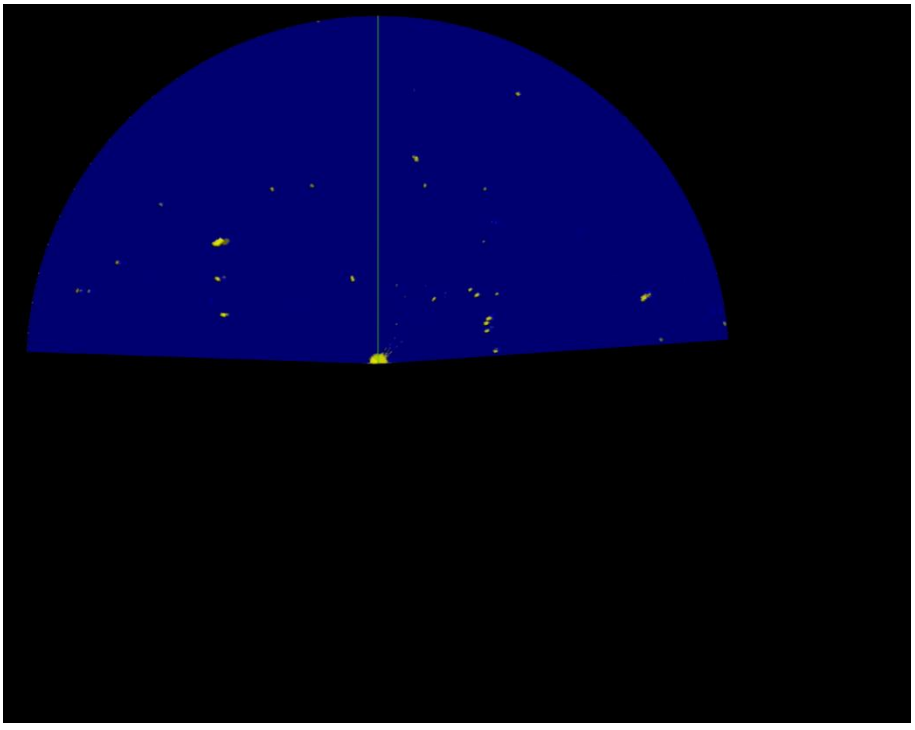

Figure 8.4 Visualisation of the image in Figure 8.1 cropped within the scan area and above a buffer around the horizon lines.

Bad weather and noise detection

Inputs: input image (RGB), scan area ellipse parameters.

Outputs: indicator of bad weather and noise in the image.

To understand the overall level of noise in the image, usually indicative of bad weather:

- The original image is cropped to the scan area above a left horizon at 290 degrees and a right horizon at 70 degrees.
- The 95 percentile of the red band within the cropped area is taken as the noise and weather indicator, for which high values indicate bad weather and/or low-quality data.

Bird filtering

Inputs: above horizon foreground mask, scan area ellipse parameters, radial artefact angles, minimum area, maximum area, minimum distance, minimum length-to-width ratio.

Outputs: coordinates of putative birds with metadata (Figure 8.5).

To extract foreground objects that are more likely to be birds:

1) Contiguous regions of the foreground mask are identified using the 'skimage' Python package.
2) Each object's locations, areas, lengths and widths are extracted.
3) The distance and angle of each object from the centre of the scan area ellipse are calculated.
4) Putative birds are filtered out based on size, shape and distance parameters.
5) Putative birds within 0.5 degrees of a radial artefact angle are excluded.

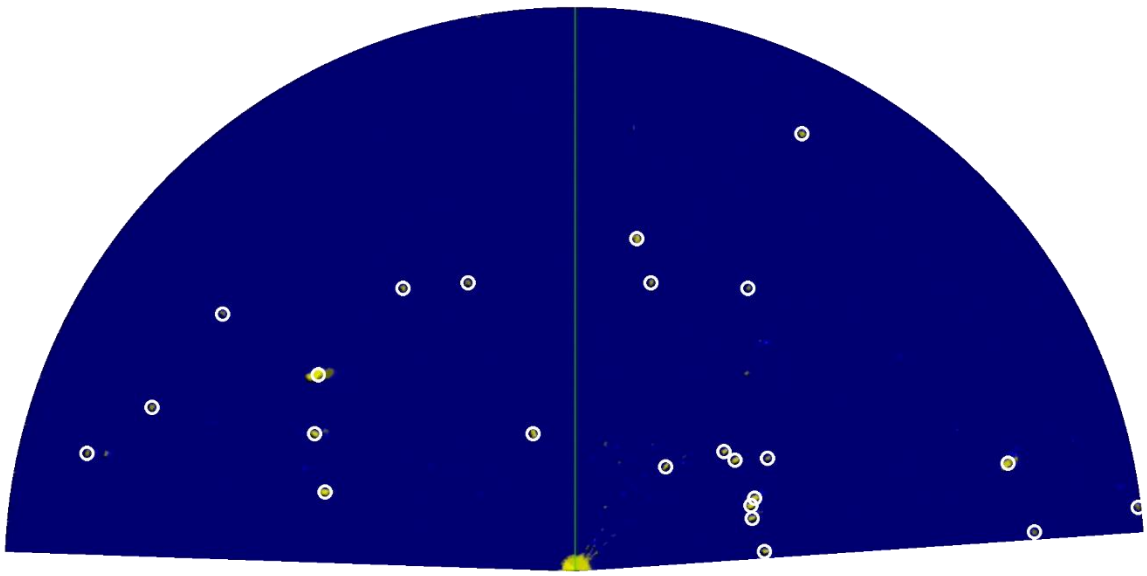

Figure 8.5 Locations of filtered putative birds (white circles) superimposed on a cropped version of the image in Figure 8.1.

Appendix 4

Ship-based survey success at observation positions

Bird observations

Table 8.4 The number of observations made at each observation position during the eight ship-based surveys conducted in the North Sea I pre-investigation area (N = 3,445).

Survey ID	Observations at observation position		
	North	Southeast	Southwest
S1	0	247	409
S2	175	86	216
S3	231	142	240
S4	208	208	165
S5	205	160	245
S6	200	125	0
S7	102	203	150
S8	116	0	75

Flight altitude recordings

Table 8.5 The number of flight altitude recordings made at each observation position during the eight ship-based bird surveys conducted in the North Sea I pre-investigation area (N = 3,206).

Survey ID	Altitude recordings at observation position		
	North	Southeast	Southwest
S1	0	232	388
S2	129	54	174
S3	171	101	155
S4	161	153	116
S5	178	149	206
S6	166	115	0
S7	85	178	137
S8	93	0	67

Individuals

Table 8.6 The number of individuals observed at each observation position during the eight ship-based bird surveys conducted in the North Sea I pre-investigation area (N = 8,070).

Survey ID	Individuals at observation position		
	North	Southeast	Southwest
S1	0	447	974
S2	218	99	466
S3	312	202	309
S4	763	405	340

Survey ID	Individuals at observation position		
	North	Southeast	Southwest
S5	400	263	541
S6	289	146	0
S7	134	1414	217
S8	180	0	69

Species

Table 8.7 The number of species observed at each observation position during the eight ship-based bird surveys conducted in the North Sea I pre-investigation area (N = 94).

Survey ID	Species at observation position		
	North	Southeast	Southwest
S1	0	24	33
S2	29	22	26
S3	13	12	14
S4	22	21	20
S5	25	31	38
S6	33	27	0
S7	11	14	14
S8	13	0	11

Appendix 5

Species observed during ship-based surveys

Table 8.8 The number of individuals of all bird species observed during the eight ship-based surveys conducted in the North Sea I pre-investigation area (N = 8,070). Species are arranged alphabetically.

Species	Survey ID								Total
	S1	S2	S3	S4	S5	S6	S7	S8	
Arctic skua	3	1	0	0	5	2	0	0	11
Arctic tern	210	16	0	52	2	0	0	0	280
Atlantic puffin	0	1	0	0	0	0	0	0	1
Barn swallow	3	11	1	0	157	0	0	0	172
Black guillemot	1	0	0	0	0	0	0	0	1
Black redstart	0	1	0	0	0	0	0	0	1
Black tern	0	2	0	0	0	0	0	0	2
Black-headed gull	0	4	0	1	11	1	5	0	22
Black-legged kittiwake	30	34	20	42	23	62	94	58	363
Black-throated diver	0	1	0	0	0	0	0	0	1
Brambling	0	0	0	0	0	1	0	0	1
Carrion crow	1	0	0	0	0	0	0	0	1
Caspian gull	1	0	0	0	4	0	1	1	7
Common guillemot	51	9	10	4	5	18	18	25	140
Common guillemot/razorbill	52	11	1	0	19	34	75	40	232
Common gull	7	11	2	9	48	20	1321	66	1484
Common kestrel	0	0	0	0	3	0	0	0	3
Common redshank	0	2	0	0	0	0	0	0	2
Common redstart	0	2	0	0	2	0	0	0	4
Common ringed plover	0	2	0	3	0	0	0	0	5
Common sandpiper	0	2	0	0	0	0	0	0	2
Common scoter	23	25	48	32	45	10	21	2	206
Common snipe	0	0	0	0	4	0	0	0	4
Common starling	0	1	0	0	0	1	61	0	63
Common swift	0	8	4	0	0	0	0	0	12
Common tern	145	0	0	99	7	0	0	0	251
Common/Arctic tern	306	1	8	63	12	1	0	0	391
Curlew sp.	1	0	0	0	0	0	0	0	1

Species	Survey ID								Total
	S1	S2	S3	S4	S5	S6	S7	S8	
Dabbling duck sp.	1	0	15	0	0	2	0	0	18
Diver sp.	3	1	0	0	0	1	2	0	7
Dunlin	0	37	0	3	31	2	0	0	73
Eurasian black-cap	0	0	0	0	1	1	0	0	2
Eurasian chaf-finch	0	0	0	0	16	1	0	0	17
Eurasian col-lared dove	0	1	0	0	0	0	0	0	1
Eurasian cur-lew	0	1	0	0	0	0	0	0	1
Eurasian sky-lark	0	1	0	0	0	11	0	5	17
Eurasian spar-rowhawk	0	0	0	0	1	0	0	0	1
Eurasian teal	9	1	2	0	7	0	0	0	19
Eurasian wigeon	0	0	0	0	20	0	0	0	20
Eurasian wren	0	1	0	0	0	5	0	0	6
European gol-den plover	3	0	0	79	3	0	0	0	85
European her-ring gull	17	6	221	9	1	37	59	19	369
European ro-bin	0	0	0	0	0	1	0	0	1
European rock pipit	0	0	0	0	0	3	0	0	3
European storm petrel	0	0	0	6	0	0	0	0	6
Falcon sp.	0	1	0	0	0	0	0	0	1
Fieldfare	0	1	0	0	0	0	0	0	1
Goldcrest	0	0	0	0	0	5	0	0	5
Great black-backed gull	22	14	4	72	59	13	14	17	215
Great cormo-rant	0	1	2	0	1	5	0	1	10
Great shearwa-ter	0	0	0	1	0	0	0	0	1
Great skua	0	0	1	3	2	0	0	0	6
Greater scaup	10	0	0	0	0	0	0	0	10
Grey heron	1	0	0	0	3	2	0	0	6
Grey plover	0	3	0	0	4	0	0	0	7
Grey wagtail	0	0	0	0	1	0	0	0	1

Species	Survey ID								Total
	S1	S2	S3	S4	S5	S6	S7	S8	
Greylag goose	0	6	0	0	0	0	0	0	6
Gull sp.	10	3	16	7	12	5	5	2	60
Lesser black-backed gull	217	409	366	835	110	1	0	0	1938
Lesser redpoll	0	0	0	0	1	0	0	0	1
Little gull	0	0	0	0	10	0	2	0	12
Meadow pipit	60	2	0	0	182	47	0	0	291
Merlin	0	0	0	0	5	0	0	0	5
Mistle thrush	0	0	0	0	0	0	0	1	1
Northern ful-mar	25	53	43	18	30	2	17	1	189
Northern gan-net	84	30	22	96	165	66	14	2	479
Northern pintail	0	0	0	0	21	0	0	0	21
Northern sho-veler	1	0	0	0	0	0	0	0	1
Northern wheatear	0	0	0	0	3	0	0	0	3
Osprey	0	0	0	0	2	0	0	0	2
Passerine sp.	1	5	0	0	6	44	0	0	56
Petrel sp.	0	0	0	1	0	0	0	0	1
Pied wagtail	5	1	0	0	4	0	0	0	10
Razorbill	9	1	0	0	29	13	46	9	107
Red knot	0	0	0	6	0	0	0	0	6
Red-throated diver	48	19	1	0	17	3	0	0	88
Redwing	0	0	0	0	0	6	0	0	6
Ruddy turns-tone	1	0	0	1	0	0	0	0	2
Sandwich tern	50	0	3	7	1	0	0	0	61
Short-eared owl	0	0	0	0	0	2	0	0	2
Skua sp.	2	0	0	0	2	1	0	0	5
Song thrush	0	0	0	0	0	2	0	0	2
Sooty shear-water	0	0	0	1	3	0	0	0	4
Swallow sp.	0	2	0	0	2	0	0	0	4
Thrush sp.	0	0	0	0	0	1	0	0	1
Wader sp.	0	0	0	25	32	1	0	0	58
Warbler sp.	1	0	0	0	0	0	0	0	1

Species	Survey ID								Total
	S1	S2	S3	S4	S5	S6	S7	S8	
Western house martin	0	4	0	0	60	0	0	0	64
Western jack-daw	2	0	0	0	0	0	0	0	2
Western yellow wagtail	0	1	0	0	0	0	0	0	1
Whimbrel	1	0	0	4	0	0	0	0	5
Willow warbler	0	1	0	1	0	0	0	0	2